ISOTHERMAL CORROSION TESTING OF FRIT FURNACE REFRACTORIES

A Thesis Submitted to the
Graduate School of Engineering and Sciences of
İzmir Institute of Technology
In Partial Fullfilment of the Requirements for the Degree of

MASTER OF SCIENCE

in Materials Science and Engineering

by
Fatih BALIKOĞLU

June 2008
İZMİR

We approve the thesis of **Fatih BALIKOĞLU**

_____
Assoc. Prof. Dr. Sedat AKKURT
Supervisor

_____
Assoc. Prof. Dr. Metin TANOĞLU
Committee Member

_____
Assoc. Prof. Dr. Selahattin YILMAZ
Committee Member

30 June 2008
Date

_____
Prof.Dr.Mustafa Güden
Head of the Material Science and
Engineering Department

_____
Prof.Dr.Hasan BÖKE
Dean of the Graduate School
Engineerind and Science

ACKNOWLEDGEMENT

I would like to thank the Materials Science and Engineering Department at Izmir Institute of Technology for accepting me into their program and giving me the opportunity to attain an M.S degree in this field. I am greatly thankful to my advisor, Assoc. Prof. Dr. Sedat Akkurt for his patience, encouragement, and guidance during this study.

I would like to thank to Research Assistants Mücahit Sütcü and Ceramic Laboratory Staff for their helps during thesis study. Special thanks are to Department of Mechanical Engineering in İYTE for providing laboratory usage.

Additional thanks are for the kind efforts and helps of İYTE Center for Materials Research Staff and to Tamsa A.Ş. and Egeferro A.Ş. for providing refractory and frit samples. I would like to thank to TUBİTAK for providing financial support for this project.

I would like to thank especially to my family for their support, patience, understanding, encouragement and help.

ABSTRACT

ISOTHERMAL CORROSION TESTING OF FRIT FURNACE REFRACTORIES

Results of a project aimed at understanding the corrosion behavior of aluminosilicate type of refractories in frit melts are presented. A refractory of largely andalusite and silimanite composition was compared to another brick of mullite and silimanite composition which was made by a different manufacturer for use in a different frit furnace. Density, porosity, microstructure and chemistry of both bricks are characterized before the corrosion tests. Isothermal tests were conducted by partially immersing a 15x15x115mm square specimen into a frit melt between 1404 and 1504^{o}C in a vertical tube furnace. The frit used had an industrially used transparent frit composition. The effects of temperature, duration of exposure and refractory type were investigated using a statistically designed set of experiments. The ANOVA (Analysis of variance) table indicated that temperature and duration were more important factor effects. Increasing exposure duration and temperature both led to increased amount of corrosion as measured by the cross sectional area loss of the corroded specimen. Postmortem microstructural analysis was also done on the specimens and extensive amount of $ZnO.Al_2O_3$ precipitation was observed along the frit-refractory interface where also other crystals of mullite and alumina were found to precipitate. Increasing amount of duration and temperature produced more $ZnO.Al_2O_3$ precipitation. As identified by SEM-EDS analysis, mullite cyrstals were in the needle like morphology while alumina crystals were generally cubic. Because of their small concentration, XRD analysis could not reveal the phases of these crystals. More experiments were done by rotating the specimens in the melt at 50 rpm of rotational speed. Due to the reduction of boundary layer thickness, more dissolution was observed from the rotated specimens. In all specimens corrosion was more pronounced in the bond phase than through the large filler grains of mullite and andalusite.

Keywords: Refractories, frit, corrosion, test.

ÖZET

FRİT FIRINI REFRAKTERLERİNİN İZOTERMAL KOROZYON TESTİ

Alumina silikat esaslı refrakterlerin frit eriyiği içindeki korozyon davranışlarının incelenmesi bu çalışmanın sonuçlarında hedeflenmiş ve sunulmuştur. Farklı sanayi kuruluşları tarafından farklı frit fırınında kullanılmak amacıyla üretilen andalusit ve silimanit komposizyona sahip refrakter ile diğer bir mullit ve silimanit içeren refrakter karşılaştırıldı. Korozyon testleri öncesi her iki refrakterin yoğunluk, gözeneklik, mikroyapıları ve kimyasal kompozisyonları karakterize edilmiştir. İzotermal korozyon testleri dikey tüp fırında, 15x15x115 mm boyutlarında refrakter örneğin frit içine 1404 ^{0}C ve 1504 ^{0}C sıcaklıkları arasında kısmen daldırılması ile gerçekleşmiştir. Kullanılan frit örneği sanayide uygulanan transparan frit kompozisyonuna sahiptir. Sıcaklık, süre ve refrakter tipinin etkisi istatistiksel olarak dizayn edilen deneylerde incelenmiştir. Anova tablosu sıcaklık ve sürenin en önemli faktörler olduğunu gösterdi. Artan sıcaklık ve test süreleri her iki korozyona uğramış örneğin kesit alanlarındaki kayıpların ölçülmesiyle belirlenen korozyon miktarının artmasına neden olmuştur. Postmortem mikroyapısal analiz örnekler üzerinde uygulandı ve büyük miktarlarda $ZnO.Al_2O_3$ çökeltileri frit-refrakter ara yüzeylerinde gözlendi. Ayrıca alumina ve mullit kristalleri de çökelti olarak bulundu. Artan sıcaklık ve süre değerleri daha fazla $ZnO.Al_2O_3$ çökeltilerine neden olmuştur. SEM-EDS analizleri ile, iğnemsi yapıda mullit kristalleri ve genellikle kübik olan alumina kristalleri belirlenmiştir. XRD analizleri az miktarlarda bulunmalarından dolayı bu kristallerin fazlarını ortaya çıkaramamıştır. Örnekler eriyik içerisinde 50 rpm hızla döndürülerek diğer deneyler gerçekleştirilmiştir. Sınır tabakasının kalınlığının azalması nedeniyle, daha fazla çözülme döndürülen örneklerde gözlenmiştir. Bütün örneklerde, korozyon bağ fazlarda, geniş mullit ve andalusit tanelere göre daha belirgindir.

Anahtar kelime: Refrakter, frit, korozyon, test.

TABLE OF CONTENTS

LIST OF FIGURES

Figures **Page**

LIST OF TABLES

Table **Page**

CHAPTER 2

REFRACTORY AND FRIT

In this chapter, some information is provided about the refractories and frits including their microstructures, properties, behaviours and manufacturing processes.

2.1. REFRACTORY

The term of refractory, from the Latin “refractorius” meaning stubborn is often used as resistant to elevated temperatures. It could be applied to any material which can be strong in a high-temperature environments such as the refractory metals W and Ta. However, the noun refractory implies a ceramic used in large volumes in extreme, corrosive environments as furnace linings for high temperature materials processing in metal, glass and ceramic manufacture (Lee and Phill 1994). In brief, refractories are ceramic materials including inorganic chemical substances, single or polyphase which have the excellent high-temperature properties such as creep and wear resistance for high-temperature applications (In his article on Refractories in the Encyclopedia of Materials: Science and Technologly, Moore noted that…). Refractories are more heat resistant than metals and are required for heating applications above 1000°F (538°C) (Refractories Institute 2008). Therefore, there are widely employed in constructions of furnaces that must resist the thermal shock, physical and chemical wear associated with iron and steel production, the smelting of metals, glass and ceramic manufacturing and similar processes (Lewis, et al. 1991). Significant consumers of refractories are the glass melting, cement and ceramic industries that are each using about 8% of production. However, the greatest user is the iron and steel industry consuming about 65% of production. A wide range of refractory types are commercially available with a variety of complex compositions and microsructures. Table 2.1. lists some of the commonly phase found in refractories (Lee and Phill 1994).

Table 2.1. Common phases found in refractory microstructures

(Source: Lee and Phill 1994)

Phase	**Chemical Formula**	**T_m(^{o}C)**	**Significant behaviour**
Silica (Quartz)	SiO_2	1723	Polymorphic transitions
Alumina	Al_2O_3	2050	-
Magnesia (Periclase)	MgO	2800	Hydrates
Calcia	CaO	2572	Hydrates
Doloma	MgO.CaO	800*	-
Andalusite	$Al_2O_3.SiO_2$	1810	Polymorphic transition
Sillimanite	$Al_2O_3.SiO_2$	1810	Polymorphic transition
Forsterite	$2MgO.SiO_2$	1890	-
Spinel	$MgO.Al_2O_3$	2135	-
Mullite	$3Al_2O_3.2SiO_2$	1810	-
Zircon	$ZrO_2.SiO_2$	1675	-
Enstatite	MgO.SiO2	1557	-
Silicate	$2CaO.SiO_2$	2130	Polymorphic transitions
Chromia	Cr_2O_3	2275	Volatilizes
Zirconia	ZrO_2	2690	Polymorphic transitions
Silicon carbide	SiC	2500*	Manmade, oxidizes
Silicon nitride	Si_3N_4	1878*	Manmade, oxidizes
Carbon	C	4000*	Oxidizes

Note: * indicates decomposition not melting.

2.1.1. Refractory Microstructure

Refractories are seldom pure, single phase materials but they generally have microstructure containing several of the phases listed in Table 2.1. The microstructure of a typical refractory consists of grain (aggregate, filler), bond (matrix) phases and pores (Zhang, et al. 2004) as shown in Figure 2.1.

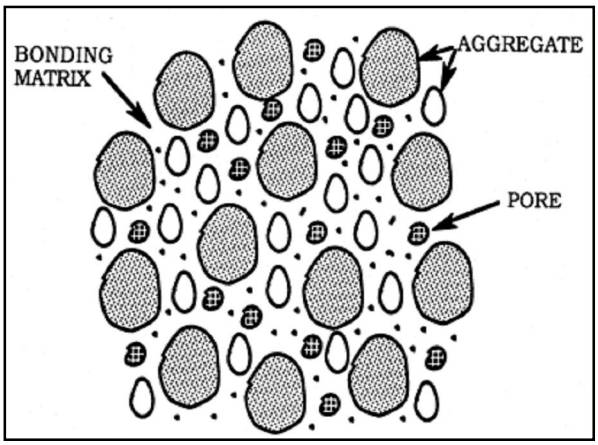

Figure 2.1. Schematic of microstructure of refractory brick
(Source: Refractories Handbook 1998)

Typical synthetic grain materials include those made by melting or fusion (Al_2O_3: alumina, $3Al_2O_3.2SiO_2$: mullite, MgO: magnesia, ZrO_2: zirconia) and sintering (MgO: magnesia, Al_2O_3: alumina, $MgO.Al_2O_3$: aluminate spinel). Fused grains are pure since many impurities volatilise during melting process while sintered grains include grain boundary impurities which are deleterious to high temperature properties. Fused and sintered grains are easily distinguished since fused grain typically contains a lower proportion of second phases at grain boundaries as shown in Figure 2.2. (Zhang, et al. 2004).

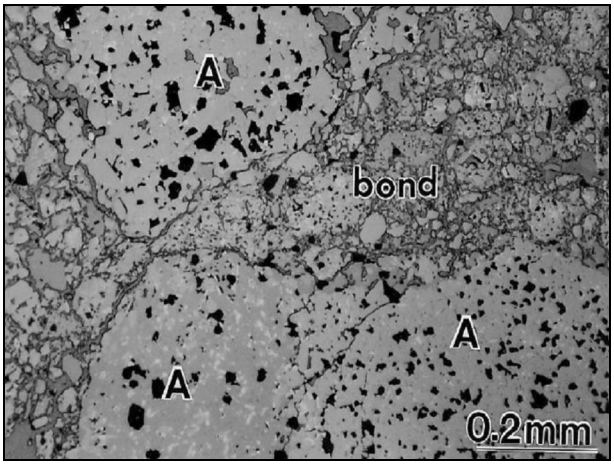

a)

Figure 2.2. a) Reflected light image of high alumina refractory containing bauxite-derived (A) which is porous (dark), predominantly sintered Al_2O_3.
b) Reflected light image of high alumina refractory containing fused Al_2O_3 and spinel matrix. (Source: Zhang, et la. 2004)

(cont.on next page)

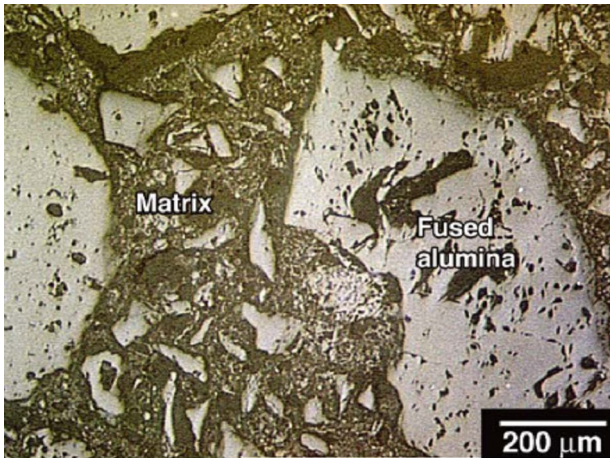

b)

Figure 2.2 shows the difference between fused and sintered alumina grains in two different refractory microstructures. While sintered corundum grain contains lighter Fe and Ti as second phases which are present at grain boundraies in Figure 2.2.a, second phases are not observed in fused alumina grain in Figure 2.2.b. Refractory grain may also be produced from natural sources such as fireclays, flint clays, quartz, dolomite, graphite, bauxite, magnesite and members of the andalucite/kyanite/sillimanite group. These materials can be directly used in the production of refractories after simple processing such as washing and calcination (Zhang, et al. 2004). The bond phase in refractories enables the aggregate/grain phases together with large components to be manufactured. Refractories are often characterized by the nature of their bond systems. Refractories are termed as “silicate bonded”, “carbon bonded”, “phospate bonded” and “cement bonded”(Lee and Moore 1998).

2.1.2. Refractory Raw Materials

Raw materials are the backbone of refractory products, whether shaped or unshaped. The progress of refractories in terms of properties, quality, service performance and economic effectiveness is closely associated with the availability of improved or new refractory raw materials (Zhou, et al. 2005). Raw materials used in the production of refractories are classified as two groups: natural (clays and rocks) and synthetic (sintered and fused alumina). Natural raw materials used for refractory manufacturing are clay minerals from the kalonite groups which are fireclay (hydrous silicates of aluminium), the commonly used rocks including chromite ($FeO.Cr_2O_3$), a complex mixture of spinel minerals ($RO.R_2O_3$), quartz (SiO_2), dolomite ($Ca,Mg.CO_3$), magnesite ($MgCO_3$) and bauxite minerals with a range of impurities and earth alkalies such as Fe_2O_3, TiO_2, CaO and MgO. Some synthetic versions of naturally occurring raw materials are produced as fused and sintered alumina (Al_2O_3), MgO, mullite ($3Al_2O_3.2SiO_2$) and zirconia (ZrO_2) (Moore 2001).

2.1.3. Refractory Manufacturing

Refractories are produced in two basic forms, shaped (bricks) and unshaped (monolithics) as shown in Figure 2.3.

a) Monolithics Refractories b) Shaped (Bricks) Refractories

Figure 2.3. Shape and Unshaped Refractories

(Source: JRSUK 2008)

The shaped refractories may be manufactured in the cold or warm processes by pressing, stamping, extrusion, slip casting or by foundry methods via smelting constituent powders to complete liquid and then casting into molds. These products are used to form the linings of furnaces, walls and floors tiles of various high temperature equipments. The unshaped refractories are also known as monolithics including mortars, ramming mixes, castables, gunning, injectable, pumpable mixes and plastics. Monolithics account for 60% of refractories production and are used as temporary for the maintenance of furnace linings (In his article on Refractories in the Encyclopedia of Materials: Science and Technologly, Moore noted that…). The major advantage of monolithic refractories is that they almost never need any high-energy requirements for their manufacturing processes like shaping and prefiring. In this way considerable amount of manpower and energy required can be saved by using monolithics instead of shaped refractories (Banerjee, et al. 1998). Refractory manufacturing involves four processes as shown in Figure 2.4, these are raw material processing, forming, firing and final processing. Raw material processing consists of crushing and grinding raw materials, followed if necessary size classification, calcining and drying processes. The raw material processed then may be dry-mixed and blending with other minerals and chemical compounds and prepared as monolithic refractories. Forming consists of mixing the raw materials and forming them into the desired shapes. This process usually occur in wet or moist conditions. Firing process involves heating the refractory to high temperatures in continuous tunnel kiln to form the ceramic bond giving the product its refractory properties. The final processing stage involves milling or direct final packaging (U.S Environmental Protection Agency 2008). Refractory bricks are generally fabricated by using powder processing or fusion cast methods. Powder processing method leads to a complicated microstructure composed of large, filler refractory grain particles held together by a continous bonding matrix often containing extensive porosity owing to large particle size distribution. Refractory bricks produced by powder processing can be installed in their service conditions as fired or unfired (pre-cast) situations (Lee and Phill 1994).

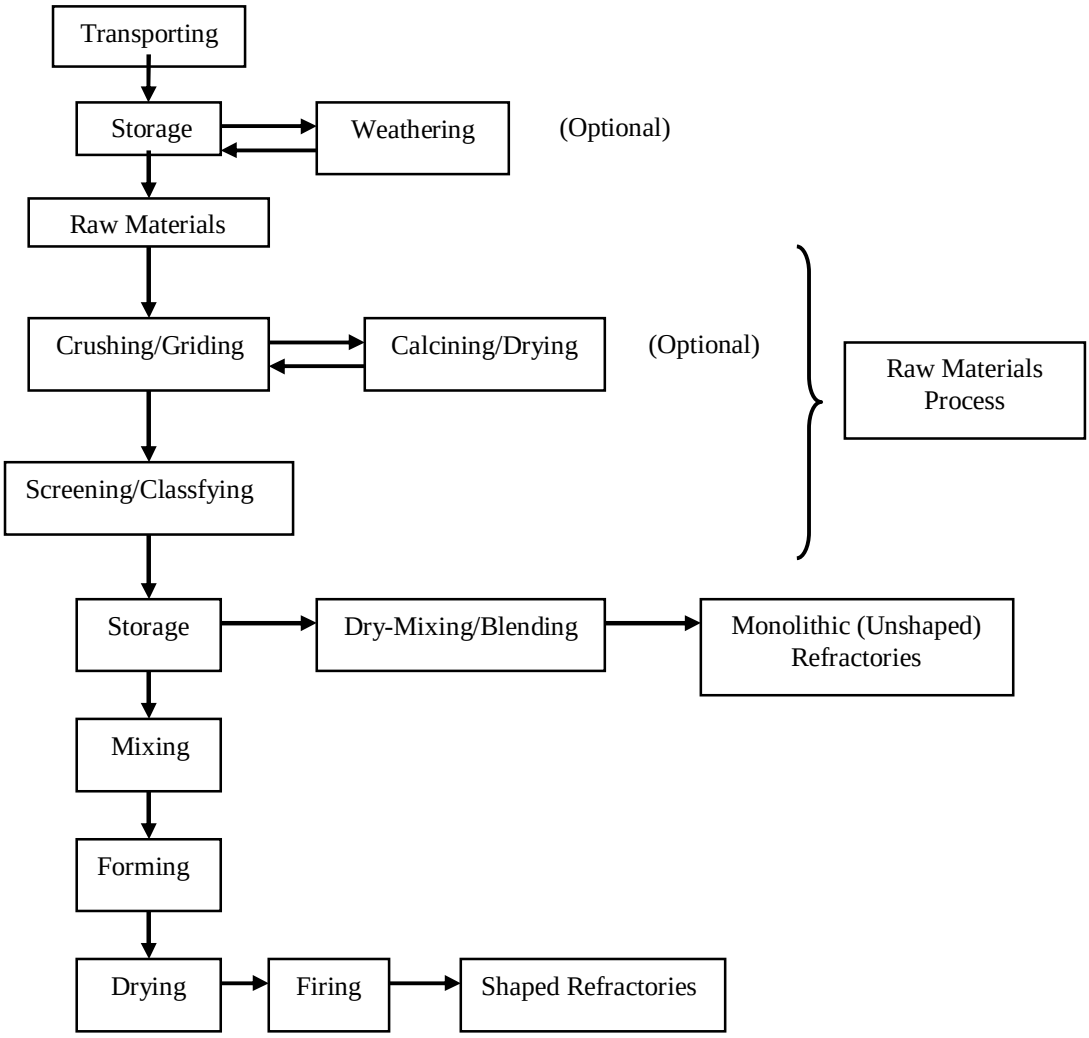

Figure 2.4. Schematic of refractory manufacturing
(Source: U.S. Enviromental Protection Agency 2008)

Refractory bricks are also produced by fused casting (electrocasting or electrofusing) manufacturing process. This process involves using an electric arc furnace to melt refractory raw materials, and then the molten materials are poured into sand-forming molds. The fusion cast method gives a microstructure like a cast metal including low levels of porosity and little glassy phase. For this reason, fused bricks are used in applications where extreme corrosion resistance is required since liquid penetration is limited by such a microstructure (Lee and Phill 1994).

2.2. Classification of Refractories

Refractories are generally classified in two ways. One is a physical classification according to manufacturing processes forming shaped (bricks) and unshaped (monolithics) refractories. The second is a chemical classification based on the different chemical compositions as shown in Table 2.2. The chemical classification includes acid, neutral and basic types. Acid refractories contain substantial amount of SiO_2 which react with basic refractories, slags and fluxes at high temperatures. They are resistant to slags that are rich in silica. SiO_2, alumina-based and clay-based Al_2O_3-SiO_2 (fireclay, high alumina and silica) refractories are members of acid refractories. Basic refractories are composed essentially of CaO, MgO or both and react with acid refractories. They are resistant to attack by slags containing high concentrations of MgO and CaO. MgO (periclase or magnesite), dolomite ($CaCO_3$.$MgCO_3$) and magnesia-chromite based refractories are classified as basic refractories. Neutral refractories are neither acid nor basic and include refractories like carbon and mullite which are resistant to attack from both acidic and basic materials, slags and fluxes at high temperatures. Neutral refractories are used for seperation as a layer when both acid and basic refractories are required in one lining of a furnace. Besides the refractories mentioned above, there is one also refractory type including such as ZrO_2, SiC and Si_3N_4 as known special refractories (Lee and Phill 1994).

Table 2.2. Classification of Refractories

(Source: Lee and Phill 1994).

Chemical Classification	Refractory Type	Base Chemical Constituents
Acidic	Silica	SiO_2
	Fireclay	Al_2O_3-SiO_2 (wt<%50 Al_2O_3)
	High Alumina	Al_2O_3-SiO_2 (wt>%50 Al_2O_3)
Basic	Magnesia	MgO
	Magnesia-Chromite	MgO-Cr_2O_3 (wt>50% MgO)
	Chromite-Magnesia	MgO-Cr_2O_3 (wt<50% MgO)
	Magnesia-Spinel	MgO.Al_2O_3
	Forsterite	2MgO.SiO_2
Neutral	Mullite	$3Al_2O_3.2SiO_2$
	Carbon	C
Special	Zirconia	ZrO_2
	Silicon carbide	SiC
	Silicon nitride	Si_3N_4

2.2.1. Aluminosilicate Refractories

Aluminosilicate refractories consist of essentially Al_2O_3 and SiO_2 contents and are classified into three groups with respect to alumina (Al_2O_3%) content: fireclay, silica and high alumina as shown in Table 2.3. Aluminosilicate refractories are basely produced from nature and synthetic raw materials. Natural raw materials source may be fireclays (hydrous silicate of aluminium), kaolin, bauxite and members of the andalucite/kyanite/sillimanite group. Synthetic raw materials used in production of those are sintered and fused mullite, alumina and calcined alumina. The simplest aluminosilicate refractories are based on the Al_2O_3-SiO_2 binary equilibrium phase diagram as shown in Figure 2.5. Refractories based on this system are defined as silica (<7wt% Al_2O_3), fireclay (7-50 wt% Al_2O_3) and high alumina (>50wt% Al_2O_3). Al_2O_3-SiO_2 binary phase diagram is useful guide to predict which phases will be present at

equilibrium in service conditions. However, aluminosilicate refractories will always not achieve equilibrium owing to substantial quantities of oxides and alkalis. These oxides and alkalis such as Fe_2O_3, TiO_2, SiO_2 and Na_2O, K_2O may be found from impurities in the natural minerals used as raw materials or may be added intentionally to facilitate processing. But their presence is critical to the high temperature strength of the brick since they can increase the amount of liquid even when present in small amounts (Lee and Phill 1994).

Table 2.3. Classsification of Aluminosilicate Refractories
(Source: Lee and Phill 1994)

Refractory	**Subgroup**	**wt % Al_2O_3**
Silica	-	<7
Fireclay	Siliceous	7-22
	Firebrick	22-38
	Aluminous	38-50
High Alumina	Sillimanite	50-65
	Mullite	65-75
	Corundum	75-98

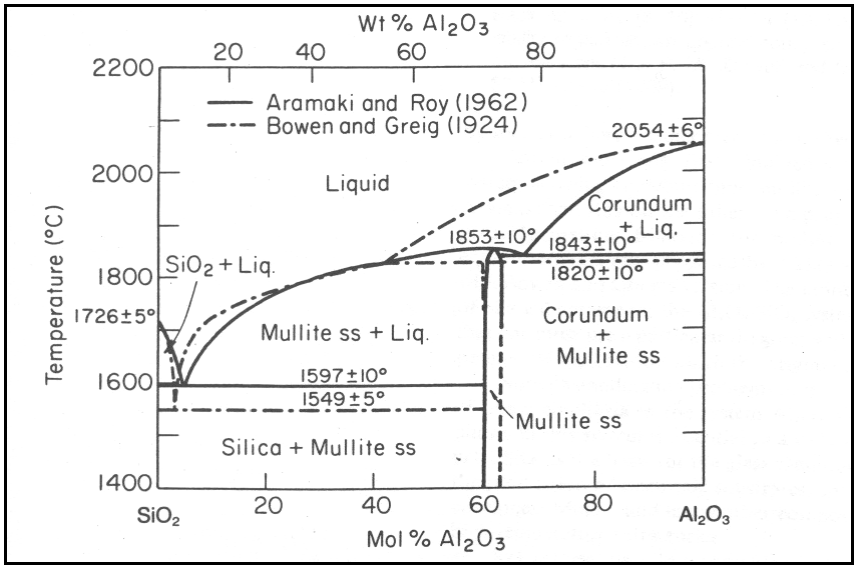

Figure 2.5. Al_2O_3-SiO_2 binary phase diagram
(Source: Lee and Phill 1994)

The fluxing effect of alkalis and oxides on the aluminosilicate glass bond is critical for high temperature properties. The general effects of higher alkali content and other oxides on the refractoriness of typical aluminosilicate refractories can be seen from Figure 2.6. The binary system based on silica divided into type A and type B in Figure 2.6. Type A binaries form eutectic phases leading to drastic reduction in melting temperature as shown in Figure 2.6.a. Type A additions to silica include alkalis such as Na_2O, K_2O and TiO_2. Small amounts of impurities flux silica in other words leads to reduction in its melting temperature to give a very fluid liquid which may have a disastrous effect on high temperature behaviour. Type B additions including oxides such as CaO, MgO and FeO lead to formation of a two liquid region in the binary pushes the eutectic to higher additive contents as shown in Figure 2.6.b. This result shows that type B additions are not as effective as on decrease in melting temperature compared with alkalis. Therefore, alkali impurities have a larger effect than other oxides on the refractoriness and must keep to a minimum in high quality aluminosilicate refractories (Lee and Phill 1994).

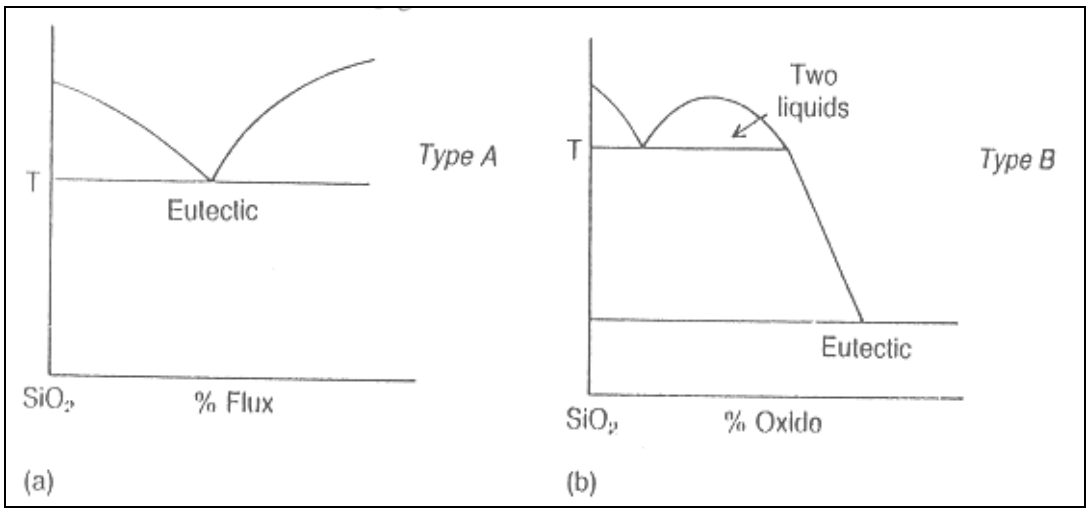

Figure 2.6. Schematic of binary phase diagram between SiO_2 and other oxides (Source: Lee and Phill 1994)

2.2.1.1. High Alumina Refractories

The increased temperatures, production with more severe environments has led to need higher quality bricks in the furnaces and other high temperature applications. The chemical composition of fireclay bricks are limited to the composition of clays used as raw materials in the production of those. Therefore, raw materials including high alumina content have been needed for the production of high alumina refractory bricks. However, high alumina refractories may not be produced by using natural clays as raw materials because of their low Al_2O_3 content (Kocabağ, et al. 2000). However, sillimanite group and bauxite minerals may be used as natural raw materials in their production. Fused/sintered alumina, mullite and calcined alumina for higher quality bricks may be also used as synthetic raw materials (Zhang, et al. 2004) The high-alumina bricks include the subgroups of sillimanite-type, mullite and corundum (bauxite) types of refractories as shown in Table 2.3. Sillimanite-type bricks are produced from the sillimanite group minerals as raw materials including andalusite, sillimanite and kyanite (Lee and Phill 1994) .Sillimanite group minerals are aluminium silicate anyhydrate minerals. Sillimanite, andalusite and kyanite are advantageous natural raw minerals for high alumina bricks. Since, mullite formation and adequate volume expansion can be observed in the sillimanite type bricks during heating or in service . Technologically, these three raw minerals have the advantages of low level impurities and valuable expansion characteristics compared with bauxite minerals. Economically, sillimanite, andalusite and kyanite save energy because they can be directly used without calcination process. Each of andalusite, sillimanite and kyanite minerals has the same chemical formula of $Al_2O_3.SiO_2$ and are known as high pressure minerals providing a typical polymorphism (Zhou, et al. 2005). However, these minerals have some differences between their crystal structures and densities when compared with each other. Another difference between them is that the three members of the sillimanite group decompose into mullite and silica at different temperatures. Andalusite decompose at 1350-1500^oC, sillimanite at 1525-1530^oC and kyanite at 1325-1410^oC. The mullite formed when these minerals decompose is lower in specific gravity than any of the three starting materials. So each changes in volume in proportion results from the differences between their specific gravities. Kyanite has the highest specific

gravity (3.5-3.6 g/cm^3) of the three. This drops considerably when kyanite decomposes. As a result, kyanite expands considerably when heated. Difference between specific gravities before and after decomposition in sillimanite and andalusite is not large as kyanite. They do not change greatly in volume when heated (Kocabağ, et al. 2000). The characteristics of the sillimanite group minerals are listed in Table 2.4.

Table 2.4. Characteristics of sillimanite group minerals
(Source: Zhou, et al. 2005)

Mineral		**Sillimanite**	**Andalusite**	**Kyanite**
Chemical Formula		$Al_2O_3.SiO_2$	$Al_2O_3.SiO_2$	$Al_2O_3.SiO_2$
Crystal system		Orthorhombic	Orthorhombic	Triclinic
Lattice Parameters	**a (A^o)**	7.47	7.8	7.11
	b (A^o)	7.66	7.9	7.84
	c (A^o)	5.76	5.56	5.57
	α	-	-	90.5^o
	β	-	-	101.5^o
	γ	-	-	106^o
Density(g/cm^3)		3.2	3.18	3.6
Decomposition temperature(^{o}C)		→Mullite 1525-1530 ^{o}C	→Mullite 1350-1500 ^{o}C	→Mullite 1325-1410 ^{o}C

Mullite is described as the chemical formula of $3Al_2O_3.2SiO_2$. Mullite is the only stable compound in the binary system of silica-alumina as shown in Figure 2.5. Mullite is almost never encountered in nature. Therefore, the only mullites used as a refractory raw materials are artificially produced (Lee and Phill 1994).Two main types of natural raw materials can be used to produce mullite. (1) Hydrous alumino-silicates based on kaolinite clay ($Al_2O_3.2SiO_2.2H_2O$), (2) Anyhydrous alumino-silicates including sillimanite, andalusite and kyanite polymorph minerals having the same composition: $Al_2O_3.SiO_2$. The characterics tics of mullite are listed in Table 2.5.

Table 2.5. Characteristics of Mullite Mineral
(Source: Schneider, et al. 2007)

Chemical Formula	$3Al_2O_3.2SiO_2$
Crystal Structure	Rhombic
Melting Point (^oC)	1830^oC
Density (g/cm^3)	~3.2
Linear thermal expansion ($x10^{-6}\ ^oC^{-1}$) 20 -1400 ^oC	4.5
Thermal conductivity (kcal $m^{-1}h^{-1}\ ^oC^{-1}$)	
20 ^oC	6
1400 ^oC	3

Sillimanite type bricks have some disadvantages arising from their nature. These bricks are undergone large volumetric expansion during firing process. For instance, while andalusite and sillimanite expand in volume approximately 0-2%, kyanite shows a large volume expansion about 15-18% (Mazel, et al. 2001). Therefore, bricks including sillimanite minerals must be used after firing and mullite formation in service conditions. Since, their large volumetric expansion values may cause disastorous effects like thermal shock when exposed to rapid heating and cooling conditions in the furnaces. The second is that these bricks may include glassy phase in their silicate-bond structure and this glassy phase may dissolve when exposed to high temperatures. This situation may conclude short service life, dissolution of materials from brick to frit melt owing to chemical corrosion, poor quality products and high maintance cost (Kocabağ, et al. 2000). However, their low thermal conductivity values as shown in Figure 2.7 (a) enable them to be used as superstructure bricks above the melt line including crown and dome, regenerators (chamber where waste heat from the furnace exhaust gas is used to heat the air intake stream) in the frit furnaces (Lee and Phill 1994).

Mullite type bricks have good strenght, creep resitance thermal shock resistance durability and resistance to chemical corrosion by glass melt. These outstanding properties enable mullite bricks to be used in many high temperature applications required (Lee and Phil 1994, Scheneider 2007, Kocabağ 2000). Mullite type bricks may be used in rapid heating changes occurred in the door of the frit furnace because of their good thermal shock resitance, in contact with the corrosive melt in the side and floor of the furnace owing to their good corrosion resistance and in the construction of the furnace on account of their good creep resistance. Mullite bricks can be chosen for the high temperature zones in the frit furnaces such as superstructures, regenerators and walls in contact with corrosive melt due to their excellent properties mentioned above (Windle, et al. 2006). Their good thermal shock resitance is arising from their low thermal expansion values as shown in Figure 2.7.b (Refractories Handbook 1998). Their good corrosion resitance results from their microstructures not including glassy phase and impruties because of only stable compound in Al_2O_3-SiO_2 binary phase diagram in Figure 2.5 (Lee and Phil 1994).

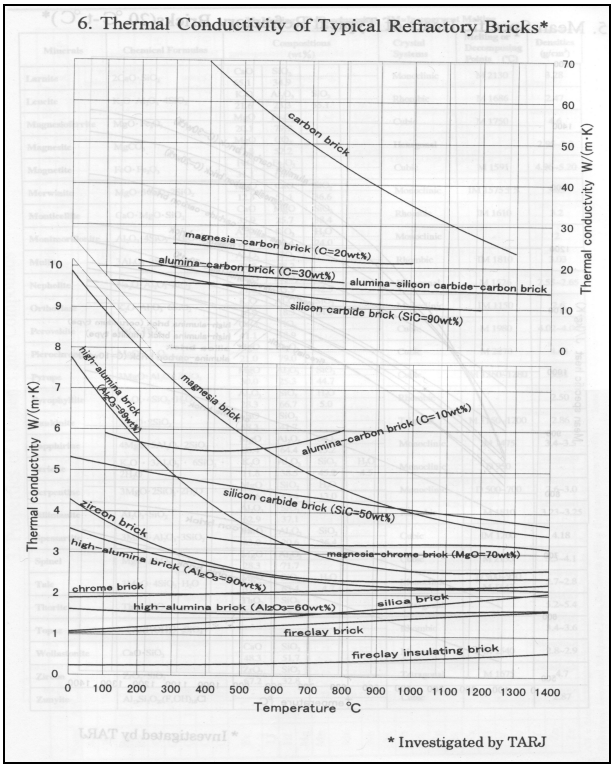

a) Thermal Conductivity of Refractory Bricks

Figure 2.7. Thermal expansion and conductivity of refractory bricks

(Source: Refractories Handbook 1998) (cont. on next page)

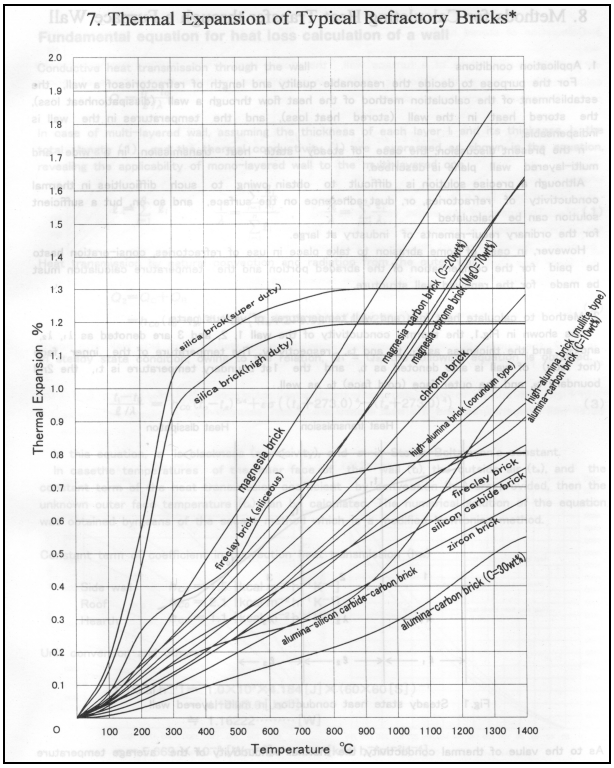

b) Thermal expansion of Refractory Bricks

2.3. Frit

Frit species are solid granules and glasses, insoluble in water and prepared by fusing suitable two or more raw materials mixture at high temperatures in a gas/oil-fired or an electric furnaces and then the molten mixture is rapidly quenching in order to be used in the preparation of glaze. Glazing is applied to provide the fired product with a series of technical and esthetical properties such as cleanability, impermeability, gloss, colour, surface texture and chemical (corrosion) and mechanical resistance. Frit species are used in glazing porcelain, pottery, ceramic wall and floor tiles and also in enameling iron and steel. Frit is also used in bonding grinding wheels, to lower vitrification temperatures, and as lubricant in steel casting and metal extrusion (U.S. Environmental Protection Agency 2008).

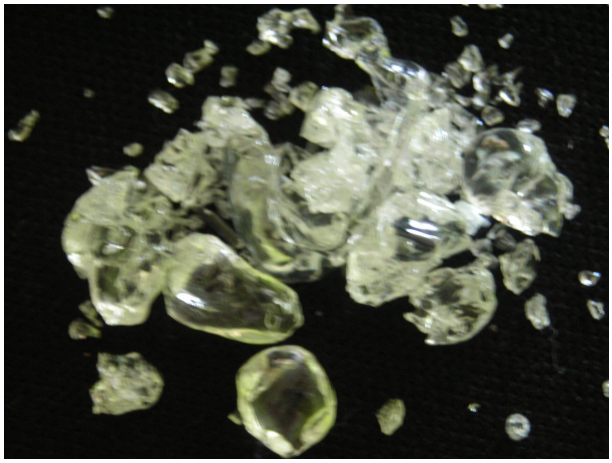

Figure 2.8. Frit (transparent frit granules)

2.3.1. Constitution and Classification of Frit

Frits can be classified according to very different criteria: in terms of chemical compositions (lead, leadless and boric), physical properties (opaque, transparent) and melting range (fluxing, hard). A variety of frits is avaliable, differing in chemical composition and physical properties. Frits are made up of series of inorganic raw materials which are responsible for differences between their properties. Commonly raw materials used in the preparation of the frits can be seen from Table 2.6 (Eppler, et al. 2000).

Table 2.6. Raw Materials Used in Frit Composition

(Source: Eppler, et al. 2000)

Oxides	**Possible Raw Materials**	**Other Oxides**
Li_2O	Lithium carbonate	-
	Spodumene	Al_2O_3, SiO_2
Na_2O	Feldspars	K_2O, Al_2O_3, SiO_2
	Soda ash (Sodium carbonate)	-
K_2O	Feldspars	Na_2O, Al_2O_3, SiO_2
	Potash (Potasium carbonate)	-
CaO	Wollastonite	SiO_2
	Calcium carbonate	-
	Dolomite	MgO
MgO	Magnesium carbonate	-
	Magnesium oxide	-
	Dolomite	CaO
	Talc	CaO, SiO_2
BaO	Barium carbonate	-
Al_2O_3	Corundum	-
	Alumina hydrate	-
	Feldspars	Na_2O, K_2O, SiO_2
	Kaolin clay	SiO_2
	Ball clay	SiO_2
	Muscovite mica	K_2O, SiO_2
SiO_2	Quartz, flint	-
	Feldspars	Na_2O, K_2O, SiO_2
	Wollastonite	CaO
	Kaolin clay	SiO_2
	Ball clay	Al_2O_3
	Talc	CaO, MgO
	Zircon	SiO_2
	Muscovite mica	Al_2O_3, K_2O
ZrO_2	Zircon (Zirconium silicate)	SiO_2

Frit may be used as a ground coat or cover coat showing difference between each other in terms of their chemical compositions of raw materials. Cover coats used as porcelain enamel include silica, fluorspar, soda ash, borax, feldspar, zinc oxide, zircon, aluminum oxide, lithium carbonate, magnesium carbonate, and titanium oxide. Cover coats are applied to provide specific colour, appearance and resistance to atmospheric and liquid corrosion, surface hardness, abrasion resistance and resistance to heat and thermal shock. Ground coats contain the same components plus smaller amounts of metal oxides such as cobalt oxide, nickel oxide, copper oxide, and manganese oxide. Ground coat is applied to directly to the metal substrate, often as an undercoat, over which other coatings are applied (U.S. Enviromental Protection Agency 2008). The glaze is made up large amounts of the various oxide molecules which are included in raw materials and supplying its properties. Firstly, these major oxides must be described in order to understand the nature of the glaze. In a given formulation for a frit composition, each oxide present has a contribution to make the glaze. The role of the common oxides is summarized as follows**:** SiO_2 is the most important oxide, by itself it will form glass if enough temperature is given. Most glaze formulations have more silica than all other constituents. It is added in many forms such as quartz, feldspar, clays or wollastonite into a glaze. It mostly acts as a glass former and controls thermal expansion. Na_2O is useful alkali flux over a wide temperature range. It functions in glaze coating as one of the potent fluxes. It is added as sodium carbonate and feldspars content into a glaze. The primary disadvantage of Na_2O is the very high coefficient of thermal expansion causing crazing defects in glazes with high soda content on many bodies. Hence, alkalis content such as Na_2O, K_2O must be controlled in glazes compositions and the glaze thermal expansion must be lower than the body expansion to avoid crazing defects. Also, glazes rich in soda content tend to be very soft and soluble in acids. LiO_2 is the most active of alkali fluxes. Due to its high cost, it is only used in glaze systems in which its fluxing power is truly needed. K_2O is very similar to Na_2O. There are a couple of minor differences. It improves the gloss of the glaze, relative to soda. Second, in many formulations, the high temperature viscosity of a potash system is higher than the equivalent soda system. Alkaline earth oxide materials such as CaO, SrO, and BaO as well as MgO are generally added as raw materials and more typically added in fritted form. They are active fluxes only at high temperatures. Below 1100 ^oC, they may even inhibit fusion rather than promote it. Their use is advantagenous as they act as powerful fluxes without having a major effect on the thermal expansion of the

glaze. CaO is avaliable and inexpensive and while it may be the principal flux in high-firing glazes, in lower-temperature glazes other fluxes, such as PbO, ZnO or Na_2O, must be used with CaO to produce the melting. Also, too much CaO content may lead to a matter surface due to crystallization in a glaze. It can be found as a content in raw materials such as dolomite, wollastonite and calcium carbonate. MgO is primarily used as a high temperature flux above 1100 ^oC and as an additive to reduce thermal expansion. ZnO is another useful flux above 1000^oC. Furthermore, it acts as a catalyst to promote the fusion of other oxides when used in small amounts. On the other hand, in large amounts, it may cause crystalline effects leading to a matte surface and surface defects such as pitting, crawling and pinholing**.** Also, the presence of ZnO has an extensive effect on the colouring of the glaze. PbO is another powerful flux up to 1150^oC. Above this temperature, volatilization becomes excessive. But besides its many advantages, its toxicity limits its use. Al_2O_3 contributes to the working properties of glaze. Alumina in a glaze increases the melt viscosity. Also in glazes containing B_2O_3 or alkaline earths, it retards phase separation or crystallization. It also increases hardness, durability and tensile strenght. ZrO_2 is primarily used as an opacifying agent. Less than 0.5 wt. % additions improve the alkali resistance. Finally, B_2O_3 is both a glass former and melting oxide. It also contributes to a lowering of the thermal expansion of the glaze (Eppler, et al. 2000).

2.3.2. Frit Manufacturing

The primary reason for the frit production is that the raw materials such as soda ash (Na_2CO_3), potash (K_2CO_3) and lithium carbonate (Li_2CO_3) required for glazes are all highly soluble in water. If such materials were used directly, the normal methods of preparation by wet grinding and application in aqueous suspension would not be possible. For this reason, these water-soluble ingredients must first be made insoluble. This is done by mixing them dry with all or some of the other glaze ingredients and premelting and then rapidly cooling them to a glasslike substance called a frit. A second important reason for using frits is melting rate. When raw glaze materials have been fritted, the reactions between them have been largely completed. Thus, there is less heat work required to fire the glaze coating. Alternatively, the firing time can be reduced for a fritted glaze. There are several other reasons for using a frit. One is the poisonous

nature of lead oxide. When lead oxide is fritted with other oxides, it becomes insoluble and less dangerous to handle. Second, some raw materials are substantially different in density from the others. Hence, these materials may settle out and layered sedimentation may occur in slip preparation. Frit produciton is a high temperature process developed for problems arising from water soluble, difference between densities of raw materials and toxic materials like lead oxide and others mentioned above (Eppler, et al. 2000)

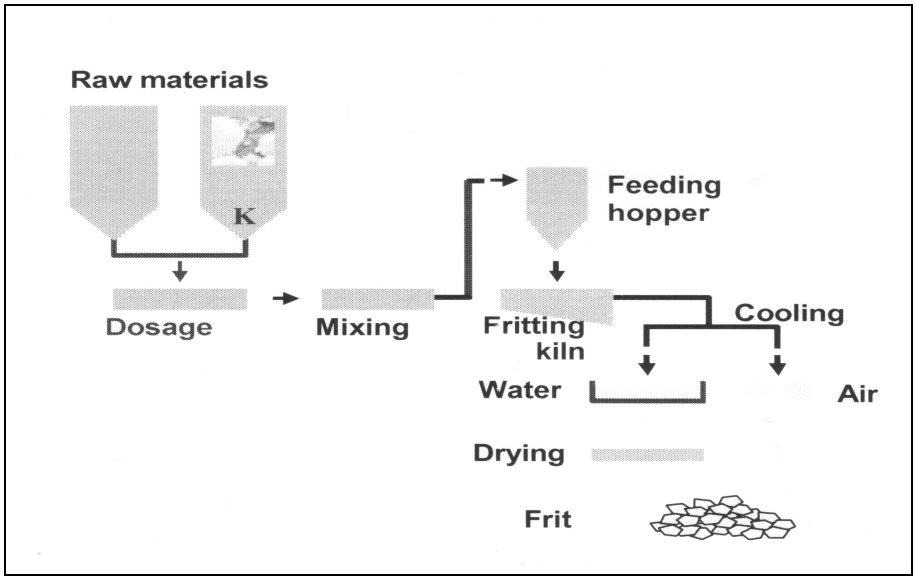

Figure 2.9. Frit Manufacturing Process
(Source: U.S. Environmental Protection Agency 2008)

The frit manufacturing consists of several stages following each other as shown in Figure 2.9. The frit production begins with weighing out the raw materials fed by from silos into a dosage or weighing hopper by a conveyor system. The next step is blending. The differrent raw materials are conveyed pneumatically to a mixer. The goal of mixing is for every grain to be adjacent to grains of other ingredients, but this random tumbling during mixing leads to random mixture. In most cases this is adequate. Raw materials differing widely in physical properties are not easy to mix homegenously. Differences in specific gravity, particle shape or grain size result in natural segregation during mixing. Heavier and smaller particles tend to sink through other lighter, larger grains. After blending, the raw materials mixture is conveyed to a hopper that feeds it into frit melting kiln by means of an screw, whose speed controls raw materials mass

flow into the kiln. The material's residence time inside the kiln is defined by the raw materials melting rate and melt flowability (Eppler, et al. 2000).

Commercial frits are melted in furnaces fired by gas, oil or electricity. They are either continous or rotary type furnace operating at temperatures of 930 ^{o}C to 1500 ^{o}C (1700^{o} to 2700^{o} F) depending on application. The frit smelting furnaces all have refractory linings exposed to high temperatures and harsh environments arising from corrosive frit melt contact with them (U.S. Environmental Protection Agency 2008). Two types of frit kilns are illustrated in Figure 2.10.

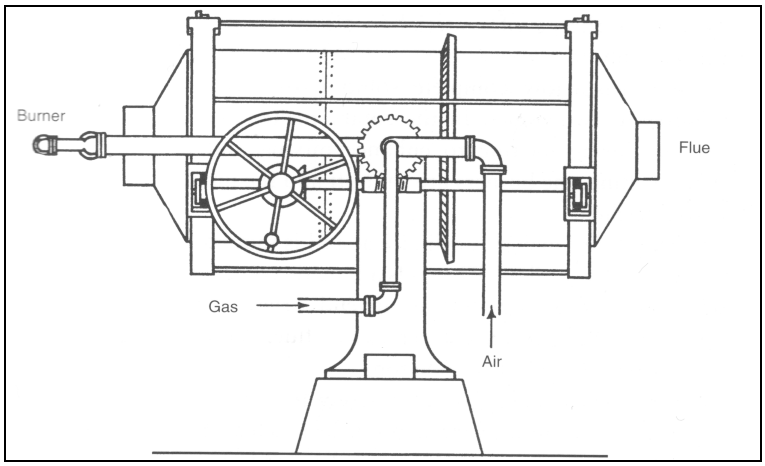

a) Rotary Frit Kiln

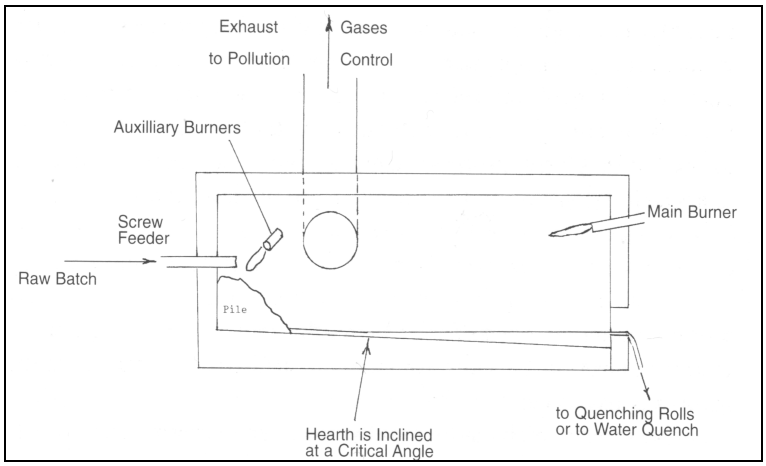

b) Continous Frit Kiln

Figure 2.10. Continous and Rotary Frit Kilns

(Source: Eppler, et al. 2000)

The rotary melter is shown in Figure 2.10.a. The rotary kiln is cylindirical and is mounted so that it can be rotated and tilted. The ends are made conical to retain the melt while rotating. An opening at one end serves for the burner, and opening in the opposite end serves as a flue. The rotary kiln is charged by a screw feeder that can reach to the back end of the furnace and deposit the raw materials mixture. The burner is then swung into the melter and lighter. During melting process, the rotary melter is slowly rotated to enhance mixing and heat distribution. After melting, the burners are shut off and molten frit discharged and quenched. However, most frit is now manufactured in continous kilns as can be seen from Figure 2.10.b. The continous kiln is of a simple incline design. Raw materials mixture is continuously added to a pile at one end of the continous kiln by a screw feeder. Burners are directed at the raw material pile, and molten material flows by gravity to the other end of the kiln and is continuously discharged and quenched (Eppler, et al. 2000). When melting process is completed, the molten frit is quenched on falling into the water as shown in Figure 2.11. Frits are removed from the water and subsequently conveyed to a dryer to eliminate any remaining moisture from quenching. After drying, the frit is finely ground in a ball mills as illustrated in Figure 2.12. Clays and other electrolytes may be added to be obtained the desired glaze formulation while grinding the frit. The latter is the preparation of aqueous suspension for glazing process. The suspension characteristics for the glazing is then adjusted with respect to the application method to be used. For instance, ceramic tile glazing is done continuously. The most common glazing methods used in the tile manufacturing are waterfall glazing and spraying as shown in Figure 2.13 (U.S. Environmental Protection Agency 2008).

Figure 2.11. The quenching process (Discharging the frit into water, EgeSeramik A.Ş.)

Figure 2.12. The grinding process (Grinding the frit in ball mill, Graniser A.Ş.)

a) Spray Glazing (Graniser A.Ş.)

b) Waterfall Glazing (Graniser A.Ş.)

Figure 2.13. Spray and Waterfall Glazing Processes

CHAPTER 3

CORROSION

In this chapter, corrosion process in ceramic materials is discussed carefully with regard to its mechanism and progress and then the previous corrosion testing methods are reviewed and classified. Finally, the corrosion test method (dip/dip or rotation test) to be employed in this study is introduced.

3.1. Corrosion in Ceramic Materials

The term of corrosion comes from the Latin word ‘corrodere’, meaning ‘gnaw away’. Corrosion is simply defined as deterioration or destruction of essential properties in a material owing to physicochemical reaction with its environments. Weakening of iron due to oxidation of the iron atoms is a well-known example of corrosion known as rust. This type of damage usually affects metalic materials. But, corrosion process may also be observed in other metals as well as in non-metallic materials, such as plastic, concrete and ceramics (Mattson 1989). Several types of corrosion can be classified in many different ways since different environment conditions can be thought as causes for the corrosion processes. One method divides corrosion into low-temperature and high temperature corrosion. Another classification is wet and dry corrosion. For instance a common example of wet corrosion is the corrosion of steel by water. On the other hand dry corrosion occurs in the absence of a liquid phase. An example for dry corrosion is attack on steel by furnace gases (Fontana 1986). Refractories used in linings of furnaces at high temperatures where they are exposed to hot air and abrasive particles, and are in contact with molten metals, slags and glasses. Attack of refractories is a complex phenomenon involving chemical wear (corrosion) and physical/mechanical wear such as abrasion and erosion processes as well as thermal shock and spalling. The mode of wear of refractories depends on the specific industrial use because of different environmental conditions (Lee and Moore 1998).

Corrosion is complicated problem among the wear mechanisms to be solved because of being effective on the refractory lifetime. It depends on a long list of factor including chemical compositions of the refractory and the melt, duration, temperatures and design parameters of furnaces (Krasnyi 2005). Corrosion of refractories happens when these materials are subjected to high temperatures in contact with corrosive substances. Corrosion may be caused by mechanisms like dissolution of the refractory in contact with a liquid , reactions in the vapor, liquid and solid phases. It may also occur due to penetration of the vapor or liquid phase in the pores, forming an altered zone. But, usually corrosion occurs due to some combination of these factors mentioned below as follows: dissolution, penetration and reaction (Nishikawa 1984).

3.1.1. Corrosion due to Dissolution

Dissolution of refractory in liquid can be estimated from the equilibrium phase diagram of the compositions of the refractory and the liquid. The rate of dissolution is critical in the actual service (Nishikawa 1984). Dissolution process can be classified into two, first known as the direct dissolution (congruent or homogeneous) involves the direct solution of the refractory species into the glass phase and leads to active corrosion. However, the refractory components may not be completely soluble in the glass melt, it may form an impenetrable barrier so that its formation may slow down further attack by the glass melt and it is called indirect dissolution (incongruent or heterogeneous) leading to passive corrosion (Zhang, et al. 2004).

Akira Nishikawa summarizes the dissolution process as follows: “When the refractory comes in contact with the melt and dissolves, a concentration gradient in the refractory composition at the boundary region is formed” as shown in Figure 3.1.

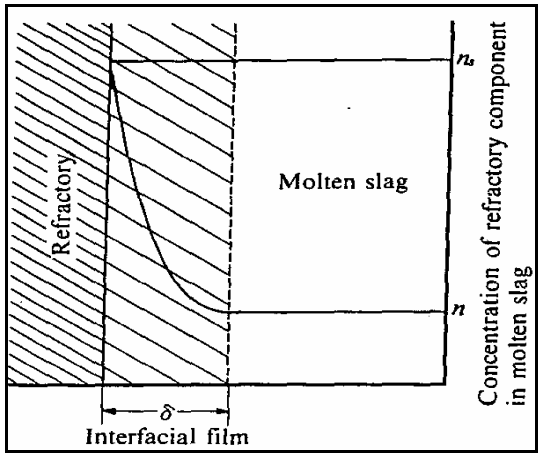

Figure 3.1. The role of the interfacial film in the dissolution of refractory components into liquid (Source: Nishikawa 1984)

The boundary layer, known as the diffusion layer or interfacial layer forms along the refractory wall. Components from the refractory diffuse through the interfacial film and dissolve in the liquid followed by the resistance of the interfacial film to diffusion. The rate of dissolution influenced by the interfacial film thickness (δ) is known as the solution rate controlled by diffusion and can be generally expressed by the following equation (3.1):

$$dn / dt = DA(n_s-n) / \delta \qquad (3.1)$$

n: concentration of the solute in liquid (g/l)
n_s: saturation concentration of the solid (g/l)
D: diffusion coefficient of liquid (cm^2/sec)
A: contact surface area (cm)
δ: thickness of the interfacial film (cm)
t: time (sec)

The above formulation summarizes that the larger the concentration gradient, the faster the rate of dissolution, while the thinner interfacial layer and/or diffusion film, refractory dissolves more readily. The thickness of interfacial film δ has an important effect on the rate of dissolution and it becomes thinner when exposed to flow of a liquid

like frit. For this reason, if the refractory is rotated into molten frit, then the relation between the speed of rotation and δ is expressed as follows:

$$\delta = 1.61 D^{1/3} . \nu^{1/6} . \omega^{-1/2} \qquad (3.2)$$

ν= coefficient of kinematic viscosity
ω=rotating speed
D=Diffusion coefficient

As can be seen from equation (3.2), the thickness of the interfacial film is reduced if the molten frit is agitated violently. Viscosity of the frit also has an effect on the thickness of the interfacial film. Presence of different oxide components leads to a change in the viscosity of the frit. Generally, zircon-rich frit have higher viscosity, whereas transparent frits without the suspended zircon particles have lower viscosity (Nishikawa 1984).

Apart from the composition of the frit, temperature of a liquid is another effect on the viscosity of the frit and the relation between viscosity and temperature is reported as follows:

$$\eta = A \exp (E/ RT) \quad \text{(Arrhenius' equation)} \qquad (3.3)$$

η : viscosity coefficient (Poise)
A: constant
E: activation energy for a viscous flow (J)
R: gas constant (g-mole/K)
T: absolute temperature (K)

According to the equations 3.3 and 3.2, higher temperatures lead to a drop in viscosity which decreases the boundary layer thickness consequently resulting in an increase in dissolution rate as given in equation (3.1). Corrosion due to dissolution was explained above in terms of the concentration gradient and interfacial film. The effect of viscosity of a frit on the interfacial film and the factors such as temperature, degree of agitation

and the chemistry of a liquid affecting the viscosity of a frit were explained to find out the dissolution process.

3.1.2 Corrosion due to Reaction

Reaction corrosion of refractories occurs between solid-solid, solid-liquid or solid-vapor phases. The rate of reaction in the solid phase is controlled by the chemical reaction at the boundary between the different phases and by the diffusion of components through the layer of reaction products. However, corrosion in refractories rarely occurs due to solid phase reaction. Mostly, refractories are corroded by a liquid phase or a reaction forming a liquid phase (Nishikawa 1984). The rate of reaction is controlled by the rate of difussion with respect to Fick's law or Jander's equation for reaction rate. Solid-liquid and solid-vapor phase reactions are believed to follow the same mechanism as the solid phase reaction. These reactions are shown in Figure 3.2.

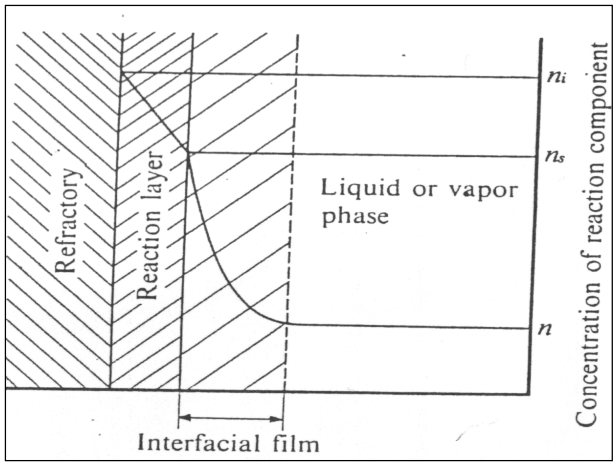

Figure 3.2. Solid-liquid or solid-vapor phase reaction
(Source: Nishikawa 1984)

Rate of reactions is controlled by the diffusion in the reaction layer, chemical reaction between refractory and reaction layer, and diffusion in the interfacial layer in solid-liquid and solid-vapor reactions (Nishikawa 1984)

Rate of the solid-vapor or liquid phase reaction is given by the folllowing equations,

- Rate of reaction is controlled by diffusion in the interfacial layer is given as follows (3.4) equation:

$$\alpha = kt \tag{3.4}$$

α : rate of reaction

t: time

k: rate constant

- Rate of reaction controlled by diffusion in the reaction layer is given as follows (3.5) equation:

$$1\text{-}3\,(1-\alpha)^{2/3} + 2\,\alpha = kt \tag{3.5}$$

- Rate of reaction controlled by chemical reaction on the surface of unreacted solid is given in equation (3.6):

$$1\text{-}\,(1-\alpha)^{1/3} = kt \tag{3.6}$$

3.1.3 Corrosion due to Penetration

Corrosion due to penetration occurs when liquids penetrate into refractory through the open pores in contact with liquid. Refractory loss due to penetration may result from two mechanisms. First, the penetrating medium may react with the matrix and form new phases with different density and expansion characteristics affecting the refractory. Such phase changes often result in a spalling loss. Secondly, if the penetrating material does not react with the matrix or the aggregate, it may lead to a

pressure differential on the matrix and eventually the refractory may be lost because of spalling. The main driving force of penetration is the suction of liquids like molten slag due to capillarity. Corrosion due to penetration proceeds at much faster rate when compared with the rate of reaction and dissolution corrosion. Since, molten frit penetrates into relatively greater depth within the refractory resulting in a thick penetrated zone. This mode of corrosion is frequently encountered in steelmaking in basic refractories in which molten slag can penetrate easily. This resulting causes layer alteration of the texture and structural spalling (Eppler, et al. 2000).

Akira Nishikawa summarizes the penetration process as follows: “Surface tension (surface energy), contact angle of liquid, and refractories are related to the suction force in capillarity occuring in corrosion due to peneration and in general, may be expressed as follows:

$$\Delta P = 2\,\gamma_L \mathrm{Cos}\,\theta / r \qquad (3.7)$$

ΔP : suction force
γ_L : surface tension of liquid
θ : contact angle
r : capillarity radius

According to Jurin’s theorem, the penetration depth is given as follows:

$$l = 2\,\gamma_L \mathrm{Cos}\,\theta / r\rho g \qquad (3.8)$$

l : depth of penetration
ρ : density of liquid
g : accelaration due to gravity

According to the above equations: The smaller diameter pores, the larger surface tension of liquid and the smaller density of liquid result in deeper penetration of liquid and speed up corrosion due to penetration in refractory.

The rate of penetration is obtained from Hagen-Poiesuille's theorem given by the following equation:

$$l^2 = (\gamma_L \, r \, \text{Cos} \, \theta / 2 \, \eta \,) \, t \qquad (3.9)$$

η : viscosity of liquid

t : time

If, $k = \gamma_L \, r \, \text{Cos} \, \theta / 2 \, \eta$ (3.10)

The above equation is simplified as follows:

$$l^2 = kt \qquad (3.11)$$

k:coefficient of penetration.

This coefficient of penetration applies to the case of cylindrical capillary tubes. For the coefficient of penetration of spherical pores, the following equation is suggested (3.12). Therefore, the shape of pore is also related to this coefficient (Nishikawa 1984).

$$k = \gamma_L \, r \, \text{Cos}\theta / 2.8 \, b^2 \eta \qquad (3.12)$$

b: loop coefficient of pore

Then, Zagar suggested the following equation including the relation between porosity and penetration (equation 3.13):

$$\frac{V}{\eta} = A\,(1/2\ P^2\ r\ \gamma_L\ t)^{1/2} \qquad (3.13)$$

V : volume of penetrated liquid

A : area of the penetrated surface

P : apparent porosity

r : average radius of pores

There must be physical contact between the refractory and the corrosive medium in order for chemical degradation to be observed. For this reason, the relation between phases with regard to contact angle must be clarified to understand at which conditions physical contact will be observed for corrosion process. The contact angle is the angle between the solid surface and the tangent to the liquid surface at the point of contact. It is related to the specific energies of the solid/vapor (γ_{SV}), solid/ liquid (γ_{SL}), and liquid/vapor (γ_{LV}) interface specific energies (Nishikawa 1984). The condition for the equilibrium of them is given in equation (3.14).

$$\gamma_{SL} + \gamma_{LV}\ \mathrm{Cos}\ \theta = \gamma_{SV} \qquad (3.14)$$

$$\mathrm{Cos}\theta = \gamma_{SV}\text{-}\gamma_{SL}/\gamma_{LV} \qquad (3.15)$$

Figure 3.3. summarizes the relation between the contact angle and penetration in solid-liquid-vapor phases. If $\gamma_{SV} > \gamma_{SL,}$ $\theta < 90\ ^{o}$, the liquid phase wets the solid phase, and if $\gamma_{SV} < \gamma_{SL}$, then $\theta > 90$, it does not. In other words, if the solid-liquid energy (γ_{SL}) is high, the liquids tend to form a ball having a small interfacial area. This condition is defined by a high contact angle ($\theta>90$) and a small solid-liquid contact area. In contrast, if the solid-vapor interfacial energy (γ_{SV}) is high, the liquid will try to cover all solid surface to eliminate solid-vapor interface. In this case, contact angle is very low ($\theta<90$) (Nishikawa 1984).

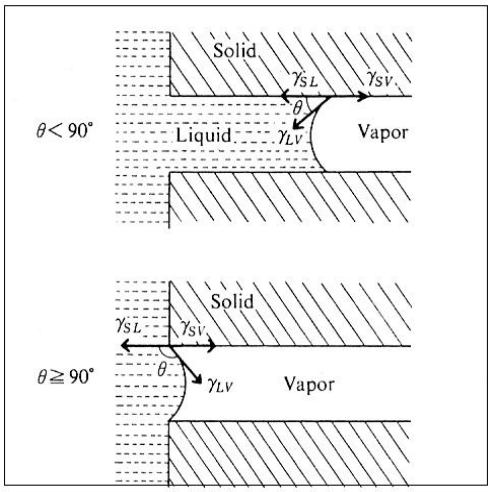

Figure 3.3. Relation between contact angle and penetration in solid-vapor-liquid phases (Source: Nishikawa 1984)

Wettability conditions in terms of angle value for corrosion process may be summarized below.

When $\theta > 90^o$ Non-wetting
When $\theta < 90^o$ Wetting
When $\theta = 0$ Spreading

For spreading to occur, the following condition must exist:

$$\gamma_{SV} > \gamma_{LV} + \gamma_{SL} \quad (3.16)$$

If the above relation is applied to penetration of liquid phase between neighbouring refractory grains as in Figure 3.4., the equilibrium is given in equation (3.17) as follows:

$$\gamma_{SS} = 2\,\gamma_{SL}\,\mathrm{Cos}\,\theta / 2 \quad (3.17)$$

If $\gamma_{SS} < 2\gamma_{SL}$, $\theta > 0$, (Figure 3.4.), the liquid phase can not penetrate. However, $\gamma_{SS} > 2\gamma_{SL}$, the liquid penetrates between the grains.

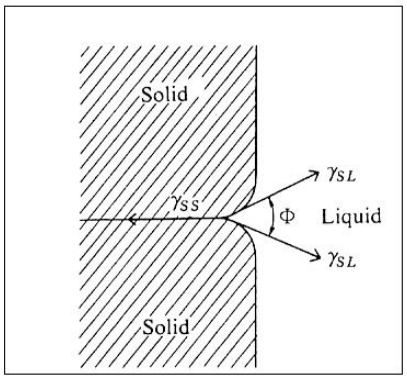

Figure 3.4. Relation between solid grains and penetration
(Source: Nishikawa 1984)

All things considered, wettability between a refractory and a liquid like molten frit is an important factor influencing penetration. In addition, surface tension (energy) of the refractory material and the molten frit and the interfacial energy between the solid and the liquid are factors related to penetration. Furthermore the surface tension of frit may change depending on its composition. In other words, the variation of surface tension due to the composition of frit may affect the degree of penetration of frit (Nishikawa 1984).

3.2. Corrosion Models

Corrosion of refractories via dissolution, penetration and reaction was explained below to understand its mechanism. Now, corrosion progress will be studied with some approaches to find out corrosion phenomenon. These approaches will be discussed in this section. Up to now, three models to explain corrosion progress have been developed as follows:

1. The General Model
2. Konig's Model
3. Endel, Fehling and Kley's Model

3.2.1. The General Model

According to the general model, corrosion of refractories is initially observed at the grain faces (phase boundraies) by frit attack penetrating into it through voids, pores and cracks as shown in Figure 3.5. Then, dissolution reactions start at the low melting bond phase between the refractory crystallites which is susceptible to attack by frit. After the bond phase dissolves in frit, the higher melting refractory crystals will be loosened from the structure. This selective corrosion of bond phase results in finger-like protrusions into the refractory. When the molten glass or frit penetrates deep into the refractory, this results in the complete disapperance of the bonding matrix of the hot face. In this way, the crystalline grains free themselves from the structure and they are transferred to the frit, where they are suspended. Then these suspended particles lead to increase in viscosity of frit penetrating intergranular area of the refractory. All things considered, corrosion phenomenon of refractory takes place in three stages in accordance with the general model: Initial stage, Intermediate stage and Final stage (Akkurt 1997).

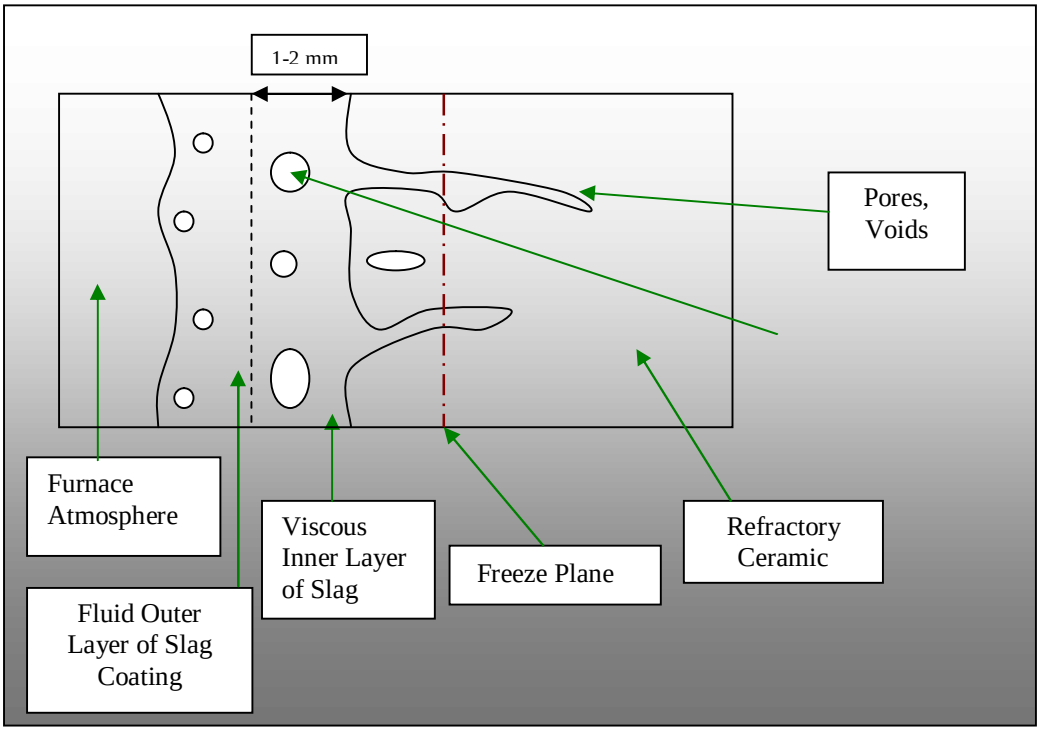

Figure 3.5. Schematic of Liquid Phase Corrosion Process

(Source: Akkurt 1997)

1) Initial stage of corrosion:

In this stage the slag wets the refractory hot face and dissolution reactions start to occur at the grain faces during which the system tries to reach the equilibrium. Initial stage of corrosion process is illustrated in Figure 3.6 (Akkurt 1997).

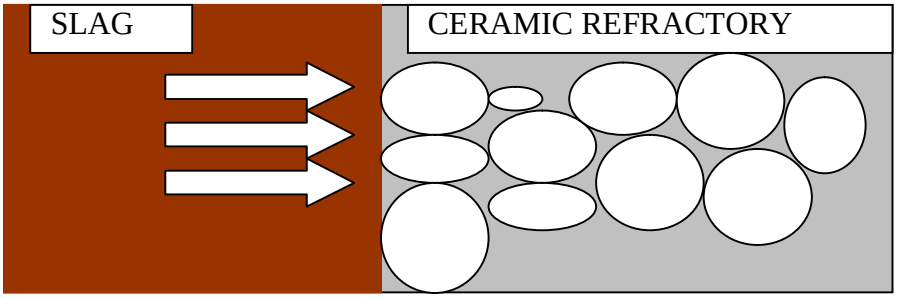

Figure 3.6. Schematic of Initial Corrosion Stage

(Source: Akkurt 1997)

2) Intermediate stage of corrosion:

In this stage two cases know as penetration and no penetration may be observed during the corrosion process. First, corrosion due to penetration may not be observed when temperature gradient is very steep and when freeze plane is closer to the face. Secondly, slag penetrates a few milimeters into the refractory by distrupting bond phase. This occurs via selective corrosion of bond phase and results in finger-like protrusions into the refractory (Akkurt 1997).

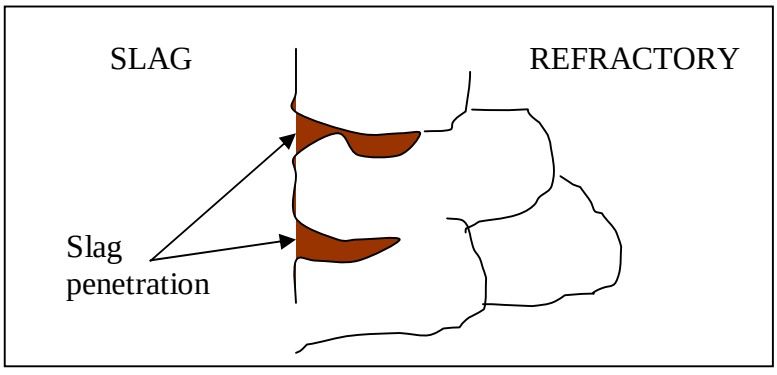

Figure 3.7. Schematic of Intermediate Corrosion Stage

(Source: Akkurt 1997)

3) Final stage:

In this stage system gets closer to the equilibrium and there is a broad temperature gradient across the brick. Slag penetrates very deep inside the refractory resulting in complete distruption of the hot face. Bond phase held the brick together disappeared except the viscosity of the slag that penetrates through and invades the intergranular area (Akkurt 1997).

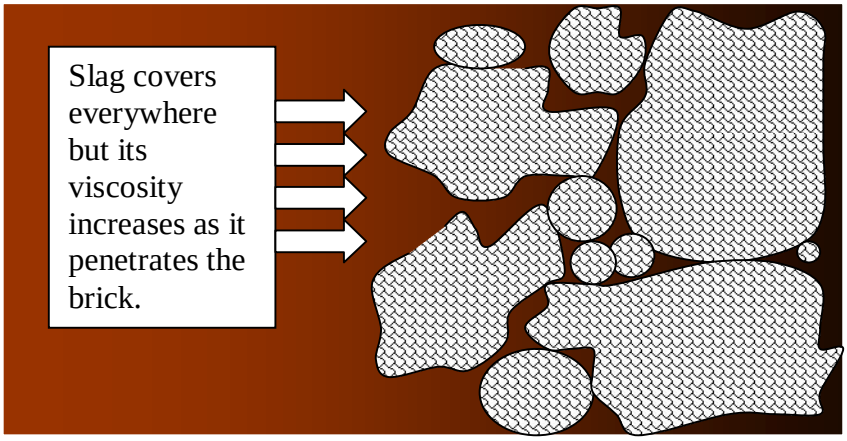

Figure 3.8. Schematic of Final Corrosion Stage

(Source: Akkurt 1997)

3.2.2. Konig's Model

Another important analysis for the refractory corrosion is the König's model for molten slag attack. König and his co workers were able to theoretically calculate the recess or critical thickness reached inside the refractory at ($T_{critical}$) critical temperature. The recess or critical thickness is somewhere between the hot and cold face of the brick. If it is closer to the hot face, the less refractory thickness is lost by corrosion. The critical temperature is actually the lowest temperature of destructive chemical reaction between the brick and slag. It is the solidus temperature of the equilibrium composition. König suggested that he could derive an equation relating the amount of corrosion to processing varibles under the conditions of constant stable furnace, constant thermal gradient across the refractory brick and solidified slag layer at the hot face. This result was achieved by equating the heat transfer rates between the furnace and the refractory brick. König assumed a stagnant slag

layer deposited on the refractory brick (König 1977). The analysis was proposed by König as follows:

$$Q_1=f_F\, A\, t\, (T_F-T_S) \tag{3.18}$$

$$Q_2=f_{eff}\, A\, t\, (T_R-T_E) \tag{3.19}$$

$$k_{eff}= 1/ (1 / f_e)+(x_R / k_R)+(x_I / k_I)+(x_{SH} / k_{SH}) \tag{3.20}$$

Equating (3.18) and (3.19) and inserting (3.20), we obtain equation (3.21) which can be applied to calculate the recess thickness of the refractor brick when the hot face reaches $T_{critical}$.

$$x_R=k_R\, \{[\, (T_R-T_E) / f_F(T_F-T_S)\,] - [1 / f_E + x_{SH} / k_{SH} + x_I / k_I]\} \tag{3.21}$$

where

T_F: Temperature inside the furnace
T_S: Temperature at the surface of the slag
T_R: Temperature at the refractory hot face
T_{SH}: Temperature at the surface of the steel shell
T_E: Temperature of the environment
f_E: Film coefficient of the environment
f_F: Film coefficient of the furnace
k_R: Thermal conductivity of the refractory
k_I: Thermal conductivity of the insulation
k_{SH}: Thermal conductivity of the steel shell
x_R: Thickness of refractory
x_I: Thickness of insulation
x_{SH}: Thickness of steel shell

König's model is very useful model because it provides us with an equation to predict the lining thickness that will remain depending on the temperature gradient and other factors. From equation (3.21) we can see that the higher thermal

conductivity, the closer the freeze plane will be to the hot face and the larger a value of x_R will result. The freeze plane is measured from the hot face of the lining and since no liquid exists beyond this plane, no material can be transferred. Corrosion process halts totally in this plane. The nearer the freeze plane to the hot face the less volume of refractory affected by dissolution (corrosion) reactions, and a thinner section wears out. In this way, the closer freeze plane to the hot face results in increasing refractory service life. A steeper temperature gradient at the refractory thickness provides this effect. However, a steeper temperature gradient means a higher rate of heat transfer through the lining resulting in large amount of loss energy. In other words refractory bricks having a high thermal conducvitiy lead to a steeper temperature gradient, the closer freeze plane to the hot face, increase in service life and also increase in gas consumption during frit production (Akkurt 1997). And finally König's model suggested that the penetration of slag never goes beyond the first stage if an effective water cooling is applied to a brick having a high thermal conductivity.

3.2.3. Endel, Fehling and Kley's Model

Endel, Fehling and Kley's model revealed a relation between corrosion rate of the aluminosilicate refractories and the slag viscosity. They used different types of slags and glasses and related the viscosity to the amount of corrosion in a dip and rotate test which did not have atmosphere control capability (Akkurt 1997). They derived an equation below:

$$a= CL_o\{T^{2/3}/\eta^{8/9}\}(\theta BA)^{1/9} \qquad (3.22)$$

a: slag attack perpendicular to the surface (cm/sec)

C: constant depending on the test furnace

L_o:solubility (kg refractory per kg slag)

η: slag viscosity (Poises)

θ: Fraction of total ash which flies to the wall

B: heat liberated in firing chamber

A: ash content of coal

As can be seen from (3.22) equation, corrosion rate decreases by increasing slag viscosity.

3.3. A Review of Laboratory Corrosion Tests

Laboratory corrosion tests of refractory bricks are used mainly for two reasons: (1) comparing and evaluating different bricks for a particular application so using suitable refractories in the furnaces, (2) understanding the corrosion mechanisms via changing the factors in controlled corrosion tests with the aim of predicting the actual service behaviour of bricks. The advantages of laboratory corrosion tests are as follows: they are faster, simpler to run, the results are not catastrophic if the brick fails when compared to the furnace conditions, different brick types can be tested and compared with each other, processing variables are controlled and changed during tests and factors affecting corrosion process can be observed to understand their potential effects. Laboratory corrosion tests have also some disadvantages like poor reproducability and difficulty to mimmick actual process conditions. The literature on laboratory corrosion tests of refractory samples was compiled by Crescent and Rigaud in 1987 and which proposed that there are three major approaches to laboratory testing of refractory corrosion: (1) thermodynamic approach which is the oldest one and is still widely used by researchers. The pill test (McGee 1981, Schurecht 1939), the crucible test (Goto 1997), Cone Test (Cramer 1901), Immersion tests are examples of the thermodynamic approach. (2) kinetic approach is the most frequently used one for studying the basic wear mechanisms. In this case the determination of the amount of wear is the major aim. This is achieved in a experimental environment within a closely controlled set of conditions. Examples of tests in this category are drip test , crucible test, finger test (dip or dip and rotation test as referred by Kobayashi), immersion test. (3) pragmatic approach was developed and used more in the industry and consequently does not target the determination of corrosion mechanisms but rather aims at evaluating service performance. It is important in such tests to closely simulate real metallurgical furnaces. For instance the thermal gradient and freeze plane within the brick are important factors to consider and

they affect the corrosion process so significantly. Therefore the reproducibility of the location of the freeze plane and temperature gradient within the brick during the experiments has considerable effect to get meaningful results from such tests (Crescent 1987). Each of the approaches improved for laboratory corrosion test methods are given Table 3.1.

Table 3.1. Laboratory Corrosion Test Methods for Refractories
(Source: Akkurt 1997)

Approaches	Reference	ASTM Code
Thermodynamic Approach		
1) Pill test	Schurecht 1939	
2) Mixing test	Kobayashi 1982	
3) Crucible test	Goto 1997	
4) Cone test	Cramer 1901	
5) Immersion test	Crescent 1987	
Kinetic Approach		
1) Dip test	Furumi 1975	C-768
2) Crucible test		
3)Dip/dip and rotation test(finger,pencil test)	Rose 1923	C-621
4) Immersion test		
5) Induction furnace test	Kobayashi 1982	
P**ragmatic Approach**		
1) Basin test		C-622
2) Rotary test	Cash 1966	C-874
3) Spray test		

3.4. Dip/Dip or Rotation Test (Our Laboratory Corrosion Test)

In case of basic research the dip/dip or rotation test is the most widely used method to investigate corrosion behaviour of refractory bricks in either static or dynamic test conditions. In our work we used it to determine the corrosion behaviour of aluminosilicate refractories used in frit melters. Dip test, either static or dynamic, is generally known with many different names. For instance, finger test, rotating finger test, static pencil test, rotating pencil test, rotating dip test. Historically, Coad-Pryor was the first to publish a corrosion test using a static dip test. Rose later proposed a rotating dip test to achieve dynamic testing conditions. The static dip test was later standardized (ASTM C-621) for glass tank refractories. In static or rotating dip tests a long narrow specimen of refractory brick is immersed into the melt (frit, glass or steel) to a known depth for a desired time. The refractory piece can be rotated in the melt if a dynamic test is desired. After completion of the corrosion test the refractory specimen is removed from the melt and raised up to allow the slag to drain. When the furnace cools the refractory brick specimen is sliced either parallel or perpendicular to its axis of longest dimension. Consequently, the amount of corrosion can be quantified via measuring the percent area loss of polished section or depth of the slag-line cut on the corroded refractory specimen. Factors affecting test conditions such as temperature, atmosphere, melt chemistry (frit, glass or steel) can all be varied to observe their potential effects on the corrosion process. Dip/dip or rotation test has some advantages as follows: this type of test enables uniform temperature throughout the brick sample and provides much better temperature control during the test. Corrosion process is accelareted in this type test because of absence of freeze plane and temperature gradient within the refractory brick. But this helps obtain reproducible results because there is no unknown thermal gradient factor associated with the test. Furhermore different types of refractory brick samples can be compared reliably with regard to the amount of erosion after testings. Moreover the corrosion tests may be carried out in controlled atmosphere or open in air. In addition to advantages mentioned above quantitative information can be obtained from this type test guite reliably and reproducably. But it has also some disadvantages as follows: The results obtained from this type test do not have a direct representation of the actual corrosion

process because of the absence of freeze plane and temperature gradient within the brick. However, these results may be used as prediction to relate those and actual process. Another disadvantage is that the melt composition is changing as the brick corrodes. Furhermore the molten slag is not totally stagnant even in the static test and free and natural convection currents are possible but can be ignored for this type test. Moreover the melt rotation can accelerate corrosion by providing fresh slag to reaction surface in this type test. Eventually the increasing test temperatures may provide more corrosion in a shorter time. This may give totally erroneous results since the test temperature may be well above the liquids temperature of the actual process and entirely different corrosion mechanism may be observed during the test. To sum up dip/dip or rotation test provides us information about corrosion behaviour of refractory brick but results obtained from this type test can be only used to predict how refractory brick reacts when exposed to actual service conditions. Furthermore it may enable different refractory brick samples to compare with each other with regard to the corrosion resistance to aggressive melts (Akkurt 1997).

CHAPTER 4

EXPERIMENTAL

In this chapter, the materials used in the thesis, the experimental setup and the procedure are explained.

4.1. Materials

Corrosion testing that was employed in this thesis required refractories to be tested and a frit melt to serve as the corrosive medium. Some frit manufacturers were contacted and industrially used specimens of two different refractories and frit were obtained. First refractory brick was a mullitic brick (coded as E) from Egeferro A.Ş. and the second brick was an andalusite brick (coded as T) from Tamsa A.Ş. This latter company also provided as with the frit samples. Further details of refractories and the frit are given in section 5.1.

4.2. Experimental Method

In this study, corrosion resistances of bricks in contact with frit melt were investigated in both static and dynamic corrosion test conditions in stagnant and turbulent molten frit, respectively. Corrosion resistances of refractories in contact with frit melt under isothermal conditions were measured in a vertical tube furnace using a bath of frit melt as the corroding medium contained in a high alumina crucible. 15x15x115mm sized refractory brick sample that was half-immersed from the top was kept as such for prescribed amounts of time and temperatures. Temperature, time and type of refractory were varied in all experiments to observe their effects on corrosion behaviour of refractory. A laboratory corrosion test protocol was constructed at our İYTE laboratory for the static and dynamic corrosion testing of refractory samples in order to mimic conditions in the frit furnaces. Our corrosion test geometry was similar to the ASTM C621 static corrosion test and can be found as “Dip/dip and rotation test ” in the literature on corrosion testing of refractory bricks (Akkurt 1997 and Velez 1997). Dip test, either

static or dynamic, has been known with many different names. For instances, finger test, rotating finger test, static pencil test, rotating pencil test, rotating dip test, etc (Akkurt 1997 and Velez 1997).

.

4.2.1. Experimental Setup

Several previous experimental setups used in dynamic and static corrosion tests were investigated to guide this study. Some apparatus of experimental setups for corrosion testing are shown in Figure 4.1.

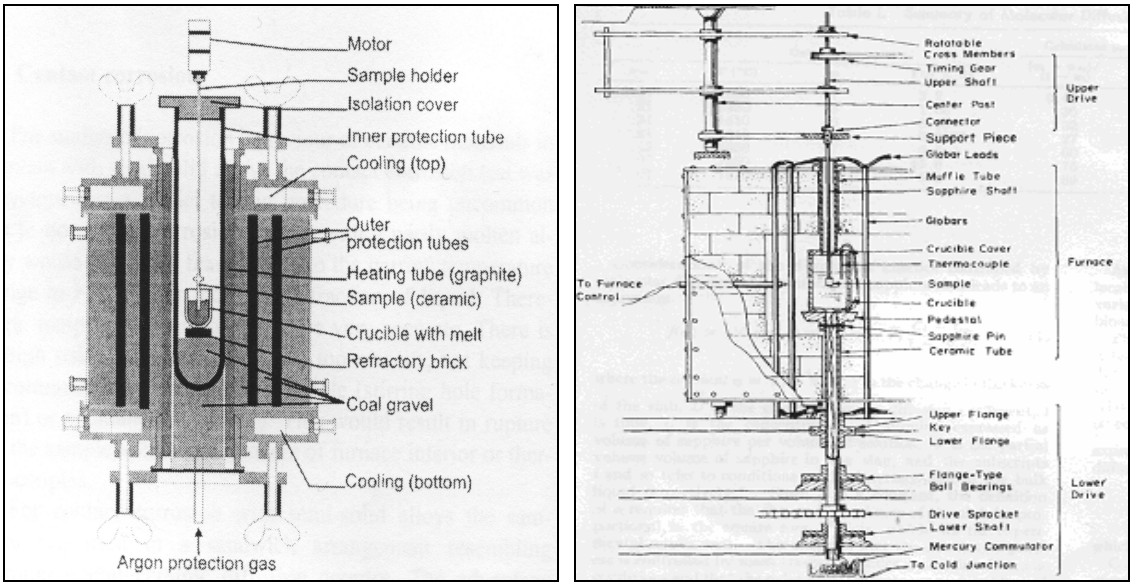

a) b)

Figure 4.1. Schematics of the previous experimental setups used for corrosion testing
a) Source:Meyer-Rau, et al. 2004 b) Source:Cooper and Kingery, et al. 1964

Corrosion test setup (Figures 4.2 and 4.3) consisted of:

1. A Nabertherm HTRV100-250/17/C42 vertical tube furnace (maximum temperature rating 1750 °C) that was heated by $MoSi_2$ heating elements (Figure 4.12.).
2. A motor assembly that allowed the refractory specimen to be rotated at 50rpm (Figure 4.3.)

The high temperature furnace was able to accommodate continuous test operation at test temperatures of 1400-1500^{o}C. Impervious high alumina crucibles were produced in-house to contain the molten frit at high temperatures in the furnace (Figure 4.4). More details about the manufacture of the crucibles can be obtained from Şenöz 2007 (Şenöz 2007). An upper end-cap on the top of the 100mm diameter alumina protection tube was also produced in-house from a castable mixture (Figure 4.5). A cylindrical block (80mm diameter and 500mm long) was made from the same castable mixture as that used for making the upper end cap. This was used as kiln furniture to support the crucible in the hot region of the furnace during the corrosion test.

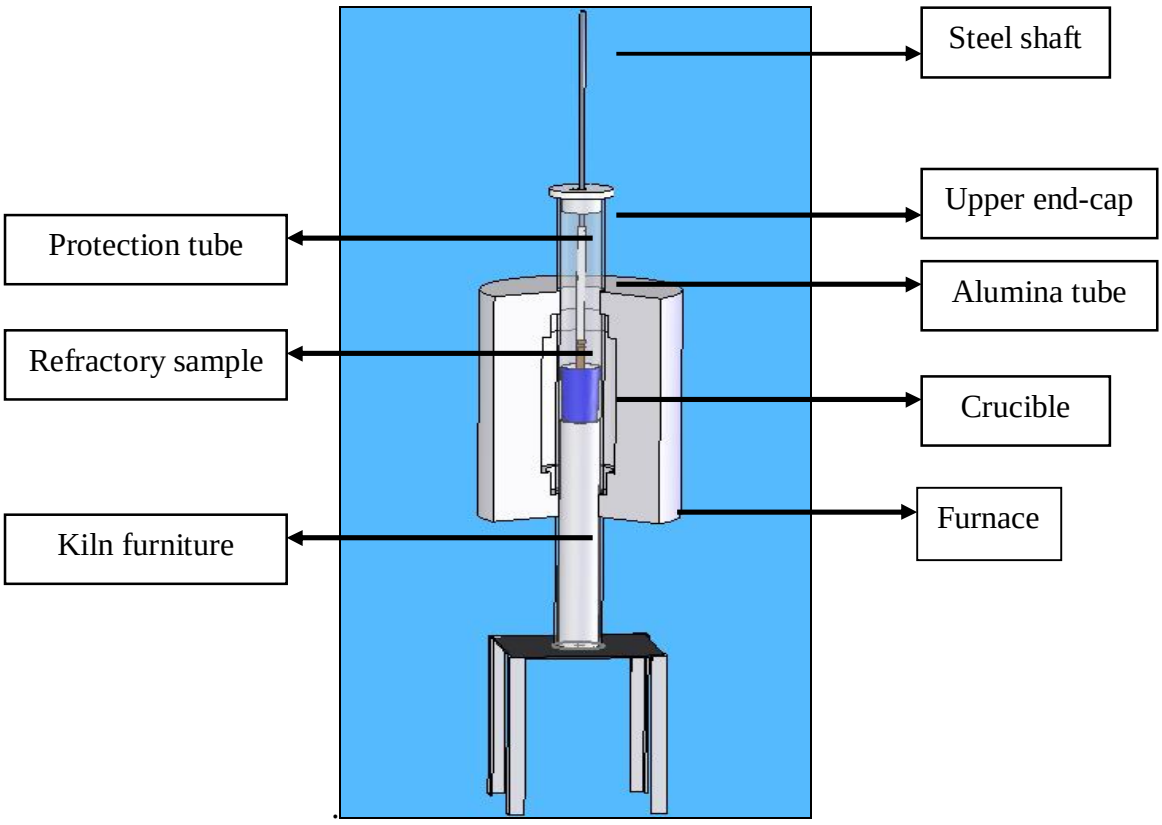

Figure 4.2. Schematic of experimental setup for corrosion testing

Figure 4.3. Photograph of experimental setup

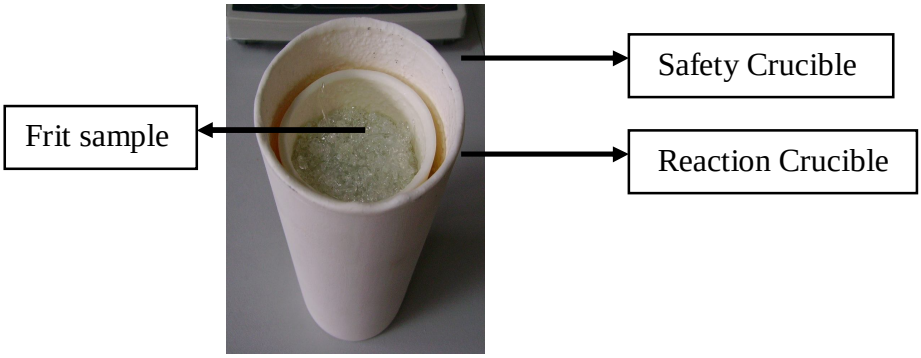

Figure 4.4. Photograph of reaction and safety crucibles

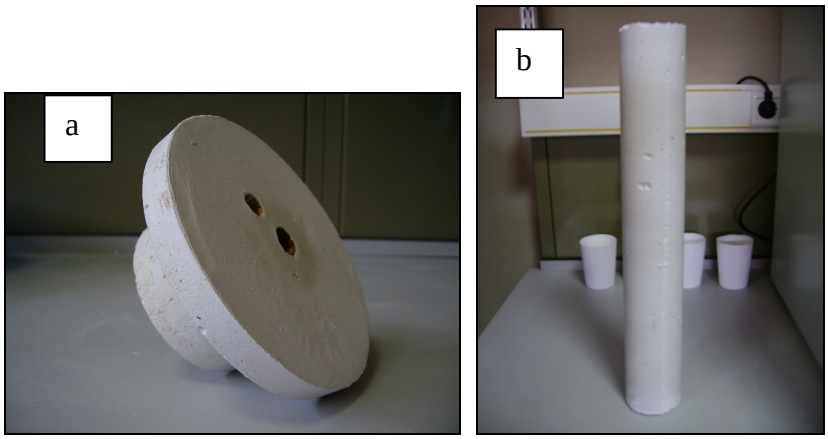

a) b)

Figure 4.5. The upper end-cap (a) and kiln furniture (b) made of an alumina castable mixture

The corrosion tests were carried out in open-air without atmosphere control which was possible using this apparatus. An alumina protection tube (1m long and 100mm diameter) was mounted vertically in the test furnace (Figure 4.3). Square refractory specimens (15x15x115mm) that were cut from larger brick, were attached to an alumina tubing (θ=20mm and l=250mm) with a platinium wire (0.5mm) and connected by a steel shaft to a motor for rotation of sample at 50 rpm (Figures 4.3, 4.6 and 4.7).

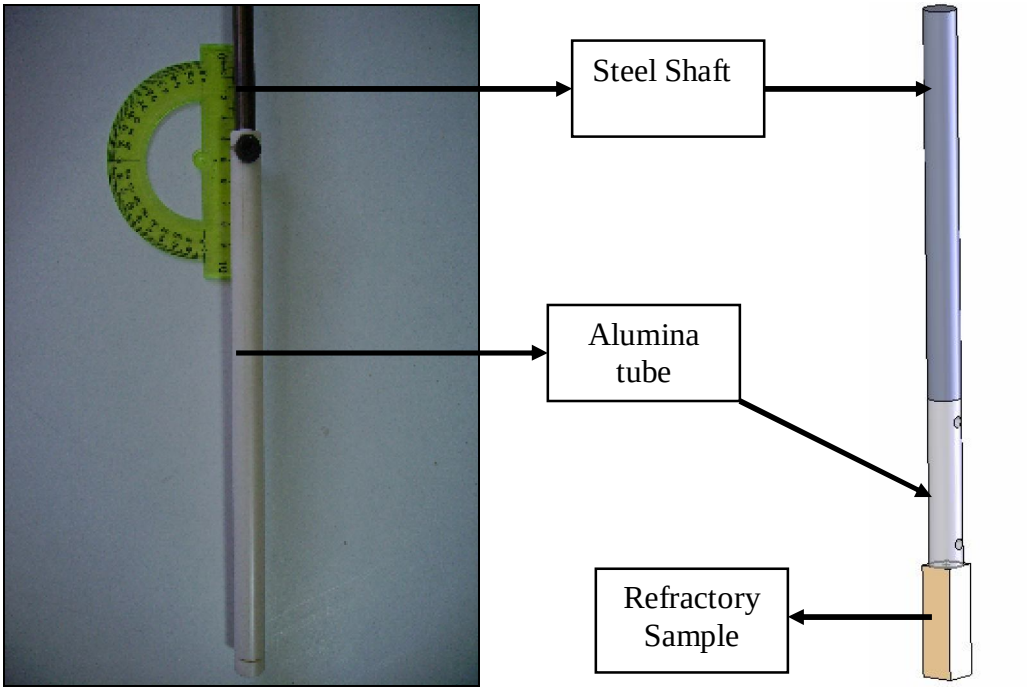

Figure 4.6. The assembly of steel shaft and alumina tubing

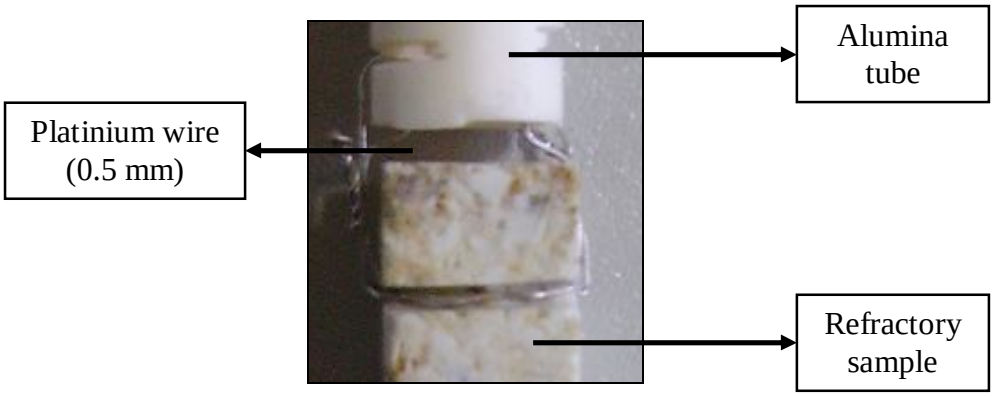

Figure 4.7. Photograph of the assembly of refractory sample and alumina tubing with platinium wire of 0.5 mm diameter

The next step was to determine the working intervals for time and temperature and to test whether the apparatus was able to safely accommodate continuous operation at test temperatures. A number of runs were done to accomplish this and a rugged test setup was finally achieved. Then experiments were started by following a set of experiments using a statistical experiment design methodology as mentioned below after the determination of the temperature and time intervals for corrosion tests.

4.2.2. Experimental Plan

Laboratory slag corrosion tests were planned by the use of statistical experiment design. The objective was to verify the previous tests on refractory corrosion and to present a mathematical model for corrosion kinetics on corrosion rate. The key in statistical experiment design is that it enables the researcher to obtain maximum possible amount of information from a limited number of runs. Because of the difficulty of experimentation in high temperature research, the statistical design is essential. The investigation started with an initial series of 8 experiments designed according to the 2^3 full factorial experiment design for static corrosion tests. The aim was to identify the more important factors affecting experimental precision and refractory corrosion. The full factorial design was used to analyze the effects of factors affecting corrosion. The factor effects chosen were duration of molten frit exposure, temperature and type of refractory. The response variable was percent area loss due to corrosion. These experiments were planned to serve as a tool for developing the mathematical model for

corrosion of frit kiln refractories. An exact theoretical model is very difficult to fit the real data in the process of corrosion of refractories in service. Most models were developed based on plant data, and suffer from poor reproducability. There was a long list of factors effecting corrosion process of refractories in the frit furnace, and it was difficult to simulate service conditions in the laboratory. Temperature, time and type of refractory were only changed in all experiments in our corrosion test protocol but refractory bricks used in the lining of the frit furnace are exposed to harsh environments at high temperatures in service. For instances, some effects like thermal shock, flow of molten frit and alkali vapor in the environment of frit melting furnace cause increase in the corrosion of refractory bricks. Consequently, the conditions included all of effects on corrosion of refractories were not completely simulated in the laboratory corrosion test.

4.2.3. Experimental Procedure

The apparatus was able to accommodate continuous operation of the simulated frit kiln environment at high temperatures (Figure 4.3). A typical run began by loading frit into the reaction crucible and heating at 10^{o}C/min. Refractory specimens were rotated in frit melt with electric motor located on the construction to simulate flowing frit attack in dynamic corrosion tests. The setup could also be run under controlled atmosphere but in this study the end caps were left open to air. By applying pre-tests, working intervals for temperature and time parameters were anticipated. The refractory specimens were then lowered into the melt and held there half-immersed for 4-24 hour static corrosion tests at 1404 and 1504^{o}C as measured by a thermocouple inserted into the alumina tube (Table 4.1). Dynamic corrosion tests were carried out by way of half immersing and rotating at 50 rpm in the frit melt for 10-60 minutes at 1418 and 1456^{o}C (Table 4.2).

Table 4.1. Parameters of static corrosion tests

Type of Refractory	Frit Sample	Temperature (^{0}C)	Time (hour)
T	Transparent	1404^{0}C	4 h 24 h
E		$1504\ ^{0}$C	4 h 24 h

Table 4.2. Working conditions of dynamic corrosion tests

Type of Refractory	Temperature (^{0}C)	Time (minute)
T	1418 ^{0}C	10
T	1418 ^{0}C	60
T	1456 ^{0}C	10
T	1456 ^{0}C	60
E	1418 ^{0}C	10
E	1456 ^{0}C	60

4.3. Percent Wear Measurement

Upon testing the brick samples for their corrosion resistances against frit melts, brick samples were analyzed by three different methods to find the percentage amounts of the losses of corroded materials from the refractory specimens as follows,

(1) photographs of corroded refractory specimens.
(2) longitudinal slicing of the corroded refractory specimens to measure the percent area losses in the cross sections.
(3) immersing into water to measure change in volume.

Measurements of change in volume and observation of photographs of corroded refractory specimens were thought to not be reliable because of slag coating on refractory specimens after corrosion tests. For this reason, (1) and (3) methods were not employed to avoid error in measurement of the percent area loss. Therefore, second technique was applied in determination of percent area loss. Corroded refractory specimens were sliced longitudinally using a low-speed diamond saw and were later polished and photographed to calculate the percent area loss in the cross section. The lost part and the remaining parts were marked on a print-out by a marker and the percent area loss was calculated as such. How to calculate percent area loss in cross section is shown in Figure 4.8. In this way, corrosion test results were obtained as numerical data to analyze statistically.

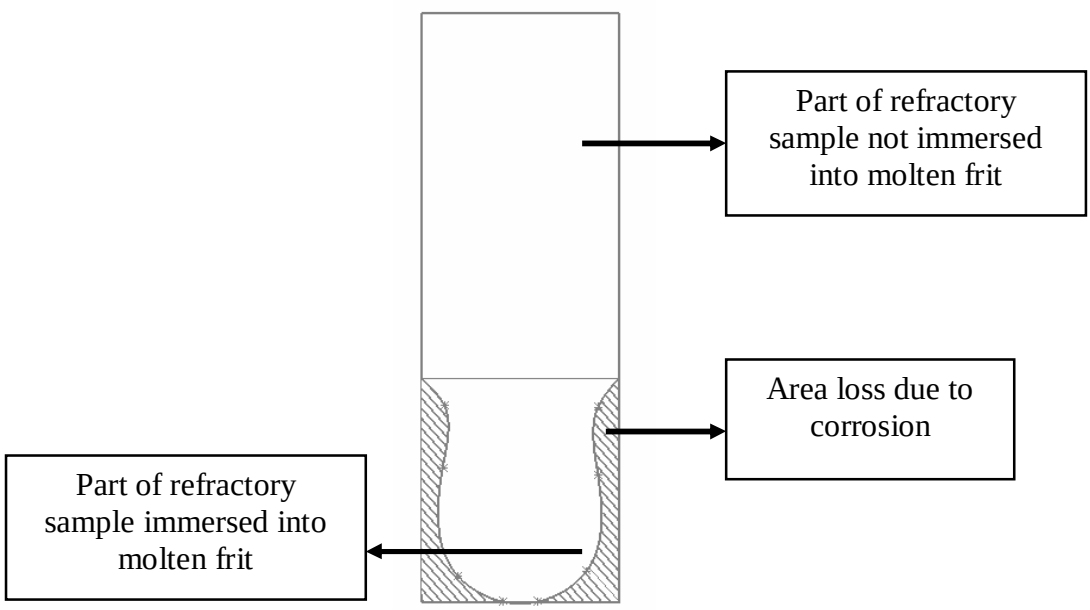

Figure 4.8. Measurement of percent area loss in the cross section of brick sample

CHAPTER 5

RESULTS AND DISCUSSION

In this chapter, results of characterization of original unused brick specimens and frits to be used for corrosion tests are given. Hence, characterization and classification of samples are completed before any corrosion tests. Secondly, the same characterization techniques like microscopic, X-ray diffraction and SEM (scanning electron microscopy) are utilized for postmortem analysis of the corroded refractory bricks after static and dynamic corrosion tests.

5.1. Characterization of Unused Brick and Frit Samples

In this study, two types of commercially available bricks were used. First one was a mullitic brick (coded as E) from Egeferro A.Ş. and the second one was andalusite brick (coded as T) from Tamsa A.Ş. Square shaped (15x15x115mm) refractory samples sliced from larger bricks for corrosion tests are shown in Figure 5.1.

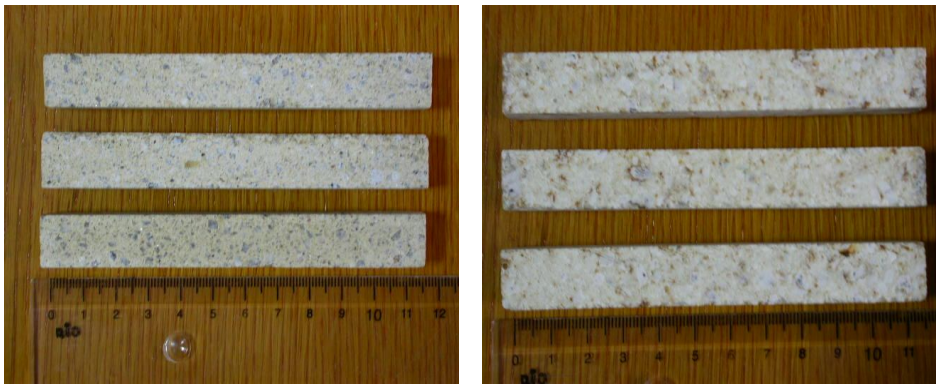

(a) T coded brick samples (b) E coded brick samples

Figure 5.1. Photographs of square shape (15x15x115 mm) brick samples for corrosion tests

The microstructures of original brick samples were analyzed by optical microscopy (OM) and Scanning Electron Microscopy (SEM). The brick samples were sliced longitudinally to prepare for microstructural analysis in their cross sections. The

cutting operation was performed with water cooling using diamond saw at low speed before polishing. Microstructural analyses by SEM and OM (optical microscope) revealed two populations of grain sizes, large grains (about 1 mm in diameter) surrounded by a matrix of fine grains (1-50 micrometers) that provided bonding during firing of the brick. Both bricks contained some sillimanite while brick T also contained large crystals of andalusite and brick E had large mullite grains embedded in fine particles of the same materials (Figures 5.2 and 5.3).

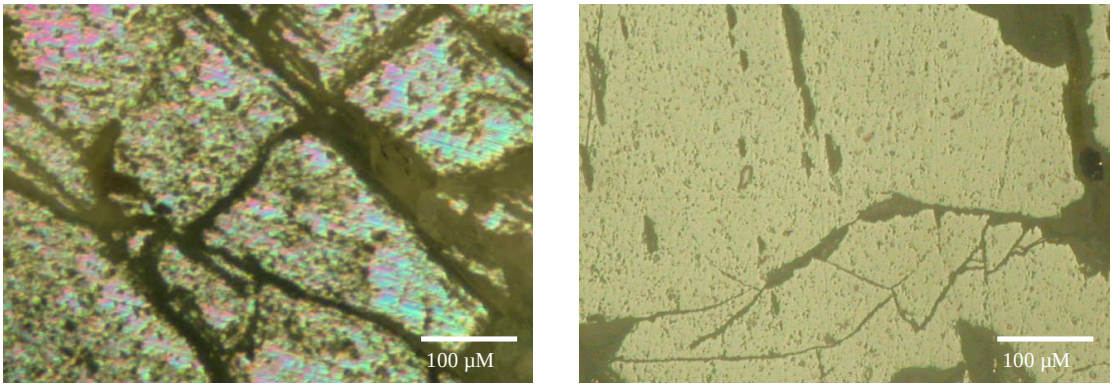

(a) T brick sample (b) E brick sample

Figure 5.2. Optical microscopy images of T and E brick samples (5X)

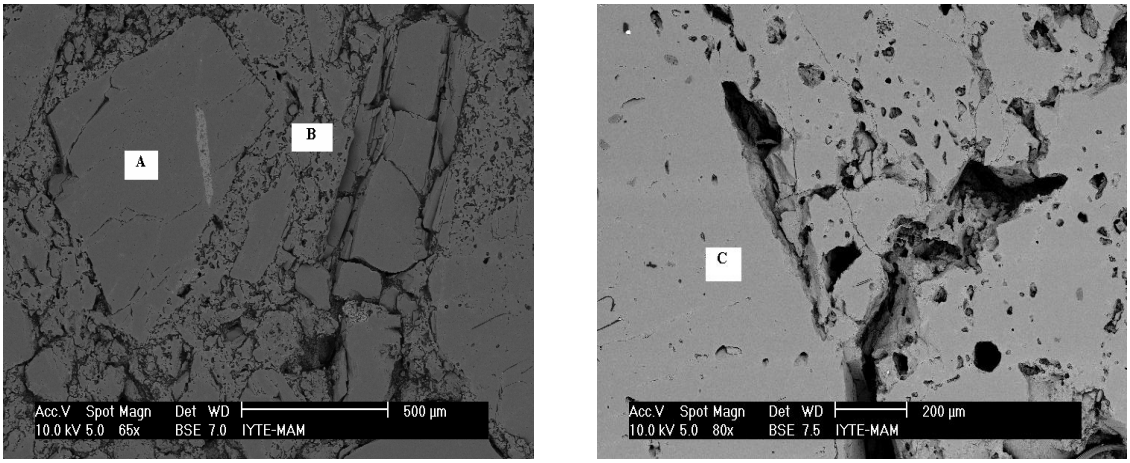

(a) T brick sample
(A) Andalusite and sillimanite,
(B) matrix composed of fine andalusite and sillimanite

(b) E brick sample
(C) large grains of mullite.

Figure 5.3. Polished cross sectional SEM micrographs of brick samples T and E

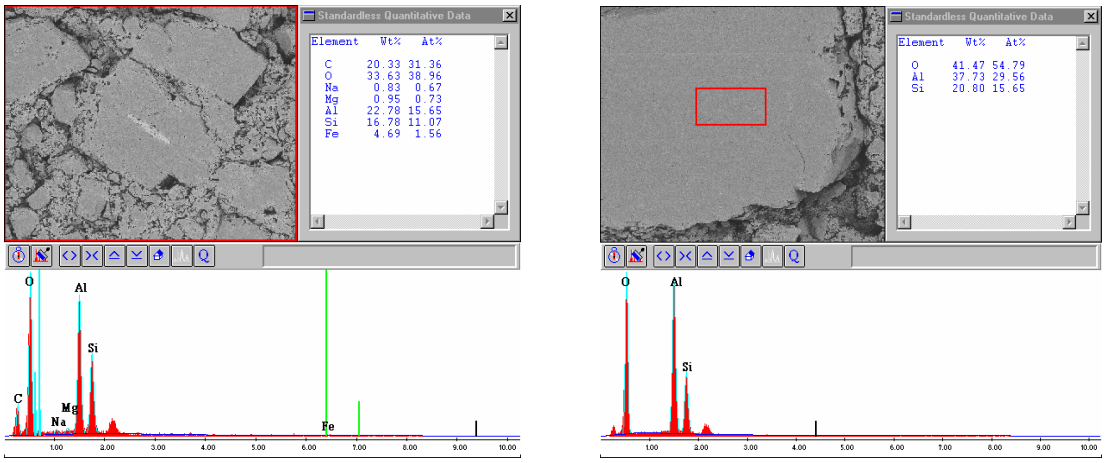

a) T(A) b) T(B)

Figure 5.4. EDX analysis of T brick sample

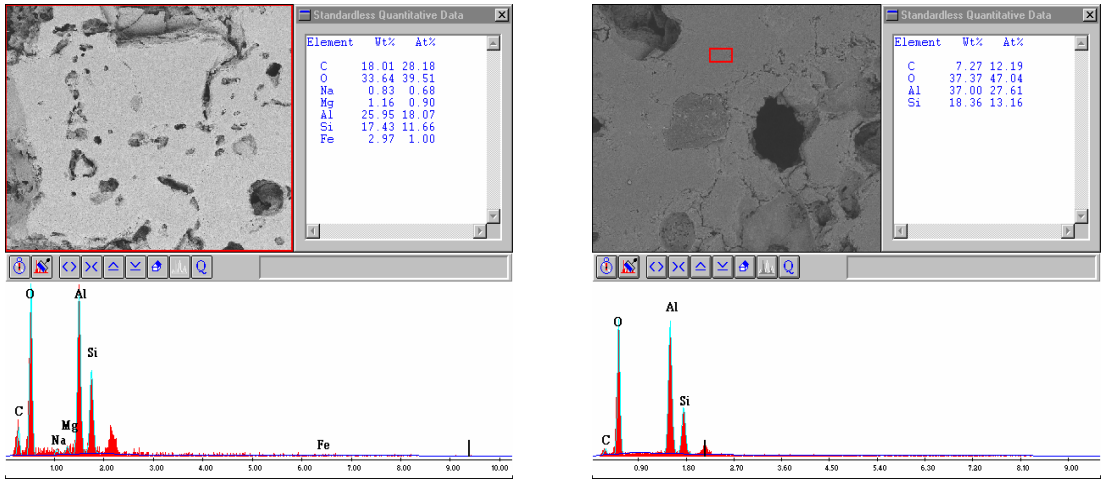

c) E(A) d) E(B)

Figure 5.5. EDX analysis of E brick sample

Compositions of different phases in T and E brick samples are given in Table 5.1. The above given EDX analysis of the predominant phase in T refractory sample confirmed that its composition was andalusite ($Al_2O_3.SiO_2$) (Figure 5.4). The existence of mullite ($3Al_2O_3.2SiO_2$) phase was confirmed in EDX results of E refractory sample (Figure 5.5). T specimens had 76-78% Al_2O_3, 22-24% SiO_2, 0.3-0.6% FeO and E specimens had 60% Al_2O_3, 37% SiO_2 and less than 1% of FeO as supplied by the manufacturers.

Table 5.1. Results of SEM-EDX analysis of refractory samples.

Element	T(A)		T(B)		E(A)		E(B)	
	wt%	at%	wt%	at%	wt%	at%	wt%	at%
O	42.2	56.8	41.5	54.8	41.0	55	40.3	53.5
Al	28.6	22.8	37.7	29.6	31.6	25.2	39.9	31.5
Si	21.1	16.2	20.8	15.6	21.3	16.2	19.8	15
Mg	1.2	1.0	-	-	1.4	1.3	-	-
Na	1.0	0.9	-	-	1.0	0.9	-	-
Fe	5.9	2.3	-	-	3.6	1.4	-	-
Ca	-	-	-	-	-		-	-

Archimedes' method was used in order to measure the percent apparent porosity and bulk density of brick samples as shown in Table 5.2. The brick samples had similar porosities. In additon to density values, some selected physical properties of the brick samples are listed in Table 5.3.

Table 5.2.Density measurement of Tamsa and Egeferro Refractory Samples by Archimedes' Method.

Sample	Apperent Porosity, %	Water Absorbtion, %	Apparent Specific Gravity, g/cm3	Bulk Density, gr/cm3	Theoretical Density,%
1T	14.6	5.6	3.0	2.6	65.6
2T	15.5	5.9	3.1	2.6	65.4
3T	8.9	3.3	2.9	2.7	67.4
1E	12.6	4.9	2.9	2.5	64.1
2E	12.7	5.0	2.9	2.6	64.3
3E	11.7	4.5	2.9	2.6	64.9
AverageT	13.0	5.0	3.0	2.6	66.1
AverageE	12.3	4.8	2.9	2.5	64.4

Table 5.3. Some Physical Properties of Brick Samples

Property	Brick T	Brick E
Apparent porosity (%)	13.0	12.3
Bulk Density (g/cm^3)	2.6	2.6
Compressive strength (MPa)	11	35

Phase analyses of refractory samples were done by X-ray diffraction method (Phillips X'Pert Pro). XRD results of original refractory samples confirmed that T specimens consisted of andalusite and sillimanite, while E refractory specimens were composed of mullite and sillimanite in the XRD patterns of Figures 5.6 and 5.7.

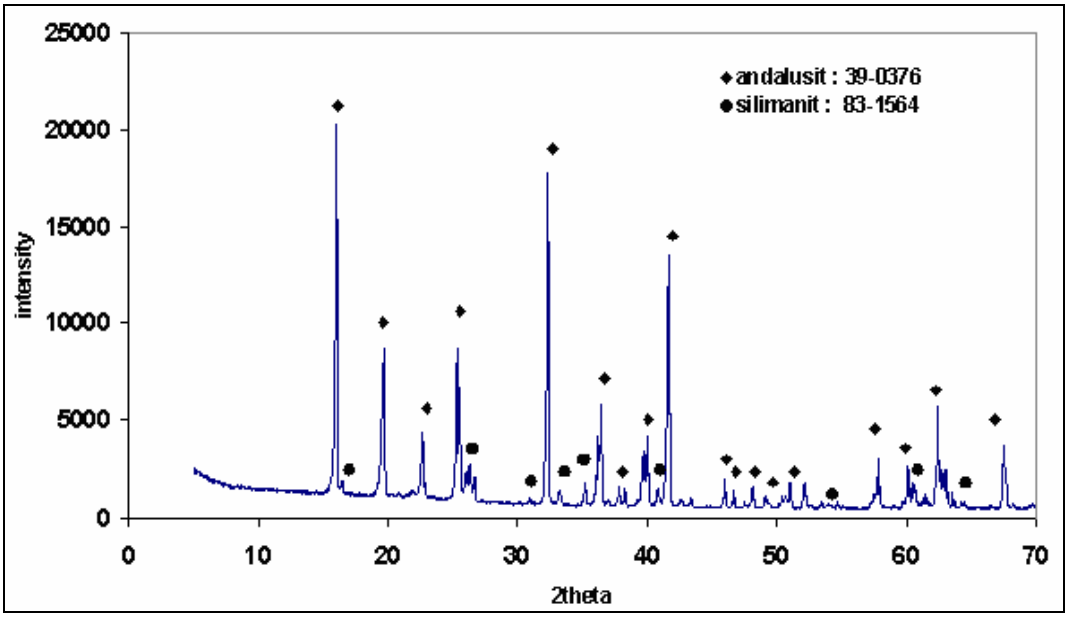

Figure 5.6. XRD pattern of original T refractory sample

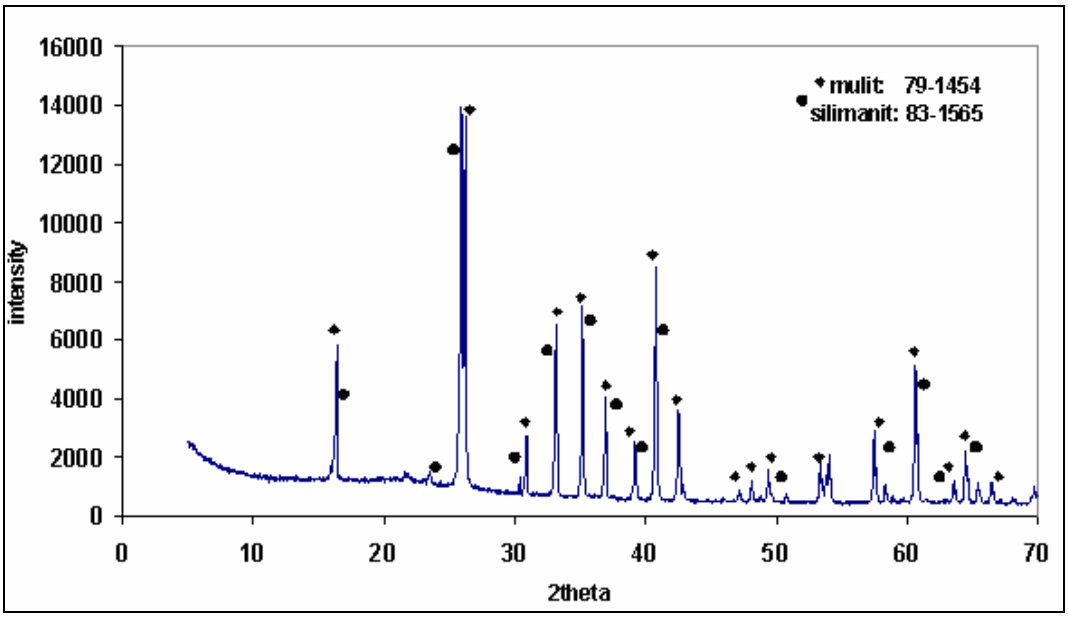

Figure 5.7. XRD pattern of original E refractory sample

SEM, EDX and XRD results showed that both refractory specimens were aluminosilicate refractories with a high amount of alumina (>50% Al_2O_3). One type of frit was planned to be used for corrosion tests. Transparent frit with high zinc and aluminium was supplied by Tamsa A.Ş. (Figure 5.8). This type of frit was commercially used for wall and floor tile glazes. Transparent frits allow light transmission due to lack of zircon opacifiers (Eppler, et al. 2000). Published chemical composition of the frit as measured by XRF is given in Table 5.4.

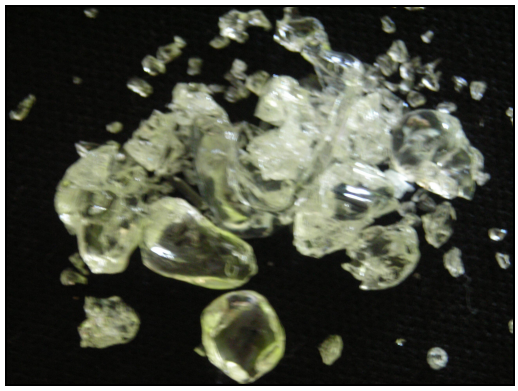

Figure 5.8. Photograph of transparent frit sample

Table 5.4. Composition of transparent frit sample

Composition	Weight%
Al_2O_3	9.3
B_2O_3	8.5
CaO	8.4
K_2O	6.1
MgO	2.2
SiO_2	52.7
ZnO	12.8

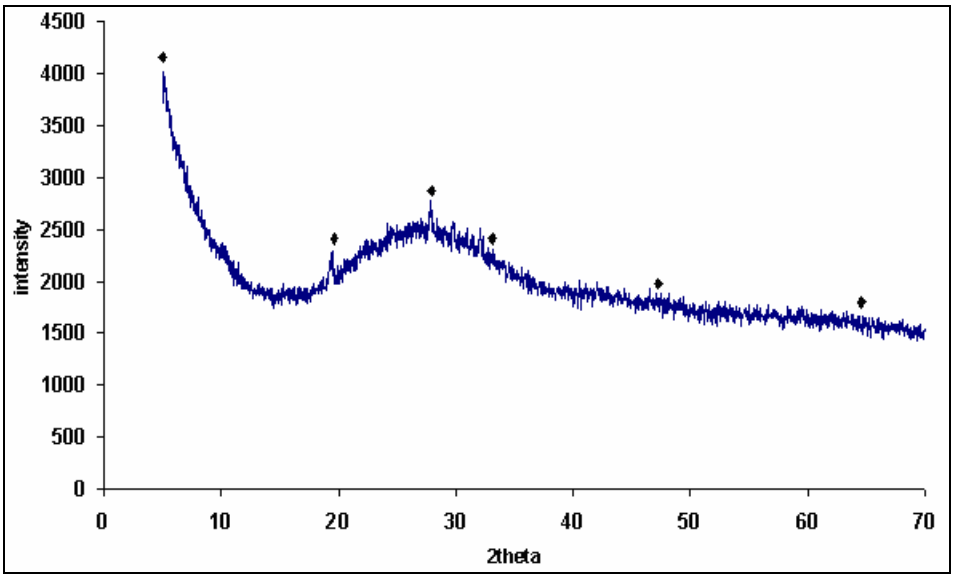

Figure 5.9. XRD pattern of transparent frit sample

X-ray diffraction analysis of transparent frit is given in Figure 5.9. As can be seen from the XRD pattern, frit sample showed entirely amorphous structure as expected. Because frit melts contain a lot of SiO_2 that is the framework of glazes and encourages glass formation upon quenching (Eppler, et al. 2000).

5.2. Results of Corrosion Tests

5.2.1. Static Corrosion Test Results

Refractory specimens were half-immersed into molten frit at temperatures in the range of 1404-1504 ^{o}C during 4-24 hours for static corrosion tests. As seen in figures 5.10 and 5.11, refractory specimens were obviously corroded after static testing and the amount of corrosion of corroded refractory specimens was significantly increased at higher temperatures and immersion times. The corroded refractory specimens were photographed after corrosion tests to measure their percent cross sectional area losses.

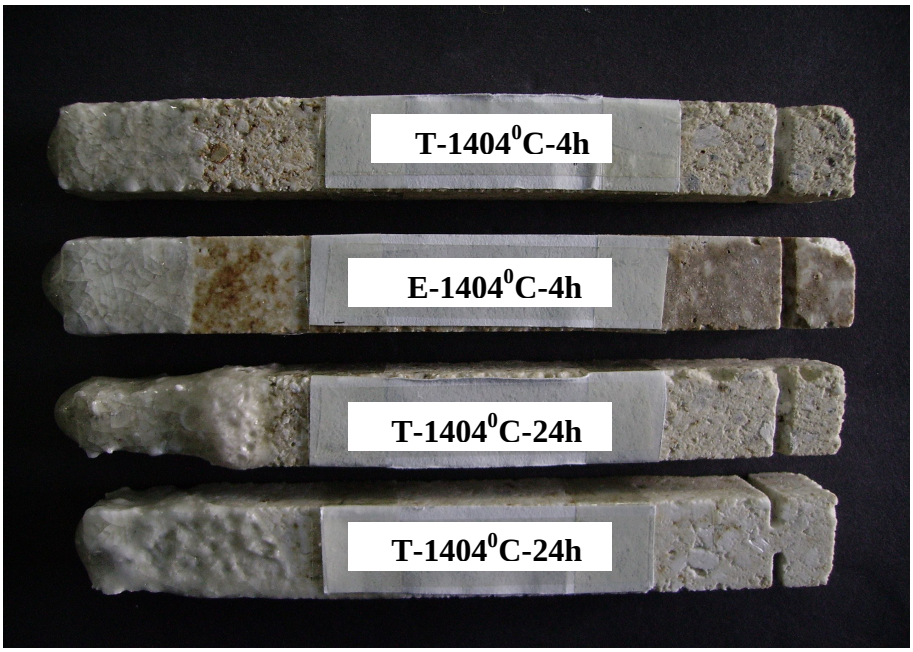

Figure 5.10. A photograph of the corroded refractory specimens tested at 1404 ^{o}C for static corrosion tests.
(T-1404^{0}C-4h : T brick was tested at 1404^{o}C for 4 hours)

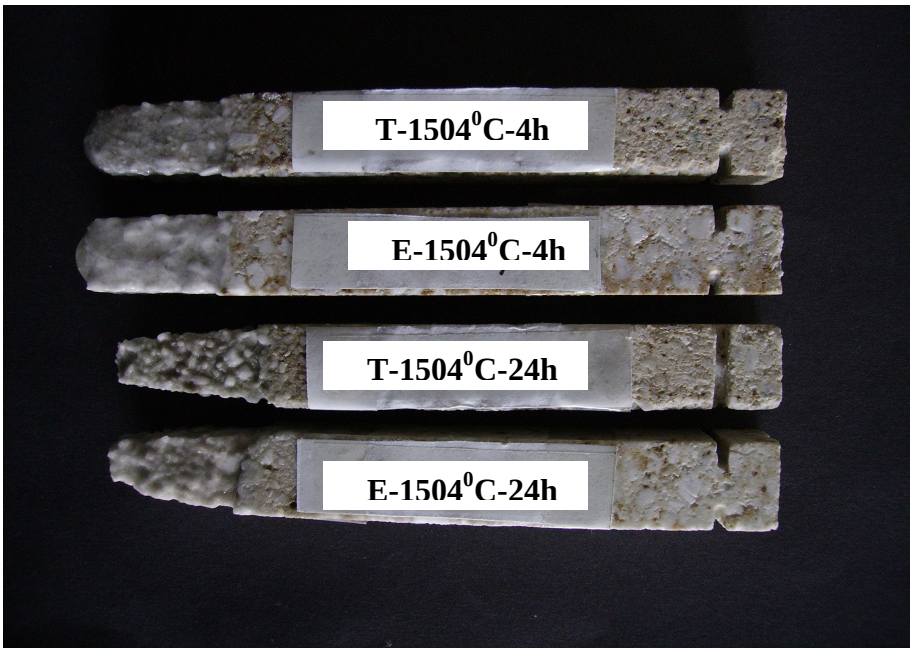

Figure 5.11. Photograph of the corroded refractory specimens tested at 1504^{o}C for static corrosion tests.

The corroded refractory specimens were sliced longitudinally using a low speed diamond saw, and were later polished and photographed to calculate the percent area loss in the cross section (Figure 5.12). The lost part and the remaining parts were marked on a print-out by a marker and the percent area loss was calculated as such.

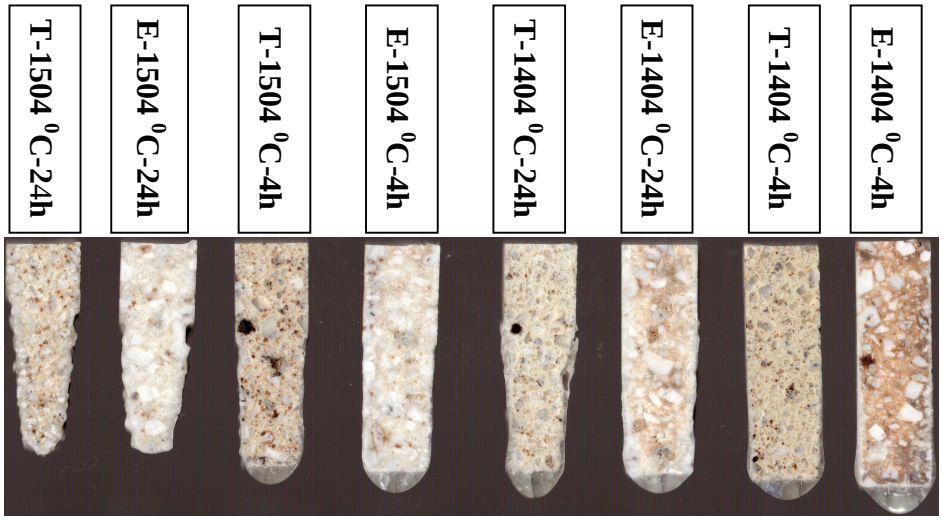

Figure 5.12. Photograph of the cross sectional areas of corroded refractory specimens after static tests.

Table 5.5 and Figure 5.13 show that the corrosive loss of material increased with increasing test temperature and duration. E brick was about 20-30% more resistant to corrosive frit melt when compared to T specimen after static tests.

Table 5.5. Percent cross sectional area losses of corroded refractory specimens after static corrosion tests.

Refractory specimens	**% area loss by observation before cutting**	**% Cross sectional area loss as measured.**
Tamsa-1404°C-4 h	0	0
Egeferro-1404°C-4 h	0	0
Tamsa-1404°C-24 h	%25	% 24
Egeferro-1404°C-24 h	%15	%18
Tamsa-1504°C-4 h	%20	%19
Egeferro-1504°C 4 h	%10	%15
Tamsa-1504°C 24 h	%40	%36
Egeferro-1504°C 24 h	%35	%30

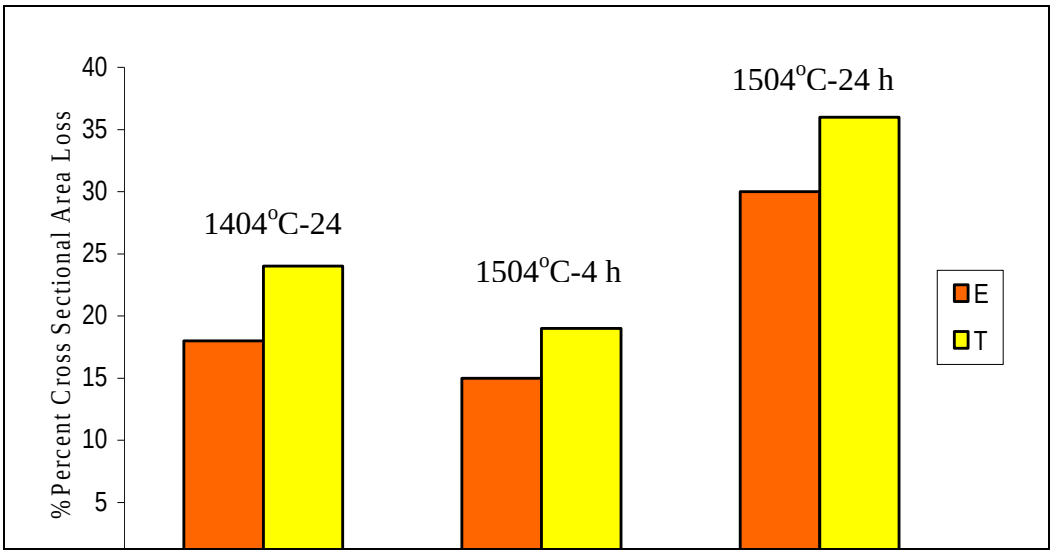

Figure 5.13. Corrosion ratings of corroded refractory specimens after static corrosion tests

Percent wear (area loss) numbers are interchangibly used with the term “corrosion” based on the assumption that erosion was not a big factor for static corrosion test method. Erosion is definitely not completely ruled out but corrosion term was used. Alternatively, percent wear numbers obtained from static corrosion test results were used for statistical study to identify the more important factors affecting experimental precision and refractory corrosion. For this reason, the 2^3 full factorial experimental design was used for static corrosion test results to analyze the effects of factors affecting corrosion (Table 5.5). Analysis of variance (ANOVA) table obtained from data are given in Table 5.6. The factors are coded as follows: A: temperature, B: time and C: type of refractory.

Table 5.6. Anova table of the corrosion data obtained from static corrosion test results

Source	df	SS	MS	F	p
A	1	420.5	420.5	210.3	0.04
B	1	684.5	684.5	342.3	0.03
C	1	32.0	32.0	16.0	0.16
AB	1	12.5	12.5	6.25	0.24
AC	1	2.0	2.0	1.0	0.50
BC	1	8.0	8.0	4.0	0.29
Error	1	2.0	2.0		
Total	7	1161.5			

Anova table of data was obtained by using Design Expert software program. As can be seen in the Anova table, the wear was very much affected by the test temperature (A) and exposure duration (B) of the refractory to the frit melt, and not much by the type of refractory specimen. There was no significant interaction term between the factor effects. R-squared value, which is an indication of the quality of the fit of the model, was 0.98. This was very encouraging because the reliability of the test method used was important.

Figures 5.14 and 5.15 show a plot of the effect of temperature and time on corrosion at varying levels of exposure durations. As can be seen from the figures not much interaction was observed between the factor effects for both bricks.

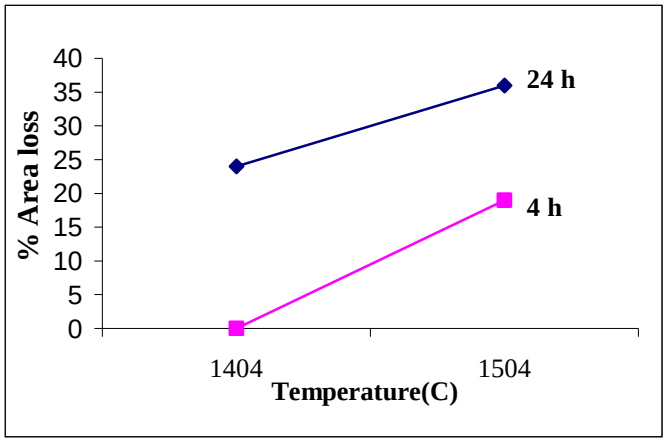

Figure 5.14. The effects of temperature and time on corrosion of T brick in static corrosion tests.

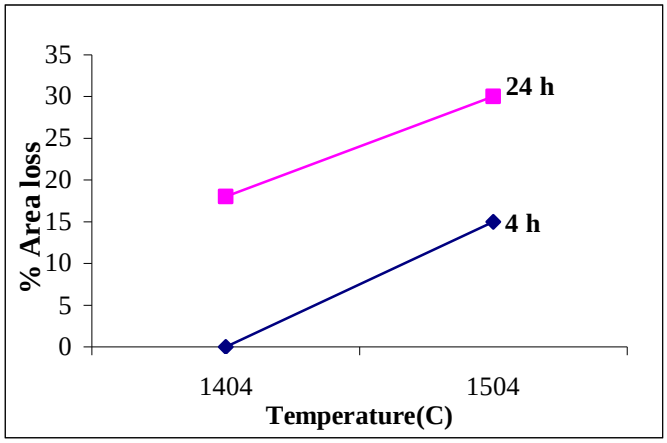

Figure 5.15. The effects of temperature and time on corrosion of E brick in static corrosion tests

5.2.2. Dynamic Corrosion Test Results

In dynamic corrosion tests, refractory specimens were also rotated into molten frit at 50 rpm at 1418-1456 ^{o}C temperatures during 10-60 minutes. As can be seen in Figure 5.16, increasing test temperature and duration led to higher amount of corrosion of refractory specimens after dynamic corrosion tests. A similar trend was also observed in the static test results.

Figure 5.16. A photograph of the corroded refractory bricks after dynamic corrosion tests. (E-1418-10: E refractory specimen was tested at 1418 C during 10 minutes)

Their percent cross sectional area loss values were calculated in the same way as was used in static corrosion tests. Table 5.7 shows that E brick was more resistant to frit melt than T brick in dynamic test conditions. Both static and dynamic test results showed that E brick based on mullite phase was less corroded in the frit melt after the corrosion tests.

Table 5.7. Percent cross sectional area loss of corroded refractory specimens after dynamic corrosion test

Refractory specimens	**% area loss by observation before cutting**	**% Cross sectional area loss as measured.**
T-1418°C-10 min.	0	0
T-1456°C-10 min.	%2	%4
T-1418°C-60 min.	%5	% 6
T-1456°C-60 min.	%10	%13
E-1418°C-10 min.	0	0
E-1456°C-60 min.	%5	%7

5.3. Postmortem Microstructural Analysis

Postmortem study in glass-melting furnaces is important to understand the mechanisms related to refractory corrosion. This kind of study can reveal useful information about the furnace's operational conditions and refractory wear. Based on this information, several actions may be taken to increase the furnace campaign. For instance, appropriate refractory brick for special industrial applications can be chosen by comparing with different types of refractory bricks in terms of their resistances to the corrosive melts. This type of study also allows evaluation of the corrosion mechanisms based on a long list of furnace's operation conditions that would not be otherwise possible to do in laboratory conditions (Paskocimas 1998, Karakus 1996). The corroded refractory specimens were investigated after corrosion tests with SEM, EDX, optical microscopy and X-ray diffraction methods to carry out their postmortem analyses.

5.3.1. Postmortem Analysis of the Corroded Refractory Specimens After Static Corrosion Tests

Detailed SEM, EDX and OM examination of the different cross sectional zones in the corroded refractory specimens cooled to room temperature after static corrosion tests is described below. Regardless of the nature of the corrosive agent used, all the corrosion profiles observed in the corroded refractory bricks consisted of four zones with different textures (Poirier, et al. 2004).

1. Remnant slag
2. Precipitation zone
3. Penetrated zone
4. Unaffected zone

These four zones are easily distinguishable in all samples after the corrosion tests. SEM, EDX and OM images of the corroded refractory specimens are given below.

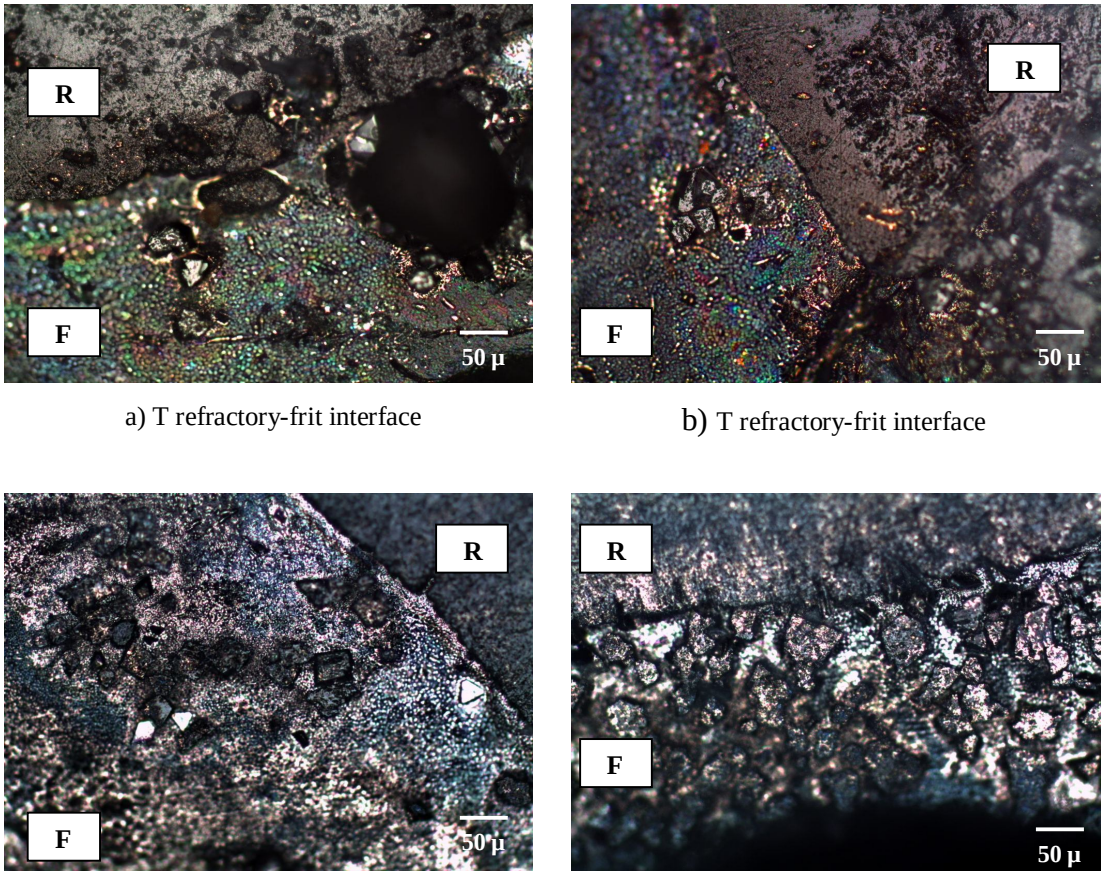

a) T refractory-frit interface

b) T refractory-frit interface

c) E refractory-frit interface

d) E refractory-frit interface

Figure 5.17. Optical microscopy images of the corroded refractory specimens tested at 1404 ^{0}C during 24 hours in static corrosion tests (magnification ratio is 20X). R:Refractory grain (unaffected zone), F: remanant slag(frit melt cooled after corrosion test on the cross sectional surface of the refractory specimen)

Optical microscopy was used for the initial microstructural examination of the above described corroded refractory specimens. Optical microscopy images of the corroded refractory specimens tested at 1404^{o}C during 24 hours indicated that along the refractory-frit interface there exists white triangular and polygonal shaped precipitates embedded within porous frit slag. The size of these small precipitates varies between 10 µm and 50 µm.

a) Precipitation zone of T refractory specimen

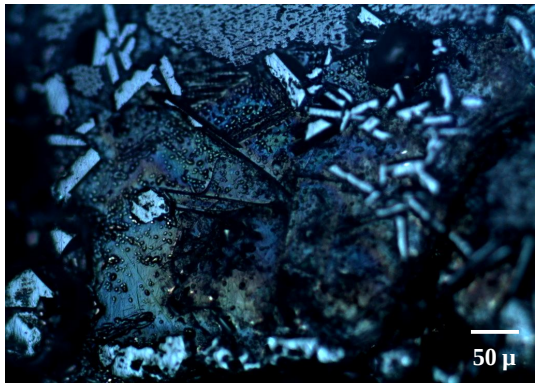

b) Precipitation zone of T refractory specimen

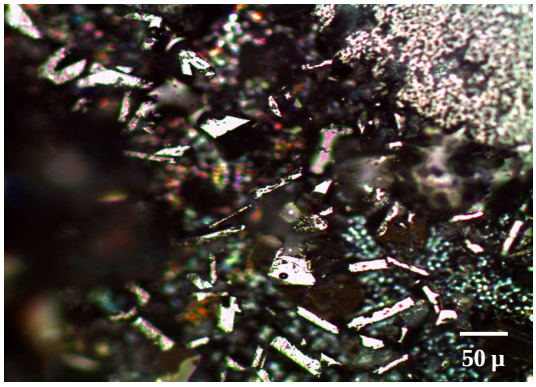

c) Precipitation zone of E refractory specimen

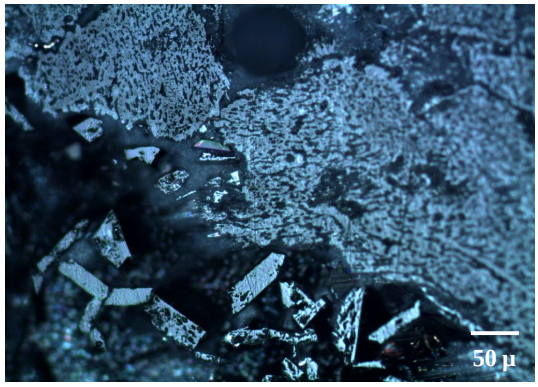

d) Precipitation zone of E refractory specimen

Figure 5.18. Optical microscopy images of the corroded refractory specimens exposed to frit melt at 1504^{o}C during 24 hours in static corrosion tests.

Optical microscopy images of the corroded refractory specimens exposed to frit melt at 1504^{o}C during 24 hours showed that small white crystals embedded within frit slag were observed again along the frit-refractory interface. Precipitation zones are located in refractory specimens in contact with frit melt (Figure 5.18). The size of these crystals varies between in 10 µm and 50 µm. The precipitated crystals were found to be new phases after static corrosion tests that were carried out at 1404^{o}C and 1504^{o}C along the refractory-frit interface. SEM-EDS analysis was carried out below for the details of the structure of these small crystals located along the frit-refractory interface.

a) E refractory-frit interface

b) Precipitates at E refractory-frit interface

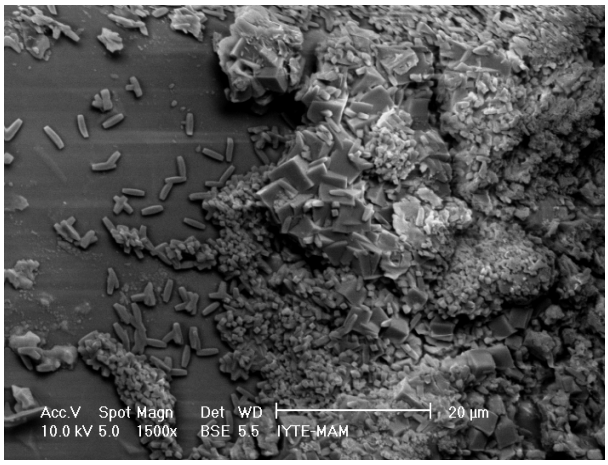

c)The pile of precipitates on the cooled frit (slag)surface of T refractory specimen

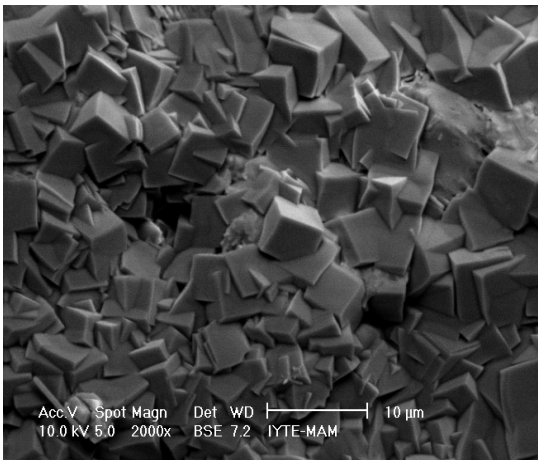

d) Cubiodal precipitates on the cooled frit (slag) surface of T refractory specimen

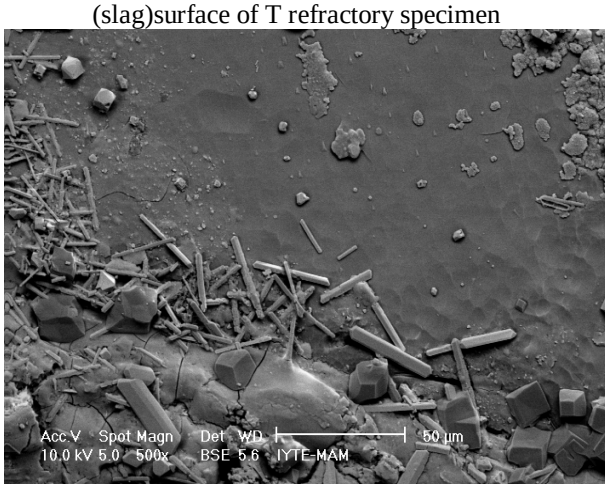

e) T refractory–frit interface

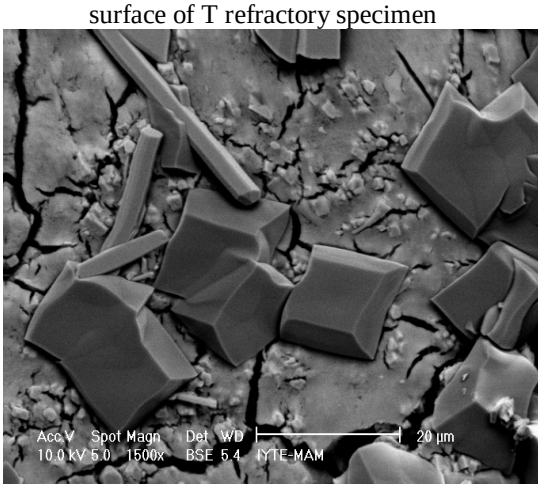

f) Cuboidial and prismatic crystals precipitated at T refractory-frit interface

Figure 5.19. SEM images of cross-sectional area of the corroded refractory specimens tested at 1404 ^{0}C during 4 hours in static corrosion tests.

SEM images of the corroded refractory specimens exposed to frit melt at 1404 ^{o}C during 4 hours are shown in Figure 5.19. SEM images at two different magnifications of the same white precipitates along the E refractory-frit interface are shown in Figure 5.19. a and b. The proportions of the elements displayed by EDX results helped confirm the identity of the newly formed phases at the refractory-frit interface. The EDX analysis of these crystals are given in Figure 5.20. EDX analysis showed that small white crystals were found to be $ZnAl_2O_4$ as new reaction products along the E type frit-refractory interface. As shown in Figure 5.21 and 5.22, precipitates with prismatic and cubiodial shapes were detected as corundum (Al_2O_3) crystals along T refractory-frit interface. Consequently, the precipitates that were observed after 1404^{o}C-4 hours static corrosion tests by the frit melt are corundum with different shapes as well as $ZnAl_2O_4$ and mullite crystals. Corundum crystals with a cuboidal habit were also observed by Xiao et al (Xiao, et al. 2000).

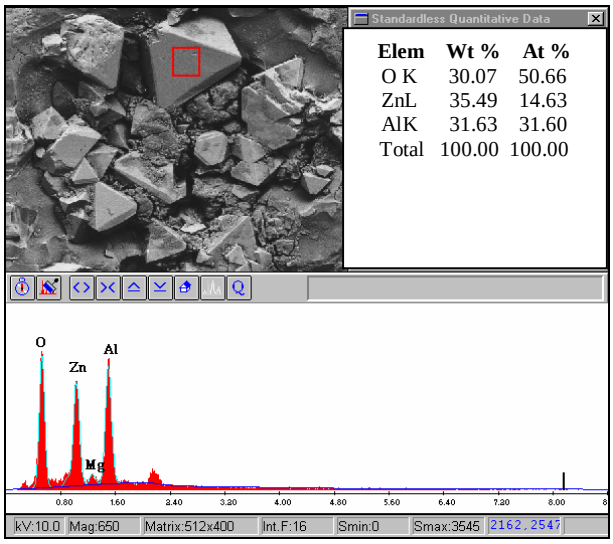

Figure 5.20. EDX analysis of the white colour crystals at E refractory-frit interface after static corrosion test at 1404 ^{0}C during 4 hours.

SEM and EDX analysis of refractory specimens that were tested at 1404^{o}C for 4 hours showed that dissolution of aluminum was clearly observed from the refractory grains to the frit melt. This result enriched the frit melt with respect to aluminium ions which on cooling precipitated out of the frit melt in the form of idiomorphic grains. EDX results confirmed that occasional precipitations of $ZnAl_2O_4$ and corundum (Al_2O_3) were observed to occur in the frit melt and along the frit-refractory interface.

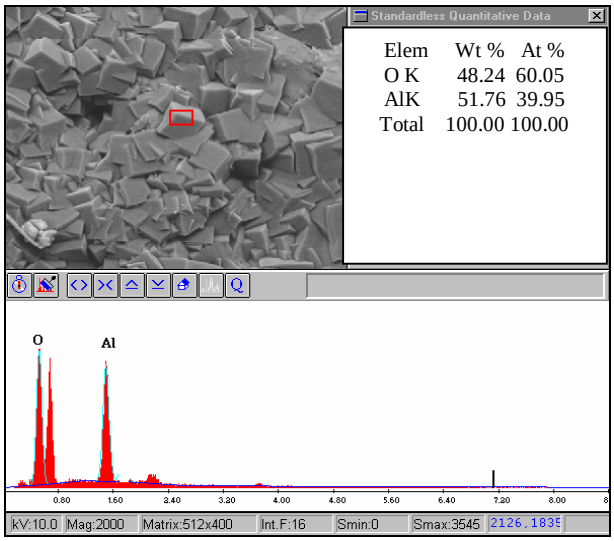

Figure 5.21. EDX analysis of the cubidial crystals precipitated on the cooled frit surface of T refractory specimen after static test at 1404 ^{0}C during 4 hours.

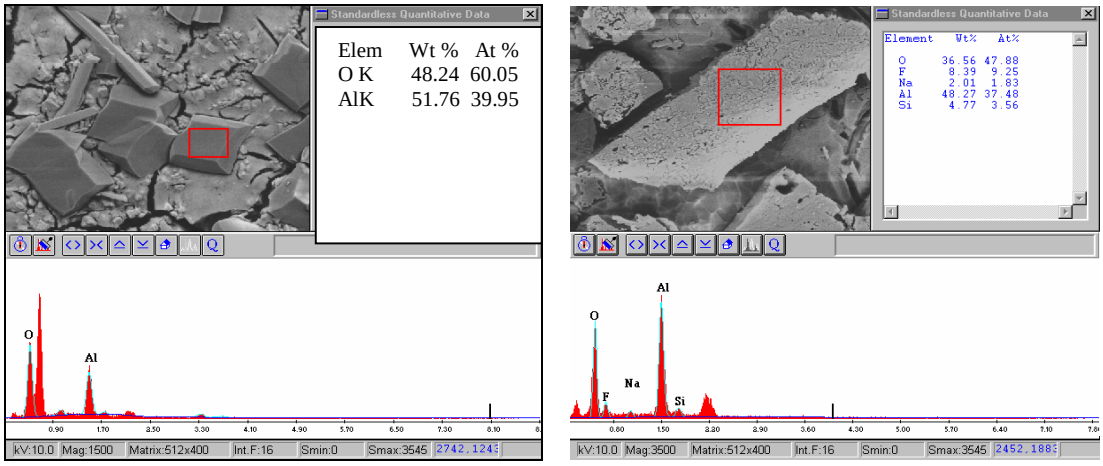

a) b)

Figure 5.22. EDX analysis of the precipitates along the T refractory-frit interface after static test at 1404 ^{0}C during 4 hours.

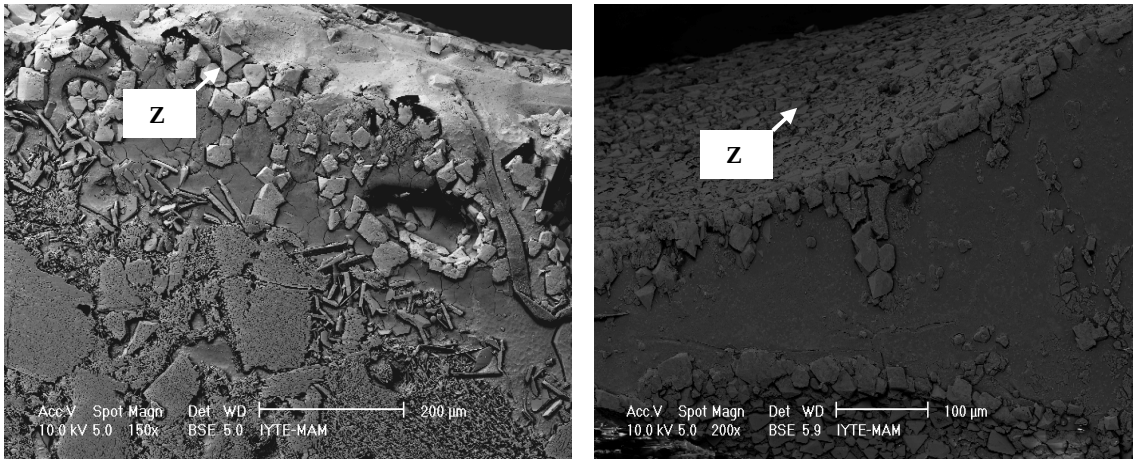

a) E refractory-frit interface b) Precipitation zone of T refractory specimen

Figure 5.23. SEM images of cross-sectional area of the corroded refractory specimens exposed to frit melt at 1404°C during 24 hours . (Z:$ZnAl_2O_4$)

SEM images of refractory specimens tested at 1404°C during 24 hours showed that precipitation of $ZnAl_2O_4$ was observed in both of refractory types in Figure 5.23. For formation of these $ZnAl_2O_4$ crystals alumina from the refractory supplied the aluminum while the frit supplied zinc. Furthermore, the amount of $ZnAl_2O_4$ crystals increased with increasing immerse time into the frit melt when compared to those that were done during 4 hour-tests.

SEM images of the corroded refractory specimens held into frit at 1504°C during 4 hours are given in Figure 5.24. Figures 5.24.a, b shows the needle-like crystals embedded within the cooled frit melt, and also $ZnAl_2O_4$ crystals clustered along frit-refractory interface and in pores. EDX analysis indicates that these needle-like crystals are mullite in Figure 5.25. Mullite crystals with neddle-like shape were also observed by Iqbal Y. and Tomba et.la (Iqbal, et al. 2001 and Tomba, et al. 1999). As can be seen from Figure 5.24.c, $ZnAl_2O_4$ crystals were observed for the corroded E type refractory specimens. EDX analysis of the precipitated crystals in Figure 5.26.b. indicated their structure to be corundum. Corundum, mullite and $ZnAl_2O_4$ crystals were observed as the precipitated products after static tests at 1504°C during 4 hours.

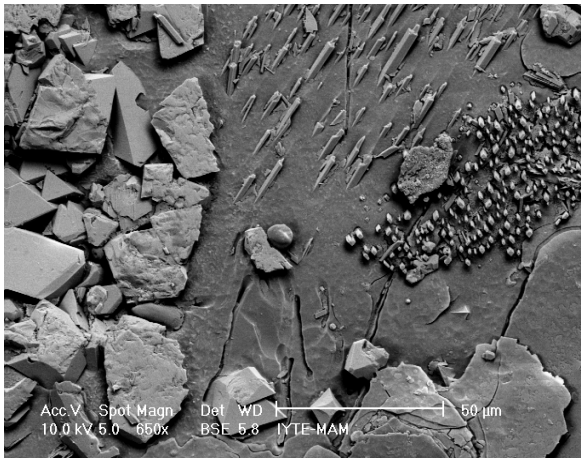

a) T refractory-frit interface

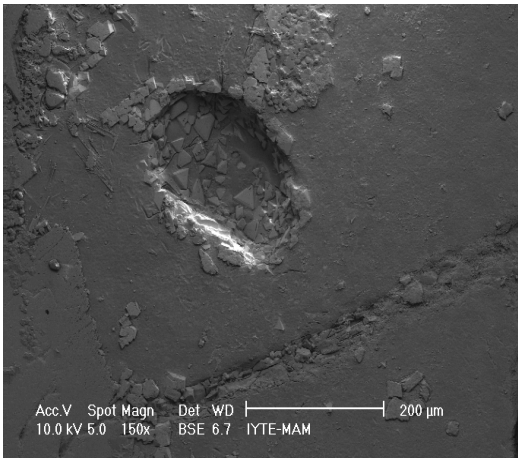

b) T refractory-frit interface

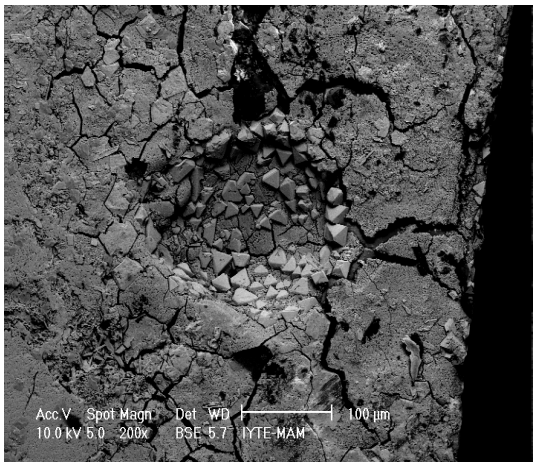

c) $ZnAl_2O_4$ precipitates gathered into pore on the slag surface of E refractory specimen.

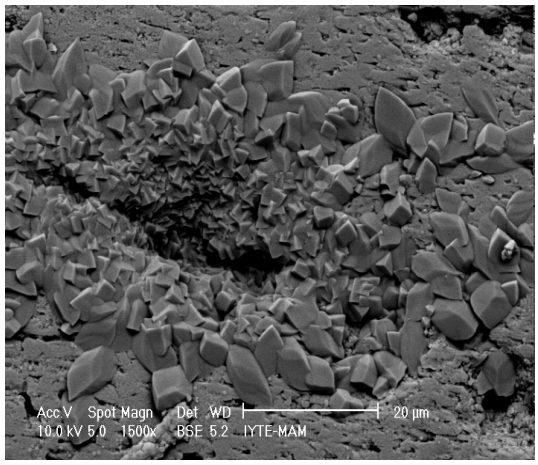

d) The pile of corundum(Al_2O_3) precipitates clustered on the slag surface of E refractory specimen.

Figure 5.24. SEM images of cross-sectional area of the corroded refractory specimens tested at 1504 ^oC during 4 hours.

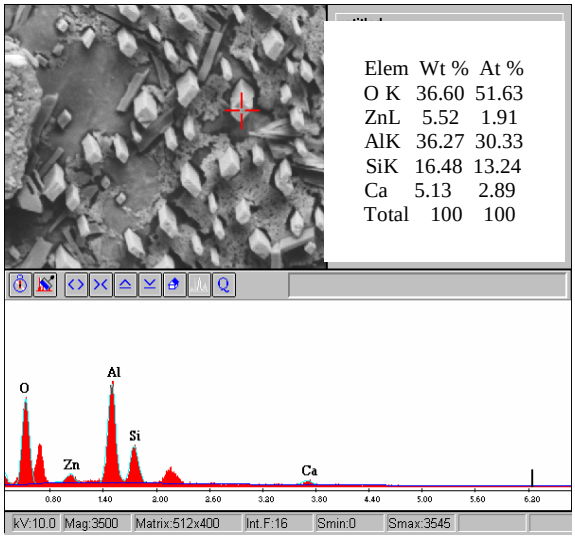

Figure 5.25. EDX analysis of needle-like crystals along T refractory-frit interface (1504 ^{o}C 4 hours).

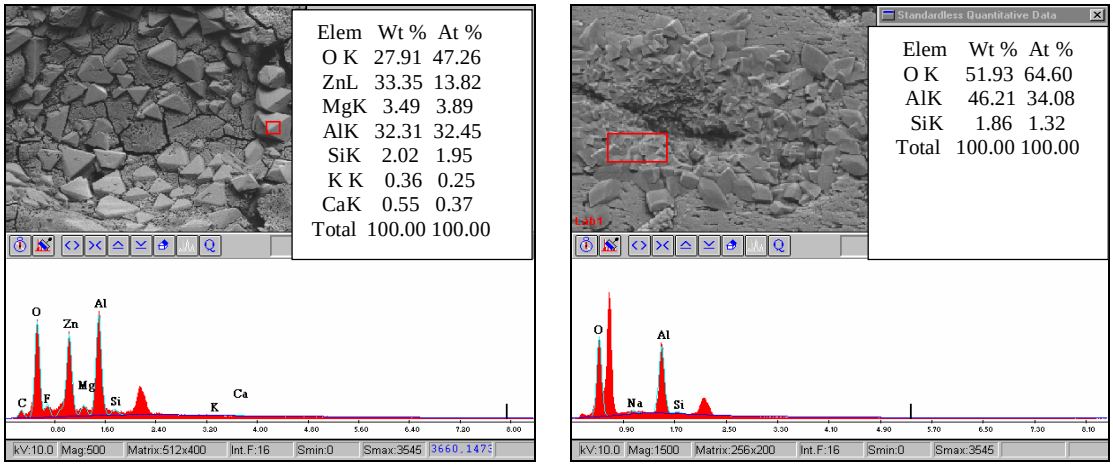

a) b)

Figure 5.26. EDX analysis of precipitates in the pore on the slag surface of E refractory specimen (1504 ^{o}C 4 hours).

SEM images of the corroded refractory specimens tested at 1504^{o}C during 24 hours displayed a bright white zone (precipitation zone) where refractory in contact with frit during static corrosion testing (Figure 5.27). EDX analysis of these precipitates indicated their structure to be $ZnAl_2O_4$ in Figure 5.28. The amount of $ZnAl_2O_4$ crystals increased with increasing immersion time and temperature. The same results were obtained after static tests that were carried out at 1404 ^{o}C during 24 hours.

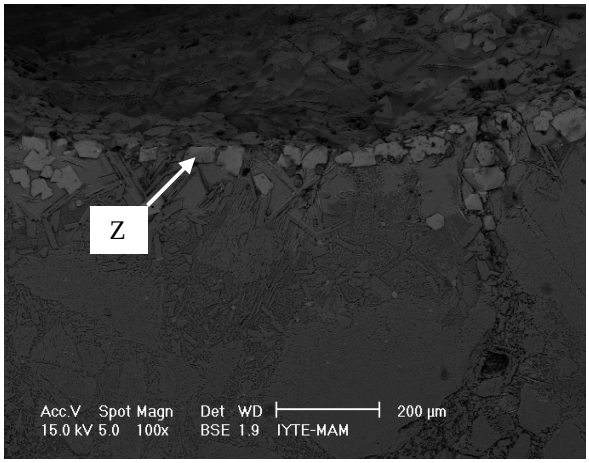

a) Precipitation zone (white crystals) of T refractory specimen in contact with frit melt during the static corrosion testing.

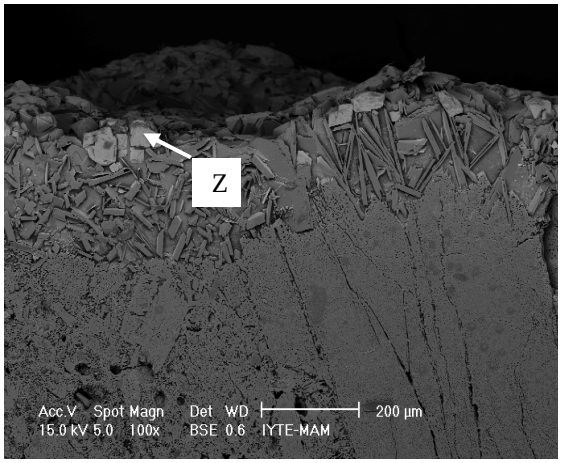

b) Precipitation zone (white crystals) of E refractory specimen in contact with frit melt during the static corrosion testing.

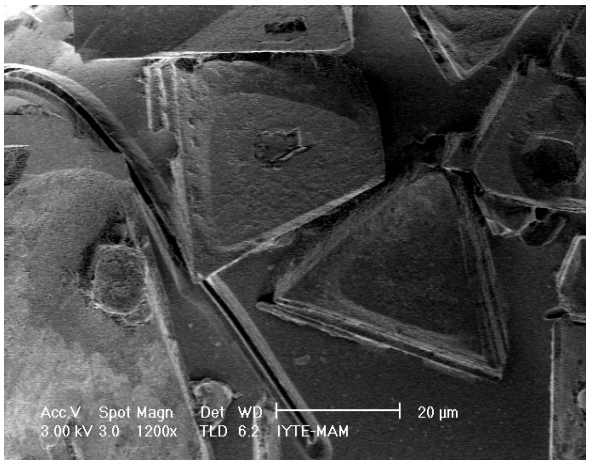

c) $ZnAl_2O_4$ precipitates with triangular shape that were embedded on the solidified frit surface of T refractory specimen.

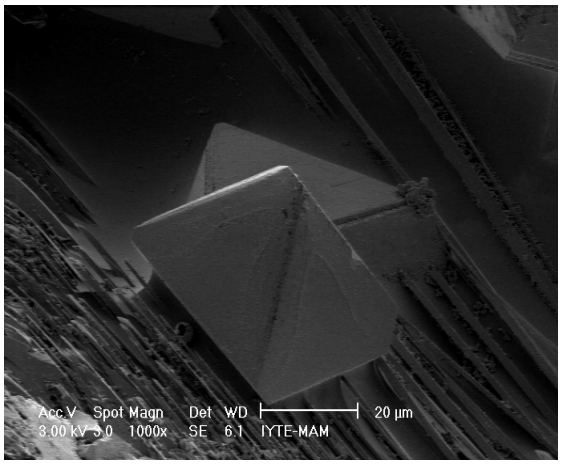

d) $ZnAl_2O_4$ crystals in pore of the corroded T refractory specimen.

Figure 5.27. SEM images of cross-sectional area of the corroded refractory specimens that were tested at 1504 ^{o}C during 24 hours. (Z:$ZnAl_2O_4$)

The effect of $ZnAl_2O_4$ on the corrosion mechanism may be clarified such that the presence of the band of $ZnAl_2O_4$ crystals could act as a limited barrier on the dissolution of the brick components because it is not continuous as shown in Figure 5.27. Furthermore its formation may increase the slag viscosity at test temperature. As a result, the frit melt could no longer penetrate easily into the refractory through the pores and grain boundaries and this result could decrease the corrosion rate. However, none such band of precipitates was observed in static tests that were carried out at 1404^{o}C-1504^{o}C during 4-24 hours. SEM, EDX results showed that occasional precipitation of corundum, mullite and $ZnAl_2O_4$ crystals were detected along the frit-refractory interface and in the cooled frit melt.

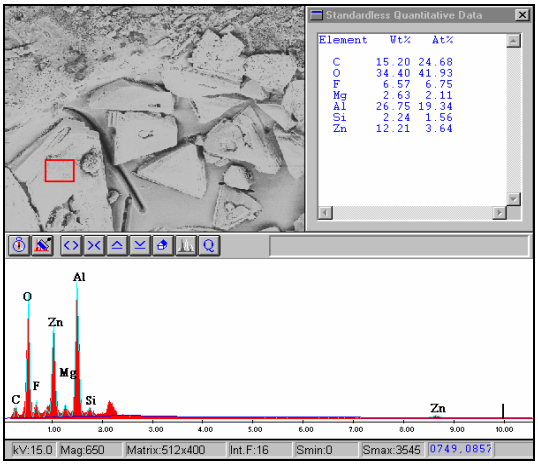

Figure 5.28. EDS analysis of $ZnAl_2O_4$ crystals with triangular shapes embedded within the cooled frit (1504 ^{o}C-24 h)

SEM images of the corroded refractory specimens after static corrosion tests showed that corundum crystals with different shapes precipitated along the frit-refractory interface. But, differences between corundum formed during corrosion process or that formed during cooling proved difficult. But, it may be considered that acicular crystals probably formed during cooling while 3D-cellular structures resulted from the frit melt during corrosion process (Poirier, et al. 2004).

Analysis of the corroded refractory specimens tested at 1504 ^{o}C during 24 hours by X-ray diffraction method did not show any significant changes in phase composure of the refractory specimens after the corrosion test in Figure 5.29.

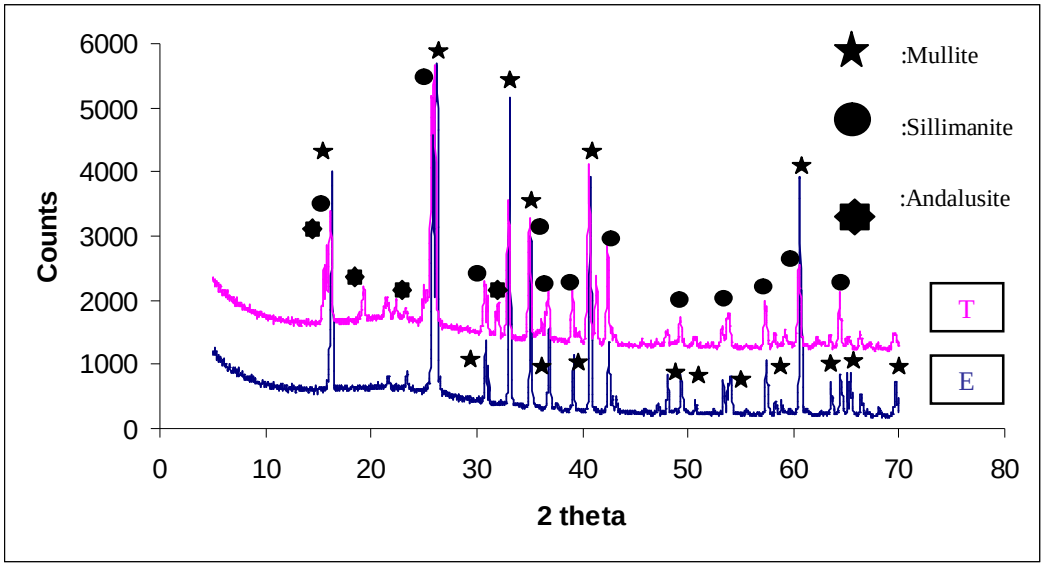

Figure 5.29. XRD pattern of the corroded refractory specimens tested at 1504 ^{o}C during 24 hours.

To sum up, the corrosion front was found to advance slowly into the refractory regardless of whether the frit is in contact with the large mullite or silimanite grain or with the grain boundary. This indicates that chemically this type of refractory is not compatible with frit melts. Dissolution occurs independent of the microstructure.

5.3.2. Postmortem Analysis of the Corroded Refractory Specimens After Dynamic Corrosion Tests

SEM, EDX and OM investigations were carried out for the corroded refractory specimens after dynamic corrosion testings. In this way, formation of new phases along the frit-refractory interface and in the cooled frit melt was observed to find out their corrosion mechanisms in dynamic conditions. Firstly, optical microscopy was used to investigate crystals precipitated because of corrosion process. Precipitation zones are marked as circled white cross in Figure 5.30. As can be seen from the microscopy images, some white crystals as corrosion products were observed along the frit-

refractory interfaces. These small white crystals were also found in SEM images of the corroded refractory specimens tested at 1418 ^{o}C during 10 minutes in Figures 5.31 and 32. SEM, EDX analysis of these precipitated crystals are given below.

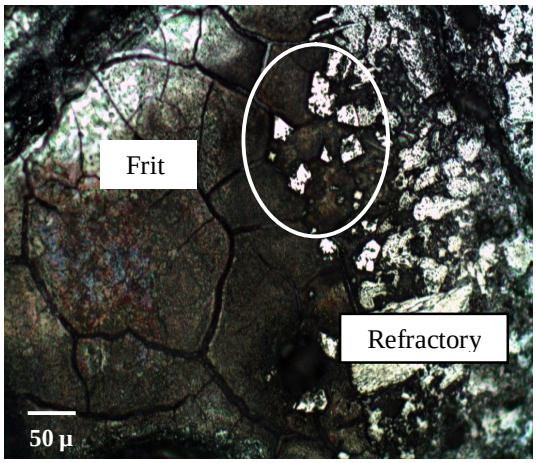

a) E refractory-frit interface
(1418 ^{o}C-10 minutes) (20X)

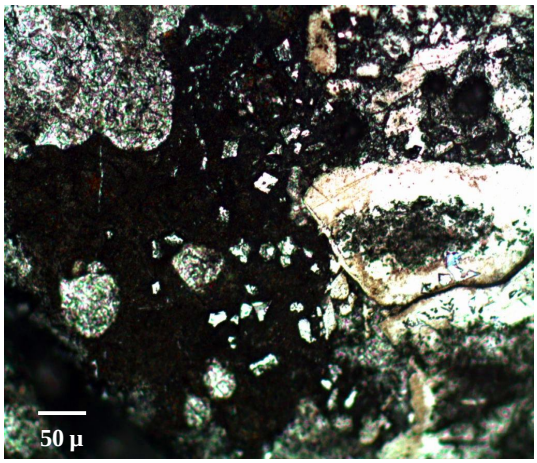

b) T refractory-frit interface
(1456 ^{o}C-10 minutes) (20X)

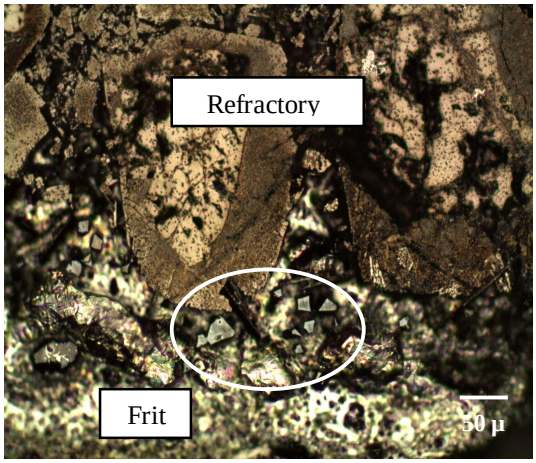

c) T refractory-frit interface
(1418 ^{o}C-60 minutes) (20X)

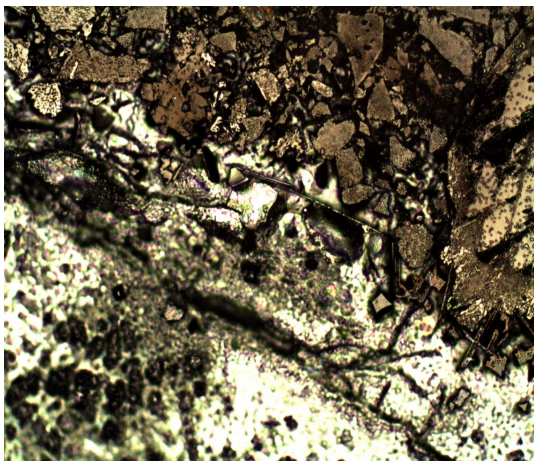

d) T refractory-frit interface
(1456 ^{o}C-60 minutes) (20X)

Figure 5.30. Optical microscopy images of the corroded refractory specimens after dynamic corrosion tests.

(cont. on next page)

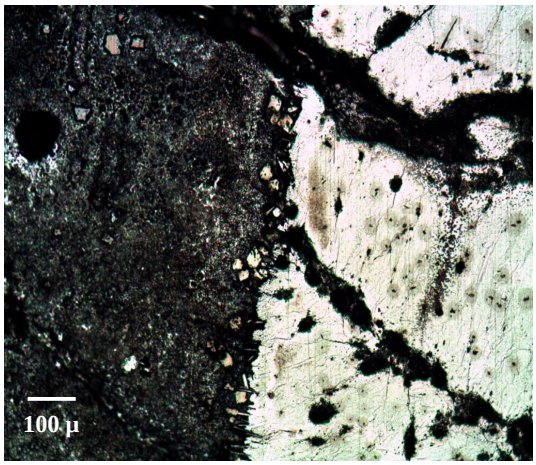

e) E refractory-frit interface
(1456 ^{o}C-60 minutes) (10X)

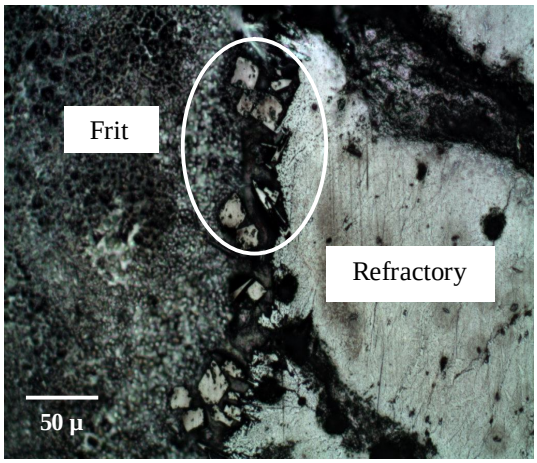

f) E refractory-frit interface
(1456 ^{o}C-60 minutes) (20X)

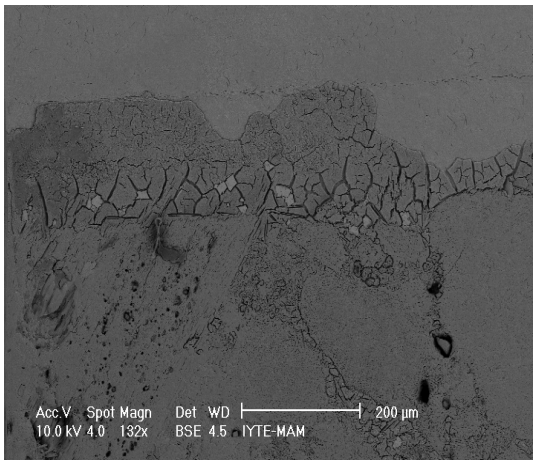

a) E refractory-frit interface
(1418^{o}C-10 minutes)

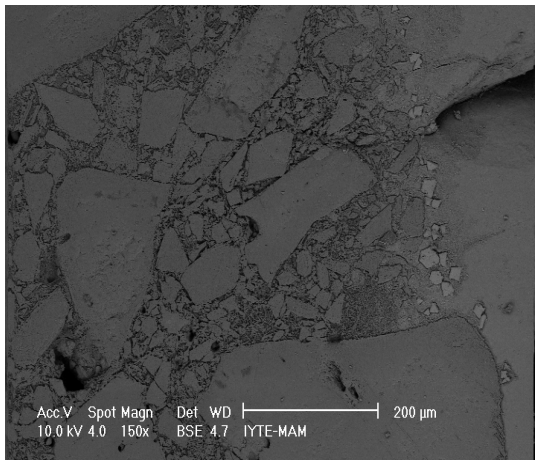

b) T refractory-frit interface
(1418^{o}C-10 minutes)

Figure 5.31. SEM images of the corroded refractory specimens that were tested at 1418 ^{0}C during 10 minutes for dynamic tests.

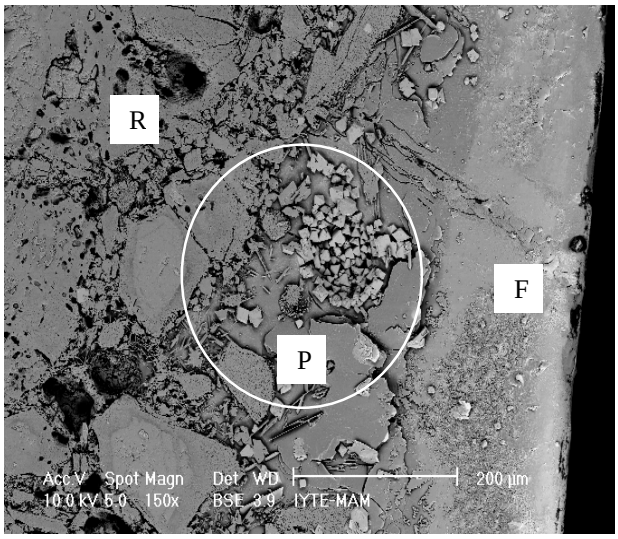

T refractory-frit interface
(1418^{o}C-60 minutes)

Figure 5.32. SEM image of T refractory specimen tested at 1418 ^{o}C during 60 minutes for dynamic corrosion test. R: Refractory structure (unaffected area), F: Cooled frit (Remnant slag), P: Precipitation zone (along the refractory-frit interface).

Figure 5.33 shows precipitation zone between refractory structure (unaffected zone) and remnant slag zone and it was investigated by observing EDX results of the precipitated crystals in Figure 5.33. EDX analyses showed the existance of $ZnAl_2O_4$ crystals in the white colour zone as seen in Figure 5.33.a. Furthermore corundum and mullite crystals embedded within the cooled frit melt were detected in Figure 5.33.b,c,d.

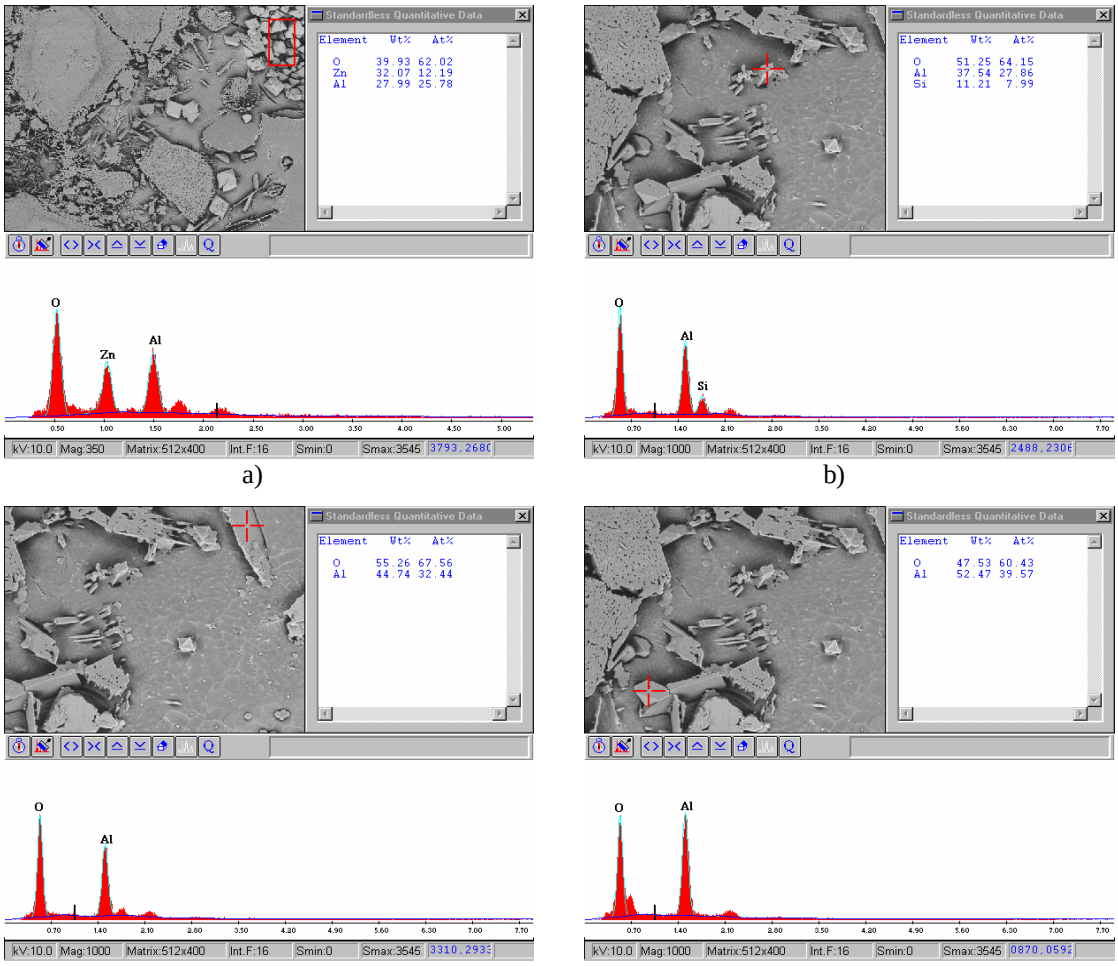

Figure 5.33. EDX analysis of T refractory specimen tested at 1418 ^{o}C during 60 minutes for dynamic corrosion test.

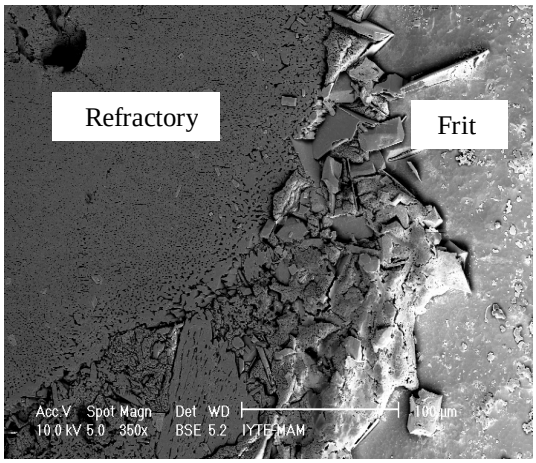

a) E refractory-frit interface

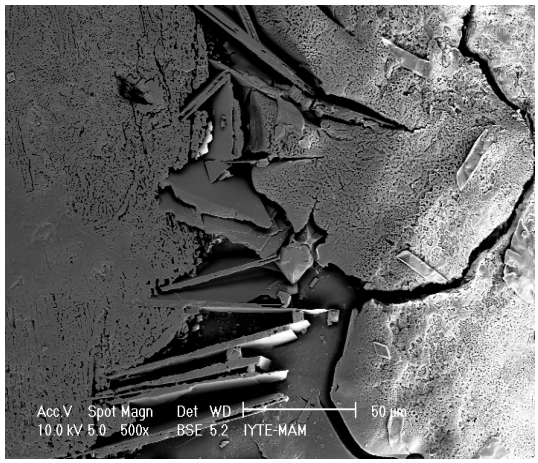

b) E refractory-frit interface

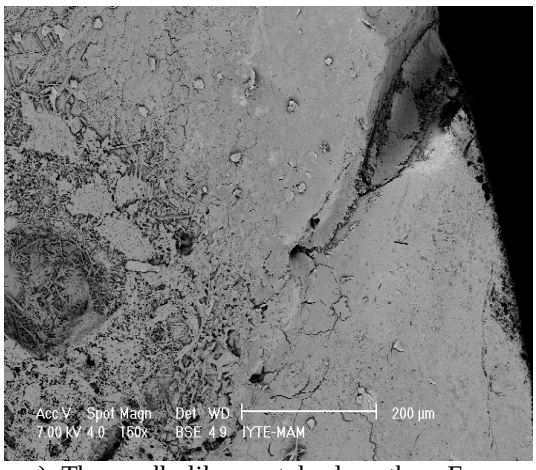

c) The needle-like crystals along the E refractory-frit interface.

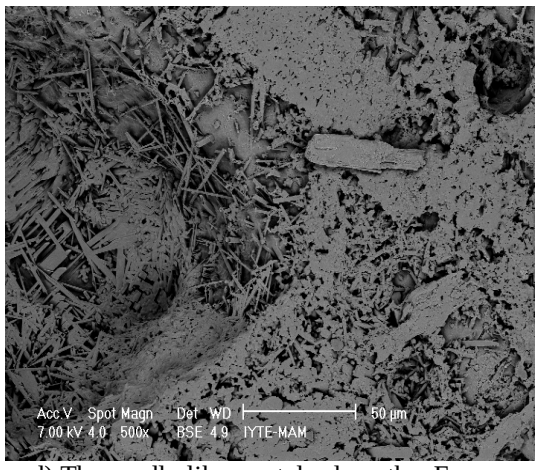

d) The needle-like crystals along the E refractory-frit interface.

Figure 5.34. SEM images of E refractory specimen tested at 1456 ^{o}C during 60 minutes for dynamic corrosion tests.
(R: Refractory structure, F: Cooled frit)

Precipitates formed as plate shapes in SEM images of the corroded refractory specimen given above were analyzed by EDX and the chemical composition of the crystals was identified as corundum in Figure 5.35.a. The needle-like crystals were found to be mullite as seen in Figure 5.35.b.

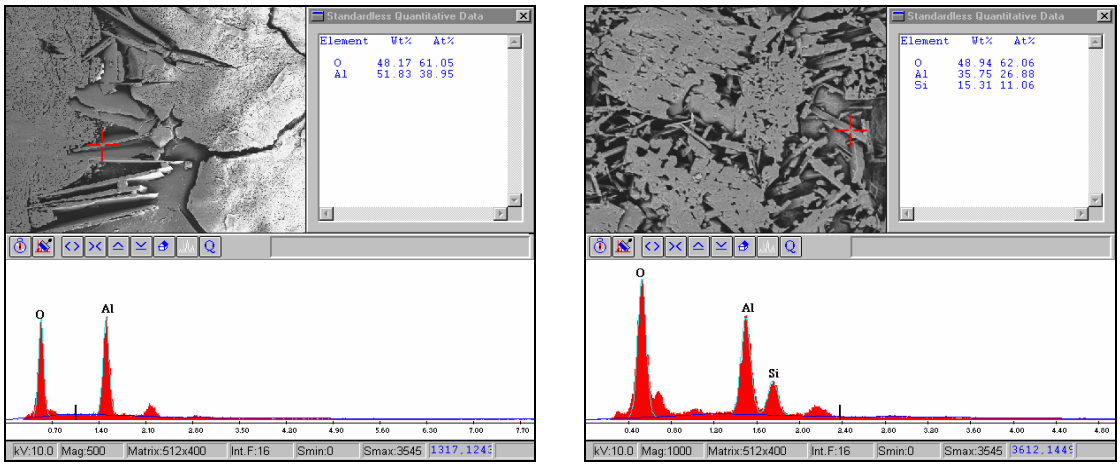

a) b)

Figure 5.35. EDX analysis of E refractory specimen tested at 1456 ^{o}C during 60 minutes for dynamic corrosion tests.

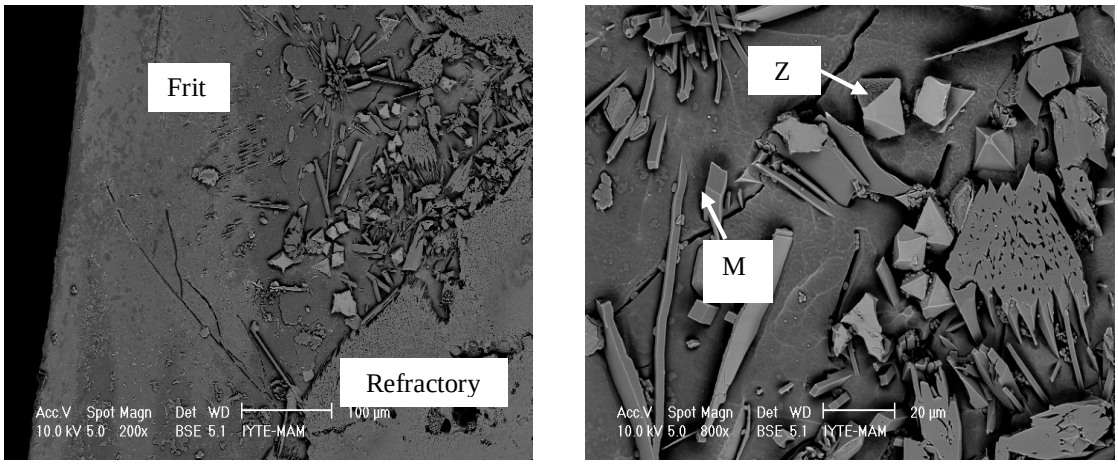

a) T refractory-frit interface (1535 ^{o}C 60 minutes)

b) Precipipates along the refractory-frit interface (1535 ^{o}C 60 minutes)

Figure 5.36. SEM images of T refractory specimens tested at 1456 ^{o}C during 60 minutes for dynamic corrosion test. (Z:$ZnAl_2O_4$, M:Mullite)

Occasional precipitation of $ZnAl_2O_4$ (white crystals) and mullite (needle-like) crystals were observed along the frit-refractory interface in Figure 5.36. EDX analysis of these crystals are given in Figure 5.37.

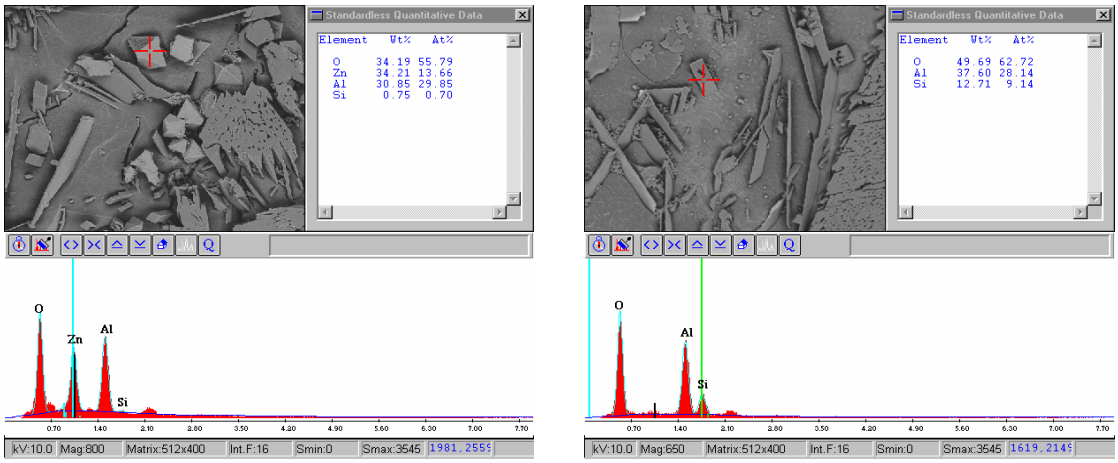

a) b)

Figure 5.37. EDX analysis of T refractory specimen tested at 1456 ^{o}C during 60 minutes for dynamic corrosion tests.

CHAPTER VI

CONCLUSIONS AND RECOMMENDATIONS

Corrosion test results indicated the following conclusions: E type bricks were found to be more resistant to the corrosive frit melt than T type bricks in both static and dynamic corrosion tests when the percent wear measurements in their cross sectional areas are compared. This result was probably due to the higher proportion of mullite in these bricks that are less suspectible to dissolution in the frit. Mullite is the only thermodynamically stable phase in the system Al_2O_3-SiO_2. Static corrosion tests were designed according to the 2^3 full factorial experimental design to analyze the effects of factors affecting corrosion process. Temperature and exposure duration were found to be significant factors affecting corrosion as indicated in the ANOVA table. In the case of static corrosion tests, increasing temperature and immersion time led to higher amount of corrosion in the cross sectional areas of corroded refractory specimens. Along the frit-refractory interface, needle-like mullite crystals, corundum crystals with different shapes and $ZnAl_2O_4$ spinel crystal formation were observed because of frit melt interaction in the range 1404^{o}C and 1504^{o}C during 4-24 hours. The amount of $ZnAl_2O_4$ spinel crystals increased with increasing immersion time and temperature by forming a discontinuous band at the frit-refractory interface. The crystallization of $ZnAl_2O_4$ is expected to be observed at 1950^{o}C in the Al_2O_3-ZnO-SiO_2 system. Therefore, its formation in this study occurred probably due to the presence of other fluxing oxides that might reduce the $ZnAl_2O_4$ formation temperature indicated at the Al_2O_3-ZnO-SiO_2 ternary phase diagram. Dynamic corrosion tests in the range 1418^{o}C and 1456^{o}C during 10-60 minutes concluded that higher temperature and immersion time resulted in higher proportion of corrosion. This similar trend was also observed in the static corrosion test results. Furthermore, more accelareted dissolution was observed after dynamic corrosion tests because of reduction of boundary layer thickness. Along the frit-refractory interface, the needle-like mullite, corundum and $ZnAl_2O_4$ crystals were observed as precipitation products. But, XRD analysis could not reveal the phases of these crystals because of their small amounts. In all specimens, corrosion was more observed in the bond phases than through large filler grains of mullite and andalusite.

Corrosion tests of different types of refractories into various frit melts can be studied for future work. Refractories used in the special industrial applications that are exposed to different corrosive environments may be tested in our test protocol to select the appropriate bricks for manufacturers.

CHAPTER 1

INTRODUCTION

Frit is a glassy material that is composed largely of silica, alumina, alkali and alkaline earths. It is an intermediate product that is used in making glaze which is itself used for coating ceramic articles. The reason for making frit is to form a water insoluble and homogeneous material for preparing glaze formulations. Many ceramic tile manufacturers also produce their own frit to better control their glaze formulations because of the freedom from dependency on frit suppliers. In Turkey, there are 15 frit manufacturers operating 31 continous and 39 rotary frit melters having a frit production capacity of 565 tonnes per day (Türk Seramik Federasyonu 2003). Frit kilns of continuous type are rectangular constructions to which raw materials are fed from one end and the frit melt is discharged from the other end. The discharged frit is rapidly poured in a water bath to quickly cool it to preserve the glassy structure. Refractory bricks are used for lining of frit kilns such as the floors, sidewalls and discharge locations which are under varying amounts of frit attack at high temperatures (Eppler, et al. 2000). Many producers suffer from premature failure of their refractories because of incorrect choice of refractories and improper choice of operating conditions. However, ceramic producers are more concentrated on the production parameters of tile or sanitary products, and they generally lack the expertise to identify the correct type of refractories for their kilns. Therefore they are often dependent on supplier's advice. It's widely recognized that large savings can be realised by extending furnace campaign lives and delaying repairs as long as possible (Evans, et al. 2006). For this reason, the effects that are responsible for campaign duration must be clarified and investigated carefully to prevent premature shutdowns in the frit furnaces. The long campaign duration for a frit melting furnace depends on many factors: properties of bricks, primarily their heat and corrosion resistance in the melt and in the aggressive gaseous atmosphere saturated with aggressive volatile glass as batch components and fuel combustion products, as well as service condition of brickwork elements (cooling and insulation), frit melting parameters (temperature level, chemistry of frit and type of fuel) (Tokarev, et al. 2006). One of the most important properties of refractory bricks

used to line furnaces for melting frit glazes is their corrosion resistance to aggressive melts (Krasyni, et al. 2005).

Corrosion of refractory bricks happens when these materials are subjected to high temperatures in contact with corrosive substances. Corrosion is a complex phenomenon depending on the chemical composition of bricks and frit, temperature levels and design parameters of furnaces (refractory position in furnace). Corrosion occurs via different types of mechanisms for each material. Corrosion of refractories involves dissolution, penetration and reaction processes. In most instances, these mechanisms occur in combination (Nishikawa, et al. 1984).

The choice of bricks used as lining in furnaces for melting frit glaze can be based on experiments determining corrosion resistance of refractories in frit melts (Krasyni, et al. 2005). But significant properties of refractories especially corrosion behaviours determined under laboratory conditions cannot provide sufficiently accurate estimate of the furnace campaign duration. This is a result of the presence of a freeze plane within the brick that complicates the corrosive processes (Tokarev, et al. 2006). In an isothermal test, where every point of the refractory specimen and the corrosive medium (frit) are at the same temperature the corrosion performance is reliable and reproducible (Annual Book of ASTM Standars 1992).

In this study, corrosion behaviours of aluminosilicate refractories in contact with frit melts are investigated to find out their corrosion mechanisms. Aluminosilicate refractories are generally employed in frit kilns due to their low cost, but their service performances are generally not satisfactory (Lee and Phill 1994). Extensive corrosion of these refractories limits their service lives. Andalusite, silimanite and mullite based fired bricks are common in such furnaces. These bricks were studied for their corrosion behavior in contact with steel slag but in the literature no study was found on the corrosion behavior of these bricks in contact with molten frit at fixed temperature without a thermal gradient during the test (Krasyni, et al. 2005, Poirier, et al. 2004). A corrosion testing method and a test protocol for frit kiln refractories is produced by mimicking the conditions in the frit kiln. Some previous experimental setups used in corrosion testings were investigated to guide this study (Kobayashi 1982, Akkurt 2003, Cooper 1962, Meyer-Rau 2005, Velez 2003, Winder 1998, Guigonis 2002). Dip/dip and

rotation test (finger, rotating pencil test) was thought to be suitable for determining corrosion behaviours under both static and dynamic conditions that involved stagnant and flowing molten frit attack on refractories. Finally, postmortem microsctructural analysis of tested brick specimens was investigated by SEM, optical microscope and XRD methods to determine the factors related to refractory corrosion.

This thesis is composed of mainly six different part beyond this introduction chapter. The second chapter presents information from the literature survey on refractories and frit. The third chapter introduces information on corrosion. Fourth and fifth chapters provide experimental setup, results and discussion. Sixth chapter summarizes the conclusions obtain from this thesis.

REFERENCES

Akkurt S. and Leigh H.D. 2003. Corrosion of MgO-C Ladle Refractories. *American Ceramic Society Bulletin* 82(5):32-40.

Akkurt S. 2007. Lecture Notes, Refractory Corrosion, High Temperature Materials. İzmir Instıtue of Technology, Mechanical Engineering Department, Urla, İzmir.

Annual Book of ASTM Standards. 1992. Section 15: General Products, Chemical Specialites, and End Use Products, Refractories; Carbon and Graphite Products; Activated Carbon.

Banerjee S. 1998. *Monolithic Refractories*. The American Ceramic Society and World Sciencetific.

Bouchetou M. L., Ildefonse J. P., Poirier J. and Daniellou P. 2005. Mullite grown from fired andalusite grains: the role of impurities and of the high temperature liquid phase on the kinetics of mullitization and consequences on thermal shocks resistance. *Ceramics International* 31:999-1005.

Cooper A.R., Kingery JR and W.D. 1964. Dissolution in Ceramic Sysytems: Molecular Diffusion, Natural Convection Studies of Sapphire Dissolution in Calcium Aluminum Silicate. *Journal of The American Ceramic Society* 47(1):37-43.

Eppler Richard A. and Eppler Douglas R. 2000. *Glazes and Coatings.* Westerville, Ohio: The American Ceramic Society.

Eti Holding A.Ş. 2003. *Seramik Sektörünün Startejik Halkası-Frit*. Ankara: Özel Bor Kimyasalları Toplantısı, Türk Seramik Fedarasyonu Yayını.

Evans Geoff. 2006. Monitoring Refractory Wear, Glass Furnaces. *The Refractories Engineer* 5:7-10.

Fontana Mars G.1986. *Corrosion Engineering.* New York: McGraw-Hill International Editions, Materials Science and Engineering Series.

Guigonis J., Larry J., McGarry C. and Nelson M. 2002. Glass Contact Application of High Chrome Refractories in Soda-Lime Glass Melters. *Ceramic and Engineering and Science Proceedings* 23(1-2):24-28.

.

Iqbal Y., Lee. W.E. 2001. Influence of mixing on mullite formation in porcelain. *Journal of European Ceramic Society* 21:2583-2586.

Jrsuk.2008. http://www.jrsuk.com/images/splashpic.jpg (accessed March 3, 2008).

Karakus M. and Moore R.E. 1996. Post-Mortem Study of Glass Melting Furnaces Refractories, *The American Ceramic Society* 23:78-84.

Kobayashi M., Nishi N. and Miyamoto A. 1982. Slag resistance tests for refractories. *Taikabutsu Overseas* 2:5-13.

Kocabağ D. 2000. *Cam Fırınları, Malzemeler, Teknolojiler, Prosesler*. Eskişehir: Etam A.Ş Matbaa.

Krasnyi B.L., Tarasovskii V.P., Kuteinikova A.L. 2005. Evaluation of Corrosion Resistance of Refractory Materials in Furnaces For Melting Frit Glazes. *Glass and Ceramic* 62(9):26-27.

Lee W.E. and Moore R.E.1998. Evolution of in Situ Refractories in the 20th Century. *Journal of American Ceramic Society* 81(6):1385-1410.

Lee W. E. Phil D. and Rainforth W. Mark. 1994. *Ceramic Microstructures, Property Control by Processing*. London, UK: Chapman & Hall.

Lewis G. 1991. *Engineered Materials Handbook*, *Ceramics and Glasses*. ASM International, Materials Park, OH.

Mattson Einar, 1989. *Basic Corrosion Concepts* in Basic Corrosion Technology for Scientists and Engineers. New York.

Mazel F., Gonon and M., Fantozzi G. 2001. Manufacture of mullite substrates from andalusite for the development of thin film solar cells. *Journal of The European Ceramic Society* .22:453-461.

Meyer-Rau S. and Telle R. 2005 Testing strategies for corrosive interactions of ceramics with semi-solid and molten metals alloys. *Journal of The Eoropean Ceramic Society* 25:1049-1055.

Nishikawa Akira. 1984. *Corrosion in Technology of Monolithic Refractories.* Minato-ku, Tokyo: Plibrico Japan Company Limited.

Paskocimas C.A., Leite E.R., Longo E., Kobayashi W., Zorrozua M., Varela J.A. 1998. Determination of Corrosion Factors in Glass Furnaces. *Ceramic Engineering Science Proceedings* 19(1):75-87.

Poirier J., Qafssaoui F., Ildefonse J. P. and Hubert P. 2004. Influence of the Liquid Phase on the Slag Corrosion of Andalusite Based Refractories. *Refractories Applications Transactions* 1(1):55-61.

Refractories Instıtute
www.refractoriesinstitute.org/aboutrefractories.html (accessed March 12, 2008).

The Technical Association of Refractories in Japan. 1998. *Refractories Handbook.* Tokyo, Japan.

Senöz C. 2007. Microstructural Analysis of The Corrosion of Al_2O_3 and ZrO_2 in Frit Melts. Thesis MS, Material Science, İzmir Instıtue of Technology, Urla, İzmir.

Schneider H., Schreuer J. and Hildmann B. 2007. Structure and properties of mullite-A review. *Journal of The European Ceramic Society* 10:1016-1032.

Tokarev V.D., Igat'ev S.S. and Popov O.N. 2006. Analysis of Service of Refractories in Glass-Melting Tank Furnaces. *Glass and Ceramics* 63(5):19-22.

Tomba A., Camerucci M.A., Urretavizcaya G., Cavalieri A.L., Sainz M.A., Caballero A. 1999. Elongated mullite crystals obtained from high temperature transformation of sillimanite. *Ceramics International* 25:245-252.

U.S. Environmental Protection Agency.2008.
http://www.epa.gov/ttn/chief/ap42/ch11/final/c11s05.pdf (accessed Februrary 15, 2008).

U.S. Environmental Protection Agency. 2008.
http://www.epa.gov/ttn/chief/ap42/ch11/final/c11s14.pdf-Frit (accessed Februrary 15, 2008).

Velez M., Karakus M., Reidmeyer M.R. Headrick W.D., Moore R.E. 2001. Characterization and Testing of Refractories for Glass Tank Melters. *Ceramica (Brazil)* 43:13-21.

Velez M., Moore R.E., Smith J. 1997. Refractory Degradation in Glass Tank Melters. A Survey of Testing Methods. *Ceramica (Brazil*) 43:283-284.

Winder S.M. , Gupta A., Selkregg K.R. 1998. Investigation of Liquid Contact Refractory Corrosion Under Oxy-Fuel Glass Melting Atmosphere. *Ceramic Engineering and Science Proceedings* 19(1):53-73.

Windle C. 2006. New Refractory Concepts in Glass Furnace Design. *The Refractories Engineer* 5:24-30.

Xiao Z., Mitchell B.S. 2000. Mullite Decomposition Kinetics and Melt Stabilization in the Temperature Range 1900-2000^{o}C. *Journal of American Ceramic Society* 83(4):761-767.

Zhang S., Lee W.E., Karakus M. 2004. Refractories: Controlled microstructure composites for extreme environments. *Journal of Materials Science* 39:6675-6685.

Zhou N., Liu J., Lin B. 2005. Refractory Raw Materials in China. *American Ceramic Society Bulletin* 84(2):20-24.

.